UNIVERSITY OF CALIFORNIA

Santa Barbara

Polypeptoid Chain Conformation and Its Role in Block Copolymer Self-Assembly

A dissertation submitted in partial satisfaction of the

requirements for the degree Doctor of Philosophy

in Chemical Engineering

by

Beihang Yu

Committee in charge:

Professor Rachel A. Segalman, Chair

Professor Glenn H. Fredrickson

Professor Craig J. Hawker

Professor Christopher M. Bates

March 2021

The dissertation of Beihang Yu is approved.

_____

Professor Glenn H. Fredrickson

_____

Professor Craig J. Hawker

_____

Professor Christopher M. Bates

_____

Professor Rachel A. Segalman, Committee Chair

January 2021

Polypeptoid Chain Conformation and Its Role in Block Copolymer Self-Assembly

by

Beihang Yu

ACKNOWLEDGEMENTS

First of all, I would like to thank my advisor, Rachel, for the mentorship to me as a scientist, for the constant encouragement and support, and for creating a group culture that made my graduate research an enjoyable and rewarding experience. I would also like to thank my committee members: Glenn, for the insights and feedback that always get to the key points of my projects. Craig, for always providing fresh perspectives to look at and present my research, and for the prompt responses to help moving things forward along the way. Chris, for the constant enthusiasm in science and in teaching, and for being always available to listen and to help.

I would like to thank my mentors/colleagues in the group, Emily Davidson, Anastasia Patterson, and Scott Danielsen. To Emily, who welcomed me into the group, for helping me as a first-year graduate student get started in lab with unending patience, for helping me through telling my first research story, for all the little things that you spent time to help, and for your support throughout my entire graduate school. To Anastasia, my longest peptoid buddy, for all the helpful experimental skills and discussions we had on our projects, for being always patient and available to help, and for the company on those many beamtime trips we have made together. To Scott, for greatly broadening my scope of knowledge and providing different perspectives to think about the science, for the numerous discussions and suggestions on my research.

The Segalman group has been an integrated part of my graduate school. Thank you to the group with its past and present members, for being an inspiring and supportive community that I always feel belonged to. To the peptoids crew, thank you for the support and helping

hands at various times. To Dakota Rawlings, I am lucky to have you in the same year in the program and in the group, to go through our graduate school together at each milestone. Thank you for being a good listener to hear my ups and downs in research and the exciting discussions about our future careers. To Seamus Jones, thank you for being my polymer physics discussion and book club buddy, for being inspiring and sharing the science that we are both excited about.

A number of instrument scientists have been incredibly important in my research, without whom the work in this dissertation would never have been possible. To Rachel Behrens, for making instruments running smoothly in the polymer characterization facility and being always available to help, for helping me to troubleshoot instrument issues–I would not have been able to maintain our GPC without your help. To Dmitriy Uchenik, for the support and helpful tips on the mass spectrometry. To Youli Li and Phillip Kohl, for the help in the X-ray facility. To beamline scientists, Ruipeng Li and Masafumi Fukuto, Eric Schaible and Chenhui Zhu, and Tim Dunn, for the dedicated support to our experiments, which has enabled much of my PhD research. I would also like to thank my collaborators. To Professor Lynn Walker at Carnegie Mellon University, for all the insights and constructive feedback on the work in the second chapter. To Ron Zuckermann and the NanoBio staff, who warmly welcomed me when I first started my research at the Molecular Foundry, for the constant support on peptoids-relevant topics throughout my graduate research.

Thank you to the Chemical Engineering department, for being an active, creative and supportive community. I am thankful to have a highly-organized home department that always help to keep us on track, with all the friendly and efficient staff who made it so easy

to move things forward and have question answered. Thank you to UCSB and Santa Barbara, a place that I will always remember and miss coming back.

To friends near and far. To Tsatsa, thank you for always being positive and sharing–you have brightened my life in ways that I would never have. To Chad, thank you for always getting the punchlines and making me laugh. Both of you have made my graduate life an enjoyable journey. Thank you to friends at UCSB, who have made my life outside research not alone with all the fun trips, hikes and dinners. To my undergrad advisor and friends, thank you for being an important part prior to my graduate school and helping set the foundation for my PhD, for the friendship and support throughout my graduate life. To friends from young, with whom I have more than ten years of friendship, thank you for the greetings and chats that always bring me good memories and make me feel there is always a place that I can come back to.

Finally, to my parents, thank you for making me who I am, for having supported me through important life choices, for giving me the courage to explore the world and unknown, and for always being there whenever I needed support and comfort.

VITA OF BEIHANG YU

January 2021

EDUCATION

Doctor of Philosophy in Chemical Engineering University of California, Santa Barbara	Sep 2016 – Mar 2021 Santa Barbara, CA
Bachelor of Engineering in Polymer Materials and Engineering Tsinghua University	Aug 2012 – Jul 2016 Beijing, China
Bachelor of Arts in English Language (second major) Tsinghua University	Aug 2013 – Jul 2016 Beijing, China

PUBLICATIONS

9. Yu, B.; Li, R.; Segalman, R. A. Tuning the Double Gyroid Phase Window in Block Copolymers via Polymer Chain Conformation Near the Interface. *Submitted*

8. Yu, B.; Danielsen, S. P. O.; Yang, K.-C.; Ho, R.-H.; Walker, L. M.; Segalman, R. A. Insensitivity of Sterically Defined Helical Chain Conformations to Solvent Quality in Dilute Solution. *ACS Macro Lett.* 2020, *9*, 849-854.

7. Patterson, A. L.; Yu, B.; Danielsen, S. P. O.; Davidson, E. C.; Fredrickson, G. H.; Segalman, R. A. Monomer Sequence Effects on Interfacial Width and Mixing in Self-Assembled Diblock Copolymers. *Macromolecules* 2020, *53* (9), 3262-3272.

6. Yu, B.; Danielsen, S. P. O.; Patterson, A. L.; Davidson, E. C.; Segalman, R. A. Effects of Helical Chain Shape on Lamellae-Forming Block Copolymer Self-Assembly. *Macromolecules* 2019, *52* (6), 2560-2568.

5. Barry, M. E.; Davidson, E. C.; Zhang, C.; Patterson, A. L.; Yu, B.; Leonardi, A. K.; Duzen, N.; Malaviya, K.; Clarke, J. L.; Finlay, J. A.; Clare, A. S.; Chen, Z.; Ober, C. K.; Segalman, R. A. The Role of Hydrogen Bonding in Peptoid-Based Marine Antifouling Coating. *Macromolecules* 2019, *52* (3), 1287-1295.

4. Patterson, A. L.; Danielsen, S. P. O.; Yu, B.; Davidson, E. C.; Fredrickson, G. H.; Segalman, R. A. Sequence Effects on Block Copolymer Self-Assembly through Tuning Chain Conformation and Segregation Strength Utilizing Sequence-Defined Polypeptoids. *Macromolecules* 2019, *52* (3), 1277-1286.

3. Ly, J.; Martin, K.; Thomas, S.; Yamashita, M.; Yu, B.; Pointer, C. A.; Yamada, H.; Carter, K. R.; Parkin, S.; Zhang, L.; Bredas, J.-L.; Young, E. R.; Briseno, A. L. Short Excited-State Lifetimes Enable Photo-Oxidatively Stable Rubrene Derivatives. *J. Phys. Chem. A* 2019, *123* (35), 7558-7566.

2. Yang, X.; Yu, B.; Zhong, Z.; Guo, B.; Huang, Y. Nevirapine-polycaprolactone crystalline inclusion complex as a potential long-acting injectable solid form. *Int. J. Pharm.* 2018, *543* (1–2), 121-129.

1. Davidson, E. C.; Rosales, A.; Patterson, A. L.; Russ, B.; Yu, B.; Zuckermann, R. Segalman, R. A. Impact of Helical Chain Shape in Sequence-Defined Polymers on Polypeptoid Block Copolymer Self-Assembly. *Macromolecules* 2018, *51* (5), 2089-2098.

PRESENTATIONS

"Insensitivity of Sterically-Defined Helical Chain Conformation to Solvent Quality in Dilute Solution," Yu, B.; Danielsen, S. P. O.; Yang, K.-C.; Ho, R.-H.; Walker, L. M.; Segalman, R. A. Materials Research Outreach Program, UC Santa Barbara, Jan 2020 (Poster).

"Effects of Polymer Helical Chain Shape on Block Copolymer Self-Assembly," Yu, B.; Danielsen, S. P. O.; Patterson, A. L.; Davidson, E. C.; Segalman, R. A. APS March Meeting, Boston, Mar 2019.

"Effects of Helical Chain Shape on Lamellae-Forming Block Copolymer Self-Assembly," Yu, B.; Danielsen, S. P. O.; Patterson, A. L.; Davidson, E. C.; Segalman, R. A. Materials Research Outreach Program, UC Santa Barbara, Jan 2019 (Poster).

"Role of Polymer Chain Helicity in Block Copolymer Self-Assembly," Yu, B.; Rosales, A.; Patterson, A. L.; Davidson, E. C.; Zuckermann, R. N.; Segalman, R. A. APS March Meeting, Los Angeles, Mar 2018 (Poster).

"Role of Sequence and Chain Shape in Block Copolymer Self-Assembly," Yu, B.; Davidson, E. C.; Patterson, A. L., Rosales, A.; Zuckermann, R. N.; Segalman, R. A. 10th Peptoid Summit, Molecular Foundry, LBNL, Aug 2017 (Poster).

HONORS AND AWARDS

Outstanding Graduation Thesis, Tsinghua University	2016
Outstanding Graduate, Tsinghua University	2016
Evergrande Co. Scholarship (scholarship for academic excellence)	2015
Dow Chemical Scholarship (scholarship for academic excellence)	2015
Silver Award in Tsinghua Summer Social Practice	2014
Scholarship for Academic Excellence	2013

TEACHING EXPERIENCE AND SERVICE

ChE 132A: Analytical Methods in Chemical Engineering	Spring 2020
ChE 126/228: Non-Newtonian Fluids, Soft Materials and Chemical Products	Fall 2018
ChE 180A: Chemical Engineering Laboratory Lab Sessions	Spring 2018
Volunteer at Local Elementary School Science Night	2018 – 2020

ABSTRACT

Polypeptoid Chain Conformation and Its Role in Block Copolymer Self-Assembly

by

Beihang Yu

Polymer chain conformation underlies polymer physical properties and impacts many of polymer functionalities. Understanding chain conformation is critical for predicting and controlling the structures and properties in polymeric systems. In block copolymers, chain conformation of the consisting blocks closely impacts the thermodynamics of microphase separation and the resultant structures, which are key to block copolymers as functional materials. However, the understanding of chain conformation effects beyond coil–coil block copolymers is yet nascent, partially due to the challenge to precisely control chain conformation without introducing other complicating factors.

This dissertation utilizes sequence-defined polypeptoids to install precise chain conformation control into traditional polymer systems, to examine the role of chain conformation in block copolymer self-assembly. First, the polypeptoid chain conformation is examined in terms of local stiffness, overall chain size, and response to solvent quality by comparing chemically identical helical and coil polypeptoids in dilute solution. The detailed understanding from molecular length scale reveals that the helical secondary structure, driven by steric hindrance from side chains, makes the polypeptoid chains locally stiffer but overall more compact than the coil analogues. Further, we show these helical chains are relatively insensitive to solvent conditions due to their sterically defined nature. Then, through the

design of model polypeptoid-containing block copolymer systems, we are able to study the effects of the helical chain conformation, which has distinct space-filling characteristics from chemically analogous coil chains, on the melt self-assembly of block copolymers. In the lamellae-forming system, the helical chain conformation is shown to decrease the order–disorder transition temperature through a combination of decreasing the enthalpic interaction between dissimilar blocks and experiencing amplified chain stretching. Further, polypeptoids are used as a conformation tuning handle and are shown to modulate network phase formation and stability as a conformationally tunable interfacial segment, which demonstrates the importance of chain conformation at the vicinity of the interface in determining the morphology of block copolymers. The findings in this dissertation highlight the importance of chain conformation on the self-assembly thermodynamics of block copolymers, and polypeptoids as highly-controlled, precise polymers to aid the fundamental understanding of polymeric materials.

TABLE OF CONTENTS

LIST OF FIGURES

Chapter 1

Introduction

Polymer chain conformation impacts physical properties of polymers, from microscopic length scale properties such as stiffness, space-filling and scaling behaviors, to macroscopic properties including mechanical, optical, and transport properties. Molecular level understanding of chain conformation is critical for predicting and controlling structures and properties of polymeric systems ranging from block copolymers, polymer composites, to polymer solutions and blends.

Block copolymers consist of two or more chemically distinct polymer blocks, and can self-assemble to form periodic patterns on the nanometer length scale, making them appealing for many technological applications. This so-called microphase separation and the resultant structures of block copolymer melts are well-known to depend on chain conformation of the constituent blocks, with a relatively comprehensive understanding for

coil–coil block copolymers, where chain conformation of both blocks can be captured by Gaussian chain statistics. Block copolymers with chain conformations beyond flexible coils are practically important, as many newly developed polymers have variations in stiffness and/or secondary structures that are central for their application as functional materials. Yet the understanding of effects from these non-Gaussian chain conformations in block copolymers remains nascent. Challenges in traditional synthetic polymers persist due to the lack of ability to independently tune chain conformation without modifying other parameters, such as chain length and dispersity, in which variations are inevitable because of the statistical nature of polymerizations.

With the adaption of solid-phase synthesis from polypeptides, polypeptoids–poly(*N*-substituted glycine)s, integrate the sequence and length specificity of biopolymers, and the robustness of synthetic polymers. Further, the conformational diversity and the ability to precisely control conformation make polypeptoids an ideal system for investigating chain conformation effects. This dissertation utilizes polypeptoids as a polymer block of tunable chain conformation in block copolymers, to study the role of chain conformation in the self-assembly of block copolymer melts. First, a background of block copolymer self-assembly with emphasis on polymer chain conformation effects is presented to set up the context. Next, strategies to control/tune polymer chain conformation are summarized. Finally, considerations of different parameters for tuning self-assembly are discussed to establish where chain conformation lies as a tuning handle for block copolymer self-assembly.

1.1 Polymer chain conformation in block copolymer self-assembly

Block copolymers self-assemble into intricate structures on the nanometer length scale including lamellae, cylinders, spheres and bicontinuous phases, which render them unique physical properties as functional materials. The relationship between molecular structures and mesoscale structures for coil–coil block copolymer melts is well established through both experimental and theoretical approaches, with the assumption of random-walk chain conformations.[1-3] While the knowledge of coil–coil block copolymers provides valuable basis towards understanding more complex block copolymer systems, the simple trade-off between enthalpic mixing and entropic chain stretching need to be carefully reexamined for non-classical polymers.

1.1.1 Thermodynamics of classical block copolymer self-assembly

In a classical linear diblock copolymer, both blocks observe Gaussian chain statistics with symmetric statistical segment lengths. The microphase separation is driven by the chemical incompatibility between the two blocks that is unfavorable for mixing, which is counterbalanced by entropic penalties from chains stretching to fill space at uniform density. As a result, the self-assembled structure reflects a free energy minimization, accounting for the enthalpic and entropic contributions. The strength of segregation is parameterized by χN, where χ is the Flory–Huggins interaction parameter that describes the free energy cost from dissimilar blocks mixing and N is the number of segments (usually normalized by some reference volume v_0). At sufficiently large segregation strength, block copolymers self-assemble into periodic structures, with morphologies determined by the relative volume of each block. Phase diagrams of linear diblock copolymers are commonly constructed with the

segregation strength (χN) and the volume fraction of one block (f_A), and have been readily established by both experimental and theoretical works (Figure 1.1).[4-6]

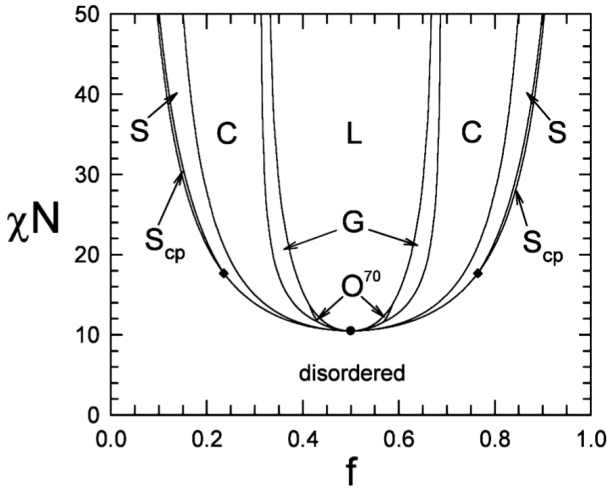

Figure 1.1 Phase diagram for linear diblock copolymer melts calculated using SCFT The thermodynamically stable morphologies include: hexagonally close-packed spheres (S_{cp}), body centered spheres (S), hexagonally packed cylinders (C), double gyroid (G), *Fddd* orthorhombic network (O^{70}), lamellae (L). (Reprinted with permission from reference 4. Copyright 2012 American Chemical Society)

A simple illustration of the theory is to consider a symmetric diblock copolymer with equal volume fractions ($f_A = 1/2$) and an overall number of segments, N.[1] The interaction energy per chain (enthalpic component) can be estimated by the product of A–B interfacial tension (γ_{AB}) and the interfacial area per chain (Σ), and the stretching energy (entropic component) can be approximated by Hookian elasticity based on the domain size (λ) and the unperturbed chain size ($\sim Na^2$), leading to a free energy expression:

$$F/k_BT = (\gamma_{AB}/k_BT)\,\Sigma + 3(\lambda/2)^2/(2Na^2)$$

Consequently, the domain period and the order–disorder transition can be determined. Interested readers are referred to works by Helfand on free energy expressions of other

morphologies,[7-9] and earlier reviews by Bates, Fredrickson *et al.* on the fundamental physics, seminal experimental and theoretical work of classical block copolymer self-assembly.[2, 6]

1.1.2 Conformational asymmetry in flexible block copolymers

In most circumstances, assuming symmetric chain conformation is sufficient to capture the phase behavior of flexible block copolymers, yet more evidence is showing that slight differences in chain conformation can lead to significant changes. Even for flexible polymer chains, chain conformations are not identical due to the intrinsic differences in their chemical structures. For example, poly(ethylene oxide) (PEO), polyethylene (PE), and polystyrene (PS), are all flexible polymers, but have different statistical segment lengths (of one repeat unit) and persistence lengths.[10] Conventionally, the conformational property of polymers can be captured by a conformational symmetry parameter, β ($\beta^2 = R_g^2/V$, a measure of space-filling vs. volume-filling of a polymer chain), then the conformational difference between two polymer blocks can be quantified by a conformational asymmetry parameter, ε ($\varepsilon = \beta_A^2/\beta_B^2$).[6, 11]

Conformational asymmetry has been shown to impact a number of aspects of block copolymer self-assembly. First, the conformational properties affect polymer–polymer interactions, inducing a nonlocal contribution to the free energy via impacting the effective coordination number that leads to changes in χ–a phenomenon exists in both homopolymer blends and block copolymer melts.[11-14] Second, conformational asymmetry induces spontaneous interfacial curvature in compositionally symmetric diblock copolymers (Figure 1.2), and therefore shifts phase boundaries and leads to asymmetric χN–f phase diagrams with some phases occurring on only one side.[6] More recently, conformational asymmetry has

been shown to be a critical factor to influence chain packing, leading to stabilization of low-symmetry phases like the Frank–Kasper phases in diblock copolymers.[15-17]

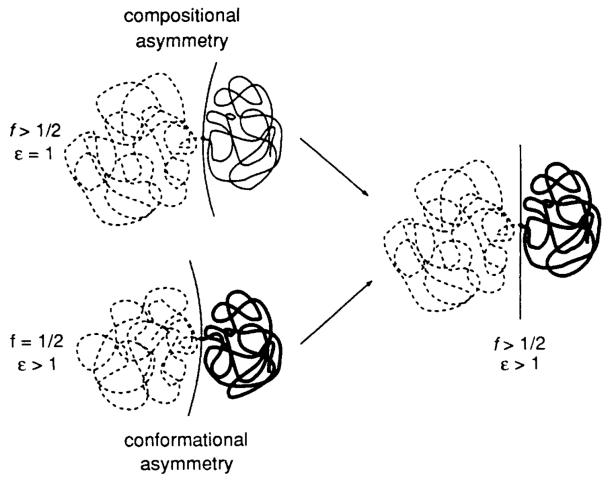

Figure 1.2 Compositional and conformational asymmetry induce spontaneous interfacial curvature
f corresponds to the volume fraction of the block on the left (dashed line), ε corresponds to the ratio of the conformational symmetry parameters of the two blocks (dashed line/solid line). When $f = 1/2$ and $\varepsilon > 1$, the interface tends to curve toward (or around) the block with a larger β^2 (i.e., occupies more space per chain volume). Proper choice of $f > 1/2$ and $\varepsilon > 1$ leads to a flat interface. (Reproduced from reference 6 with permission from the Royal Society of Chemistry)

The conformational differences between polymers essentially reflect the differences in intra- and inter-molecular correlations of polymer segments. Polymer chains with identical volume do not necessarily fill the same amount of space, and this asymmetry in space-filling in polymer blends and block copolymers leads to excess contributions to the free energy. The concept of conformational asymmetry, although mostly used to depict coil–coil block copolymers, is introduced in this section to set context for the emerging conformational differences when polymer chains adopt secondary structures, which is the topic of this dissertation.

1.1.3 Block copolymer self-assembly with semiflexible and rod-like chains

Beyond the flexible chain conformation regime, polymer chains can be semiflexible or rod-like (e.g., conjugated polymers, helical biomacromolecules). The self-assembly thermodynamics involving stiff chains is very different compared to that with coil chains, due to drastic differences in chain conformation and additional interactions between stiff chain segments. These lead to variations in the free energy and distinctly different phases in rod–coil systems.

The additional liquid crystalline interaction between stiff chain segments is the most remarkable difference as polymer chains become rigid, and this alignment interaction can be parameterized by the Maier–Saupe interaction parameter, μN.[18-20] There is also conformational mismatch between the rod and coil blocks that will affect the immiscibility[21] and chain packing,[22] because the covalently linked blocks share the same interface and need to fill space at uniform density. Furthermore, chain stiffness impacts interfacial curvature and chain stretching entropy, and the orientational effects of stiff chains also give rise to strong fluctuation effects.[18]

The semiflexible regime is more challenging to study experimentally, and tuning semiflexibility while keeping other parameters constant is almost prohibitive in most synthetic polymers. Therefore, works that specifically look at effects of varying semiflexibility are mostly theoretical studies, with the wormlike chain model (describes chains as connected rods of certain length to reflect chain flexibility) commonly used.[18, 21-22] The semiflexible–flexible or semiflexible–semiflexible block copolymers share similarities with rod–coil systems in terms of additional alignment interactions and chain packing

considerations, both of which are also factors to be considered when secondary structures change chain stiffness and the way chains occupy space.

1.1.4 Polymer secondary structures in block copolymer self-assembly

Another category of chain conformation that is gaining more attention is polymers with secondary structures. This dissertation focuses on polymers with helical secondary structures, a conformation that is observed in both biological and synthetic polymers (major helical polymer families: poly(amino acid)s, poly(isocynanide)s and poly(acetylene)s),[23] and plays a critical role in polymer functionality.

Adopting secondary structures automatically leads to chain conformation changes, as the monomers (repeat units) do not follow random-walk statistics, but instead are arranged along contours dictated by the specific secondary structures. This then leads to stiffness variations due to the additional correlations between monomers, which make the polymer chain persist over a longer distance in one direction (Figure 1.3). Indeed, polymers with helical secondary structures usually exhibit longer persistence lengths (l_ps). For example, double stranded DNA and the synthetic helical polymer, poly(*n*-hexyl isocyanate) have l_ps in the range of 30–60 nm; another helical polymer, poly(γ-benzyl-L-glutamate), has a $l_p \sim 150$ nm, while most flexible polymers have l_ps below 1 nm.[10] The persistence lengths of helical polymers are also shown to be larger than their chemically analogous counterparts under identical conditions.[24-25] Besides changes in stiffness, secondary structures also impact how polymer chains fill space. It should be noted that although helical secondary structures increase chain stiffness, monomers are also packed more densely; therefore, with the same number of monomers, a helical chain has fewer but stiffer segments (based on Kuhn length/persistence length) than

the equivalent coil chain, and this can lead to a smaller radius of gyration (R_g) of the helical chain (Figure 1.3).

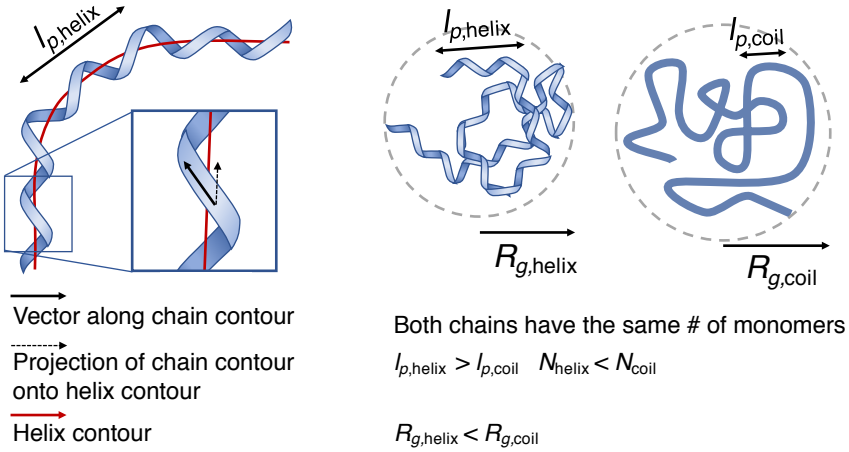

Figure 1.3 Helical secondary structures impact stiffness and space-filling of polymer chains
For polymer chains adopting a helical secondary structure, the helix contour is defined as along the red line, which has a longer persistence length, $l_{p,\text{helix}}$ (left: adapted with permission from reference 26. Copyright 2018 American Chemical Society). As the monomers are packed more closely due to the helical secondary structure, the helical chain fills less space than an equivalent coil chain with the same number of monomers.

Many helical building blocks studied in block copolymers are rod-like, such as poly(*n*-hexyl isocyanate), poly(isocynanide), poly(γ-benzyl- L-glutamate), all with persistence lengths on the order of tens of nanometers. Therefore, the self-assembly behavior resembles that of rod–coil block copolymers discussed in the last section, where the alignment interaction between the rigid blocks and the stiffness asymmetry between the rod and coil blocks are key factors impacting the self-assembly behavior.[27-30]

Most helical secondary structures in polymer chains involve chirality and an intriguing phenomenon is the chirality transfer across difference length scales. Ho and coworkers have studied block copolymers of polystyrene (PS) and a helical poly(L-lactide) (PLLA) block and

observed a long-lived metastable helical phase (H^*) with *P622* symmetry between the lamellar and cylindrical phases.[31-32] The evolution of homochirality from molecular chirality into phase chirality is explained by a twisting and shifting mechanism of the disk-shaped block copolymer microdomains, a specific geometry driven by the locally stiffer chiral PLLA chain with helical steric hindrance.[33] Diverse helical structures can be constructed from the self-assembly of polymers and block copolymers, either in synthetic or biological systems.[34] Understanding how chirality and helicity interact with the conventional driving forces in block copolymer self-assembly will lead to exciting opportunities for developing new functional materials, as well as understanding the homochiral evolution that could trace back to the origin of life.

1.2 Chain conformation control in polymers

With chain conformation being critical to polymer property and functionality, it is desirable to gain control over polymer chain conformation to utilize it as a handle to tune relevant properties. Besides the conformational differences associated with different backbone chemical structures, there are isomeric variations (sequence/positional, structural/geometric, stereo isomerism) that give additional conformational space for polymer chains. This section focuses on strategies to tune conformational properties of polymers including stiffness, size (radius of gyration), and secondary structures that closely correlate with the physical properties of polymeric systems.

1.2.1 Strategies for intrinsically tuning polymer chain conformation

Most synthetic polymers are coil-like and observe Gaussian chain statistics when exceed certain chain lengths, although their local chain stiffness varies depending on the specific backbone and side chain chemical structures. The Flory's characteristic ratio, C_∞, reflects the local chain stiffness, which typically falls in the range of 7–9 for many flexible polymers.[35]

Without alternation in the chemistry, chain stiffness can be tuned through isomeric variations. For example, regioregularity of conjugated polymers, which is associated with the position of side chains on adjacent thiophene rings, significantly impacts the persistence length of poly(3-alkylthiophene) (P3AT) polymers.[36-38] Tuning the persistence length of P3ATs could impact the electronic properties and complex morphological behavior of the polymeric materials.[39] Further, the *cis*/*trans* configuration also affects chain conformation, with *trans* favoring a planar conformation that leads to stiffer chains (e.g., in poly(*p*-phenylenevinylene) derivatives[40]); however, adopting *cis* or *trans* configuration is mostly dictated by the steric hindrance of side chains.

Tacticity/Stereoregularity is another factor that affects polymer chain conformation, and is often closely related to polymer secondary structures. A large category of synthetic helical polymers are isotactic polyolefins and other vinyl polymers adopting helical conformations in the solid state (crystalline regions), with tacticity controlled through synthesis using specific catalysts (e.g., the Ziegler–Natta catalyst for olefin polymerization).[41] The helical chain conformation in solid state is interconnected with crystallinity to achieve optimized intra- and inter-chain packing, while in solution these isotactic polymers only attain highly dynamic conformations with short helix segments in solution.

Biopolymers adopt a wider range of chain conformations, and have another tuning parameter–sequence, to further tune chain conformation. Natural proteins derived from 20

naturally occurring amino acids fold into hierarchical structures, with polypeptide chain segments adopting a variety of secondary structures including α-helix, β-sheets (two main secondary structures).[42] The α-helix is regarded as the default conformation, while there are strategies like branching at the β-carbon, introducing side chains containing hydrogen-bond donors/acceptors, and incorporating steric residues to destabilize the α-helix structure.[43]

1.2.2 Polymer chain conformation and surrounding environments

Polymer chain conformation is almost always discussed in the context of its surrounding environments, either in melts/glasses (surrounded by other polymers of the same type), or in solution (including polymeric solvents). Essentially, polymer chain conformation is determined by the interplay between polymer–polymer (intra-molecular) and polymer–molecule (inter-molecular) interactions. The studies on polymer chain conformation in dilute, semi-dilute, and concentrated solutions are comprehensive.[44] Here the discussion is focused on scenarios when specific interactions present within polymer chains and/or between polymer chains and their surrounding environments.

The chain conformations of biopolymers and biomimetic polymers are closely related to the solvent conditions (mostly aqueous) and undergo structural or conformational changes in response to external stimuli like temperature, pH, etc.[45] For example, the most common conformational change, coil-to-globule transition, is mediated by hydrophobic interactions between solvents and polypeptide residues[46]–a concept that inspired designing protein-like polymers with sequence-dependent conformations.[47-48] Further, the presence of secondary structures, which are stabilized by intra- and inter-molecular interactions including hydrogen-bonding, electrostatic interactions, and hydrophobic interactions, adds to the diversity of

polymer conformation variations. Depending on the specific driving forces, polymers with secondary structures exhibit unique stimuli-responsive chain conformations and therefore physical properties. For example, the helix-to-coil transitions of poly(L-lysine) and poly(L-glutamic acid) can be controlled by pH, which is attributed to the competing electric repulsion between the side chains and hydrogen-bonding interactions.[43] Some synthetic helical polymers also have solvent-dependent or temperature-dependent chain conformations.[49-50] Meanwhile, specific designs are also possible to produce relatively stable secondary structures that are insensitive to external stimuli.[51] Understanding the molecular origin and the interactions that determine the chain conformation of polymers is key to predict and design polymer chains with tunable chain conformations.

1.2.3 Tunable chain conformation of sequence-defined polypeptoids

Polypeptoids are a class of bioinspired polymers that allow high structural tunability resembling natural biopolymers. The ability to precisely control the sequence, and high synthetic yields enabled by solid-phase synthesis (Figure 1.4),[52-53] make polypeptoids an attractive candidate to achieve the structural and functional complexity comparable to biopolymers, yet with a larger library of available side chain functionalities.[54]

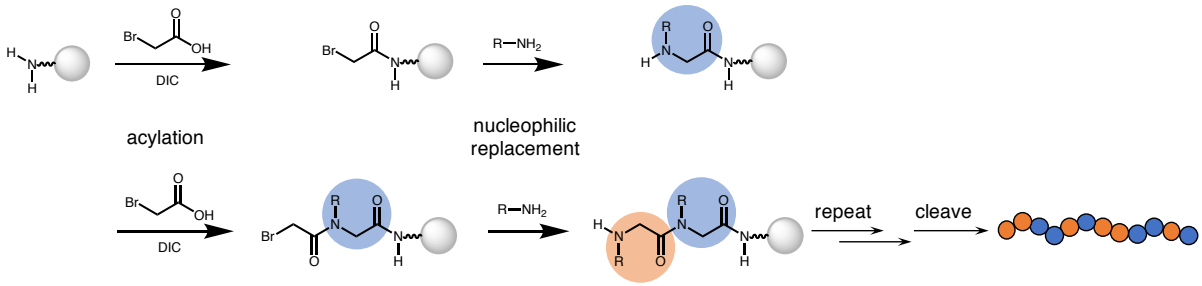

Figure 1.4 Solid-phase synthesis of polypeptoids
Polypeptoids are synthesized via a two-step submonomer process: 1) acylation of a secondary amine with a haloacetic acid, 2) nucleophilic displacement of the halogen with a primary amine–a step to introduce side chains of interest.

One intriguing feature of polypeptoids is the capability to form secondary structures, despite the lack of chiral centers and hydrogen-bond donors on the backbone. Helical conformations are the main category of secondary structures observed in polypeptoids, and are mainly stabilized by steric hindrance from bulky side chains (and electrostatic repulsion between backbone carbonyls and π clouds of side chain aromatic rings).[55] Repeat units with different types of side chains have been shown as helical conformation promoting residues, all of which possess the bulkiness in the side chain with chiral centers (Figure 1.5).[56-59] The steric hindrance from side chains makes the backbone favor the *cis* configuration, which promotes helix formation. Studies by Kirshenbaum *et al.* further show that different side chains lead to different *cis/trans* ratios of the backbone configuration, and a higher ratio is likely related to more persistent (stiffer) helical chains.[58-59] Design rules regarding sequence and chain length of making stable helical secondary structures are also established.[55, 60-61] Further, the polypeptoid helices are highly dynamic, which is distinctly different from the rod-like peptide α-helix. This is an important feature of polypeptoid helices and is further studied in Chapter 2.

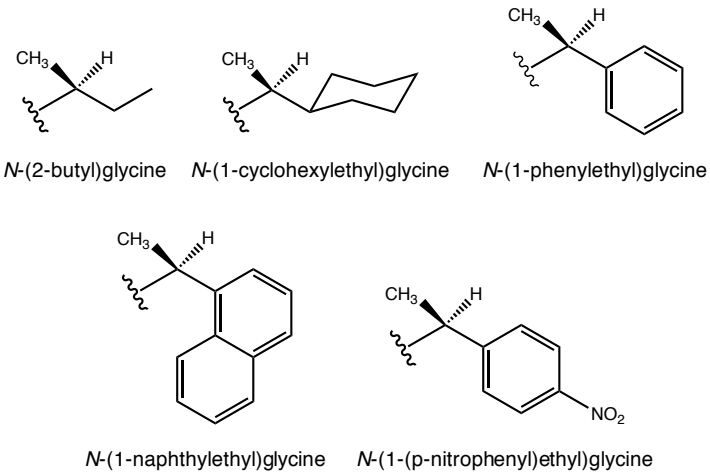

Figure 1.5 Side chains promoting helical conformation in polypeptoids

Other types of secondary structures including ribbons, square-helices have been observed for polypeptoid chains in solution.[62-63] Further modifications have also been attempted to the peptoid backbone to make N/C_α-substituted peptoid analogues. These peptide/peptoid hybrid chains are more rigid, but are synthetically very challenging to access long chains.[64] The large library of side chain chemistry, together with precise sequence control and high synthesis yields, make polypeptoids an ideal system to study design rules of hierarchical foldings, as well as investigate chain conformation effects in block copolymers.

1.3 Consideration of parameters for tuning block copolymer self-assembly

1.3.1 Common tunable parameters and scaling behaviors

There are a variety of strategies and parameters for tuning the self-assembly behavior of block copolymers: chain length (N) and molecular weight distribution (MWD), homopolymer blending, and architectural variations (multiblock, branched, star, miktoarm) etc. Here we constrict the discussion to strategies that do not alter the chemical identity of

constituent blocks and corresponding domains, as the chemistry of block copolymer materials oftentimes needs to be kept constant for specific chemical functionalities purposes.

Chain length is probably the first parameter studied and tuned for block copolymer self-assembly (except for volume fraction). Relationships between chain length/molecular weight (N) and the length scale of self-assembled structures are well established, with a scaling relation of the domain size $d \sim \chi^{1/6}N^{2/3}$ at strong segregation predicted by theoretical studies[65-66] and proved by experimental results.[67-68] The order–disorder transition of a symmetric linear diblock copolymer, is predicted to be at $\chi N = 10.5$ ($\chi N = 10.495 + 41.022\ N^{-1/3}$ when fluctuation effects are considered[69]).[3] Further, interfacial width (t) is shown to be independent of N, but has a scaling relation of $t \sim \chi^{-1/2}$ with respect to the Flory–Huggins interaction parameter.

Polydispersity is intrinsic for traditional synthetic polymers due to the statistical nature of polymerizations. For block copolymers prepared with living anionic polymerization, the molecule weight distributions are typically narrow, and the assumption of monodispersity works reasonably well for theoretic predictions. Nevertheless, as more synthetic methods are developed and block copolymers with broader molecular weight distribution (MWD) are commonly seen and used in commercial products, it is important to evaluate the effects of MWD on the phase behavior of block copolymers. In general, an increase in block polydispersity will bring the disordered melt closer to its spinodal (the order–disorder transition, ODT) at fixed segregation strength (χN), increase the domain periodicity and interfacial thickness relative to the monodisperse counterpart, and shift phase boundaries, as summarized in the review by Lynd and Hillmyer.[70] Many of the effects are attributed to the changes in entropy as a broader MWD favorably lowers the entropic penalty to stretch an

ensemble of chains. Furthermore, researchers are now able to control the shape of MWD via temporal regulation of initiation,[71-73] and the morphology, domain size and mechanical properties of block copolymers can be tuned correspondingly.[74-76] Homopolymer blending shares similar merit with increasing polydispersity in terms of changing the thermodynamics of self-assembly and therefore is abbreviated here to avoid repetition.

Beyond the simplest AB diblock copolymers, there are unlimited variety of different architectures for two-component block copolymers (e.g., ABA, ABAB…, AB_n). The phase diagrams of symmetric ABA triblock and infinite linear (ABAB…) multiblock copolymers are very similar to that of the AB diblock copolymer, while comb, miktoarm star block copolymers typically have phase boundaries deflected.[4, 77-78] The deflection of phase boundaries allows access to morphologies at extreme volume fractions, which could find useful application for thermoplastic elastomers with unique mechanical properties.[78-81]

1.3.2 Significance/Amplitude of chain conformation effects compared to other parameters

Compared to the aforementioned parameters, chain conformation is much less investigated and nowhere near a systematic understanding. This is partially due to the challenge to establish appropriate experimental systems, as well as the diversity and complexity chain conformation could possibly get. The conformational asymmetry parameter, ε, and the geometric asymmetry parameter, *v*, are examples of parameterizing chain conformation effects in coil–coil and rod–coil block copolymers, respectively. However, they are not likely to capture as well for chains with secondary structures and those accompanied by complex inter- and intra-molecular interactions.

Pure conformational effects are likely subtle compared to changes induced by polydispersity and architectural variations. For example, upon a symmetric polydispersity increase from 1 to 1.5, $(\chi N)_{ODT}$ changes approximately from 10.5 to 4 for symmetric diblock copolymers,[70] while the χN difference observed between block copolymers of different chain conformation is smaller than 1 in this dissertation. Chain length (N) is a less interesting parameter to tune as it mostly moves vertically along χN, while chain conformation provides the opportunity to explore wider phase space in both directions (χN, f) and beyond. Further, when polymer chain conformation is accompanied with other interactions (hydrogen-bonding, charge–charge interactions) or induces specific inter-chain packing, more drastic effects on self-assembly are expected.

Developing universalized rules to capture chain conformation effects will be challenging, yet understanding and predicting phase behaviors of block copolymers with complex chain conformations require much more progress as molecular designs are getting complicated with an unprecedented speed.

1.4 Motivation and dissertation outline

In this dissertation, sequence-defined polypeptoids are leveraged as conformational tunable polymer blocks to understand the effects of chain conformation on the thermodynamics of block copolymer self-assembly. Polypeptoids are unique at the crossover between synthetic and biological polymers, and integrated some of the important features of biopolymers (sequence control, monodispersity) and synthetic polymers (synthetic yield, chemical robustness). As molecular precision and perfection being the overarching considerations in the state of art of block copolymer design (the 50th anniversary perspective

on block copolymers[82]), polypeptoids come in as an ideal candidate to investigate some of the most fundamental questions, as have been demonstrated by previous studies on the effects of precise monomer composition and sequence.[83-86] The role of chain conformation in self-assembly has been a persistent topic in the block copolymer community, especially as more block types with various chain conformations are incorporated into block copolymers. Understanding how these non-classical polymer blocks impact the melt self-assembly and the underlying governing rules is critical to the design of next generation of block copolymer materials.

This dissertation studies polymer chain conformation, with the focus on the helical chain conformation and its role in block copolymer self-assembly, using polypeptoids as a block of tunable chain conformation. Chapter 2 comprises a study on the local stiffness, overall chain size, and responses to solvent quality of polypeptoid helical chains relative to their coil counterparts in dilute solution, providing a detailed understanding of the molecular characteristics of these sterically defined helical chains. Chapter 3 investigates the effects of helical chain conformation on the order–disorder transition and alteration of the Flory–Huggins interaction parameter (χ) in lamellae-forming block copolymer melts. Chapter 4 further explores the polypeptoids as a conformation tuning handle to study the role of chain conformation near the interface in accessing network phases (the double gyroid phase) in block copolymers. Chapter 5 summarizes the major conclusions of this work and provides perspectives on the future challenges and opportunities. The appendix includes the development of a block copolymer system with imidazole-bearing polypeptoids, for studying precise ion placement on ion aggregation, self-assembly, and ionic conductivity in block copolymers.

1.5 Permissions

Parts of this dissertation were reproduced in part with permissions from:

1. Yu, B.; Danielsen, S. P. O.; Yang, K.-C.; Ho, R.-M.; Walker, L. M.; Segalman, R. A., Insensitivity of Sterically Defined Helical Chain Conformations to Solvent Quality in Dilute Solution. *ACS Macro Lett.* **2020,** *9* (6), 849-854. Copyright 2020 American Chemical Society.
2. Yu, B.; Danielsen, S. P. O.; Patterson, A. L.; Davidson, E. C.; Segalman, R. A., Effects of Helical Chain Shape on Lamellae-Forming Block Copolymer Self-Assembly. *Macromolecules* **2019,** *52* (6), 2560-2568. Copyright 2019 American Chemical Society.
3. Yu, B.; Li, R.; Segalman, R. A., Tuning the Double Gyroid Phase Window in Block Copolymers via Polymer Chain Conformation Near the Interface. *Submitted to Macromolecules.* Copyright 2021 American Chemical Society.

Chapter 2

Insensitivity of Sterically Defined Helical Chain Conformation to Solvent Quality in Dilute Solution

2.1 Abstract

The interplay between polymer–polymer and polymer–solvent interactions as well as interactions that impose secondary structures determines the conformation of polymer chains in dilute solution. Polypeptoids–poly(*N*-substituted glycine)s have been shown to form helical secondary structures primarily driven by steric interactions from chiral, bulky side chains, while polypeptoids with a racemic mixture of the same side chains lead to unstructured coil chains with a shorter Kuhn length. Small-angle neutron scattering (SANS)

of the polypeptoids in dilute solution reveals that the helical polypeptoids are only locally stiffer than the coil chains formed from the racemic analogue, but exhibit overall flexibility. We show that chain conformations of both helical and coil polypeptoids (in terms of radius of gyration, R_g) are insensitive to solvent quality (parameterized by the second virial coefficient, A_2). Potential effects from the bulky, chiral/racemic side chains dominating chain conformations are excluded by comparison with an achiral polypeptoid lacking side chain chirality. The specific interactions between polypeptoid segments are likely dominating the chain conformations in this type of polypeptoids as opposed to polymer–solvent interactions or energetic contributions from the helical secondary structure.

2.2 Introduction

Polymer chains, whose conformations in dilute solution are determined by the balance of enthalpic interactions due to contacts with self or solvents, entropic interactions from chain stretching, as well as chain connectivity, deviate from ideal chain conformations depending on the quality of the suspending solvent.[35, 44, 87] Polymer chain conformation in dilute solution is critical in dictating properties ranging from solution viscosity[25, 88] to solubility[49] and light scattering[89]. While traditional scaling theories and protein crystallization clearly occupy opposite ends of a spectrum of possibilities from completely random chain trajectories to trajectories entirely dictated by specific and designed interactions, the ability to predict and understand chain conformations between these extremes under different conditions is critical for the future development of functional polymer solutions. For polymers containing secondary structures, the chain conformations are dictated by interactions (intra-chain interactions or polymer–solvent interactions) that stabilize the

secondary structures. These interactions may depend sensitively on solvent conditions, leading to altered chain conformations as in the cases of polypeptides altering their secondary structures upon solution pH change,[43, 90] and synthetic helical polymers–poly(2-oxazoline)s, exhibiting unique temperature dependence of helicity in hydrogen-bonding solvents.[49] In sterically defined helical polymers, the driving force comes from the steric hindrance of side groups, which contrasts with those specific interactions that are highly dependent on external conditions, and it raises questions on how sensitive the driving force is to solvent conditions. Nevertheless, the helical secondary structure alters the chain trajectory and possibly also affects the polymer–solvent interactions compared to chemically identical coil polymers. The chain trajectory of the helical chain differs from an unstructured coil chain because the monomers are arranged along the helical contour; thus, the correlation between monomers is substantially different from that in a coil chain. Additionally, the entropic penalty from chain stretching is also likely to change with the presence of the helical secondary structure. It is not clear how these contributions from the sterically defined helical secondary structure impact the chain conformation and its response to solvent quality compared with the coil analogues (Figure 2.1).

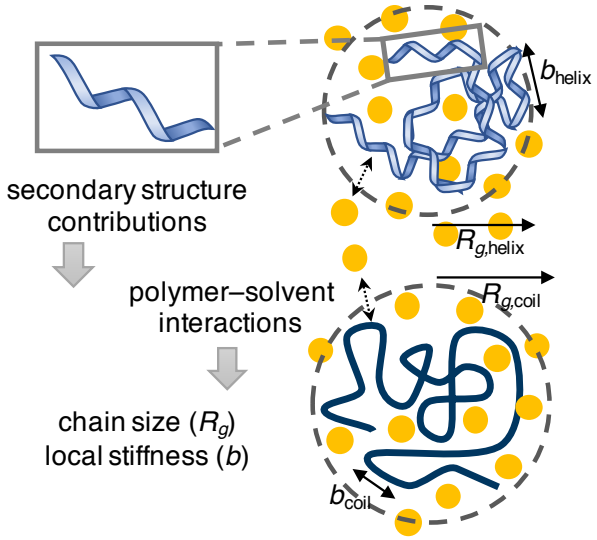

Figure 2.1 A schematic overview of the questions addressed within the study
Effects of polymer–solvent interactions and contributions from the helical secondary structure on polymer chain conformations are examined. The Kuhn length of the helical chain (b_{helix}) is defined over the helical contour, as opposed to the coil chain Kuhn length (b_{coil}) defined over the chain contour.

Helices are a common secondary structure in both synthetic and biopolymers. Helical polymers can be relatively stiff, rod-like helices such as poly(hexyl isocyanate),[91-92] or have relatively flexible helical secondary structures, where the helix persists over length scales that are much shorter than the helical contour length.[93] Here, polypeptoids–poly(*N*-substituted glycine)s, which are capable of folding to well-defined, repetitive helical secondary structures, are used to investigate the chain conformations of helical polymers in dilute solution.[56, 58-59] Unlike helical secondary structures in biological macromolecules, which are usually induced by charge–charge or hydrogen-bonding interactions, helices in polypeptoid systems are primarily driven by steric interactions. Polypeptoids used in this work are designed to form either a helical secondary structure or an unstructured coil, depending on the chirality of the side chains (chiral or racemic) (Figure 2.2).[60] This class of

polypeptoids forms a polyproline I-type helix with 3 residues per turn and a helical pitch ~ 6 Å, which has been confirmed by circular dichroism and 2D NMR.[56, 94]

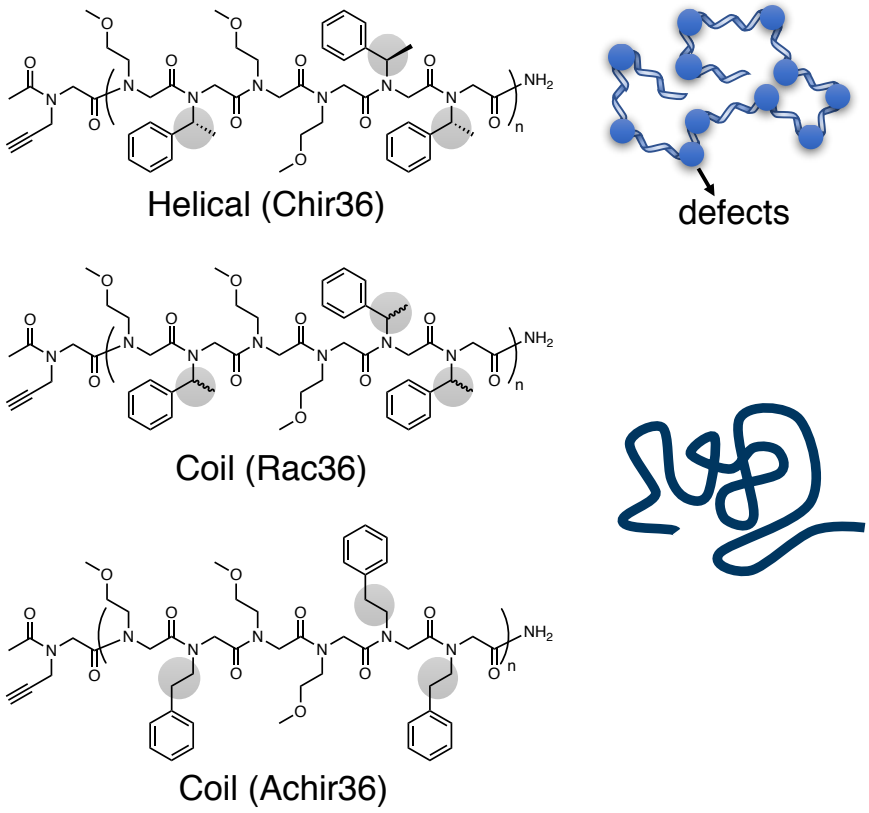

Figure 2.2 Molecular structure and chain shape of polypeptoids
Chiral, bulky side chains with the same chirality induce helix formation in Chir36, while a racemic mixture of the same side chains or chemically analogous achiral side chains result in unstructured coil chains in Rac36 and Achir36. Chir36 is a flexible helical chain made of jointed helix segments due to defects (shown as filled blue circles) along the chain. Number of repeat units, n = 6, and number of residues, m = 36.

The helical polypeptoids have been shown to be flexible (i.e., the helical chain is made of jointed helix segments rather than one stiff helix) in a marginal solvent acetonitrile, with a larger helical persistence length than the chemically identical coil chains.[24] The flexibility comes from the defects along the chain, which likely form due to some residues adopting *trans* backbone configuration that interrupt the helical turns, whereas the *cis* configuration

promotes helix formation.[56, 59] In polypeptoids with α-chiral, aromatic side chains, helices are primarily stabilized by steric hindrance from the bulky side chains (as well as electrostatic repulsion between backbone carbonyls and π clouds of aromatic rings).[55, 95] Due to the absence of hydrogen-bonding and other specific interactions such as charge–charge interactions, these polypeptoids serve as a simple model system to compare the response of chain conformations of chemically identical helical and coil polymers to solvent condition changes. This also sheds light on the melt chain conformations of these sterically defined helical polypeptoids, which have been incorporated into block copolymers that exhibited different chain packing and thermal stability of the self-assembled structure in bulk.[26, 96]

2.3 Experimental section

2.3.1 Materials

Solvents and reagents were purchased from commercial suppliers and used without further purification, unless otherwise noted. HPLC-grade acetonitrile (ACN), tetrahydrofuran (THF), acetone (ACE), and *N*,*N*-dimethylformamide (DMF) were used for static light scattering measurements. Deuterated solvents (ACN-*d*3, THF-*d*8, ACE-*d*6, DMF-*d*7) were purchased from Cambridge Isotope Laboratories, Inc., and used for small-angle neutron scattering measurements.

2.3.2 Synthesis and purification of polypeptoids

Polypeptoids were synthesized on a custom robotic synthesizer using commercially available amine submonomers. Rink amide resin (100-200 mesh, Novabiochem) with intermediate loading (~ 0.50 mmol g^{-1}) was used. Rink amide resin was first swelled in DMF

for 10 min, and deprotected twice with 4-methylpiperidine (68 equiv., 20 % v/v in DMF). Bromoacetylation: bromoacetic acid (12 equiv., 0.6 M in DMF) and diisopropylcarbodiimide (DIC, 12.5 equiv., 59 % v/v in DMF) were added and mixed for 20 min. Nucleophilic displacement: Amine (methoxyethylamine, ((*R*)-(+)-α-methylbenzylamine, phenylethylamine, or propargylamine, 16 equiv., 1 M in DMF) was added and mixed for 1 h. For the Chir36 and Rac36 sequences with chiral aromatic side chains, bromoacetylation steps were performed twice to enable high yields of the desired product. For the Npe36 sequence, 1.5 h displacement step was used for the second half of the repeat units to improve reaction efficiency. The resin was washed with DMF between each synthetic step. The chain end was finally acetylated with equimolar acetic anhydride and pyridine (11.4 equiv., 0.4 M in DMF) for 30 min, washed with DMF, then dichloromethane (DCM), and dried with nitrogen flow.

Polypeptoids were cleaved from the resin using a trifluoroacetic acid (TFA) cleavage cocktail (DCM: TFA (4:1, v/v) with another 2.5 % HPLC grade H_2O) for 10 min. The resin was filtered and rinsed with more cleavage cocktail and then DCM twice. The collected solution was dried *in vacuo* and lyophilized from ACN : H_2O (1:1, v/v) solutions to yield white powders. The crude product was then dissolved in ACN at a 10 mg mL^{-1} concentration. H_2O was added until the product started to precipitate, and another 20 % v/v H_2O was added to enable sufficient precipitation of the desired product. Precipitates were collected and lyophilized from ACN : H_2O (1:1, v/v) solutions to yield white powders of purified product.

2.3.3 Ultrahigh-pressure liquid chromatography mass spectrometry (UPLC-MS).

UPLC-MS was performed on a Waters Xevo G2-XS, equipped with a time-of-flight mass spectrometer. Polypeptoid samples were dissolved at ~ 0.5 mg mL^{-1} in ACN : H_2O (1:1, v/v)

mixtures (with 0.1 % formic acid). Separation was achieved on a Waters BEH C18 column with eluent gradients changing from 50 % ACN/50 % H_2O to 100 % ACN over 10 min. Polypeptoid materials were detected by UV absorption at 214 nm, and charged polypeptoid species were detected in the mass spectrometer (Figure 2.3).

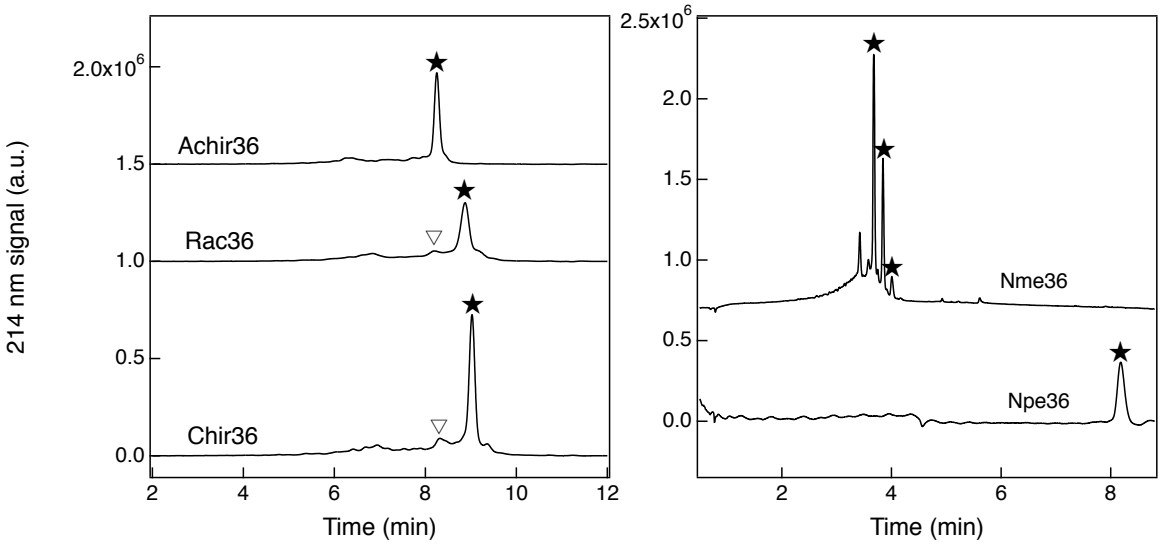

Figure 2.3 UPLC traces of polypeptoid 36-mers
Polypeptoids were detected by UV absorption at 214 nm, and charged polypeptoid species were detected in the mass spectrometer. Chir36, Rac36, and Achir36 (main product peak labeled with ★) have the same chemical formula and a molecular weight of 5128.2 g mol^{-1} (theoretical m/z: 5126.73 (100 %), 5127.74 (90.6 %), …). For Chir36 and Rac36, peaks labeled with ▽ before the main product peak are peaks of 36-mers with one methylbenzyl side chain (104 g mol^{-1}) cleaved off (m/z: 5022.67 (100 %)). Nme36: 4203.8 g mol^{-1} (theoretical m/z: 4202.3 (100 %), 4203.3 (97.9 %), …), and all three peaks labeled with ★ are target product but with different types of charges, therefore eluded at different times; Npe36: 5862.4 g mol^{-1} (theoretical m/z: 5861.1 (100 %), 5862.1 (94.8 %),…).

2.3.4 Circular dichroism (CD)

CD measurements were performed on a J-1500 CD spectrometer. Polypeptoid solutions were prepared at a concentration of 0.1 mg mL^{-1}, and CD spectra of the solutions were collected using quartz cells (Starna Cells) with a 1 mm path length. A scan speed of 200 nm min^{-1} was used, and 5 measurements were averaged for each sample. Vibrational circular

dichroism (VCD) measurements were performed on a JASCO FVS-6000 VCD spectrometer. Polypeptoid solutions were prepared at a concentration of 26 mg mL^{-1}, and VCD spectra of the solutions were collected using liquid cells with a 0.5 mm path length. A resolution of 4 cm^{-1} min^{-1} was used, and 4000 accumulations were averaged for each sample.

2.3.5 Static light scattering (SLS)

For each polypeptoid–solvent pair, ~ 300–500 mg polypeptoids were dissolved in double filtered solvent and sonicated for 30 min. The solution was then filtered twice (filtered with Teflon filter with 0.2 μm pores) to remove dust particles and transferred to volumetric flask to make a 10 mL solution. The solution was then transferred to a 20 mL scintillation vial for SLS measurements. Volumetric flasks and scintillation vials used were rinsed with double filtered solvent and dried in an oven. SLS measurements were taken on a Brookhaven BI-200SM light scattering instrument with a HeNe diode laser at 532 nm. The sample cell was equilibrated for 15 min in a Decalin bath with temperature set to 20 °C before the measurements were taken. The solution was diluted to another 5 lower concentrations to get averaged scattering light intensity at angles of 90°, 105°, 120°, 135°. The second virial coefficient, A_2, was extracted from the slope of $Kc/R \sim c$ (Figure 2.3). After SLS measurements, the solution was dried on a EZ-2 Genevac (SP Scientific) and materials were lyophilized from ACN : H_2O (1:1, v/v) solutions to determine the actual solution concentration used for SLS. Refractive index increments were determined using a Waters e2695 GPC equipped with a 2414 refractive index detector. The flow cell in the RI detector was purged with corresponding solvents before injection of samples. For each polypeptoid–solvent pair, 3 concentrations were prepared and each injected with injection volumes of 10,

20, 30, 40 μL. Polystyrene (in THF and DMF) and poly(methyl methacrylate) (in ACN and ACE) solutions were measured in the same way to determine the calibration constant for the RI detector to give the correct refractive index increment (*dn*/*dc*) value for each polypeptoid–solvent pair (Table 2.1).

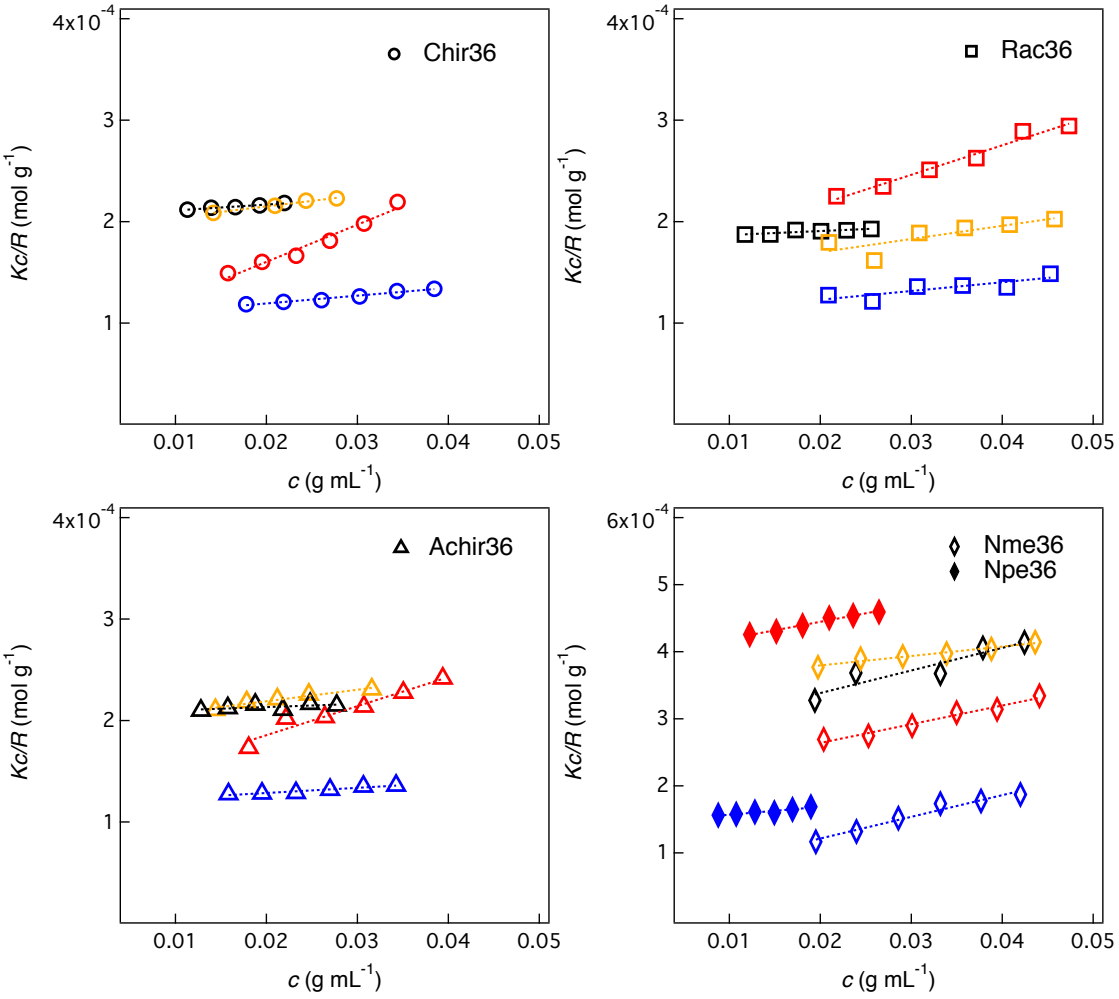

Figure 2.4 SLS of polypeptoids in different solvents
The scattering intensity showed minimal angular dependence as these polypeptoids are relatively small, therefore averaged values of intensity at angles of 90°, 105°, 120°, 135° were used to calculate *Kc*/*R* (symbols: black-ACN, blue-THF, yellow-ACE, red-DMF).

Table 2.1. Refractive index increment (*dn/dc*) of each polymer–solvent pair

polymer–solvent pair		*dn/dc* (mL g^{-1})	polymer–solvent pair		*dn/dc* (mL g^{-1})
THF	PS	0.185	ACE	PMMA	0.134
	Chir36	0.129 ± 0.006		Chir36	0.206 ± 0.007
	Rac36	0.131 ± 0.006		Rac36	0.199 ± 0.011
	Achir36	0.131 ± 0.006		Achir36	0.204 ± 0.010
	Nme36	0.090 ± 0.009		Nme36	0.163 ± 0.010
	Npe36	0.141 ± 0.013		Npe36	/
DMF	PS	0.159	ACN	PMMA	0.137
	Chir36	0.113 ± 0.001		Chir36	0.196 ± 0.018
	Rac36	0.112 ± 0.004		Rac36	0.193 ± 0.020
	Achir36	0.106 ± 0.005		Achir36	0.190 ± 0.016
	Nme36	0.068 ± 0.009		Nme36	0.160 ± 0.016
	Npe36	0.177 ± 0.017		Npe36	/

dn/dc values for PS–THF and PS–DMF: reference 97, PMMA–ACE and PMMA–ACN: reference 98.

2.3.6 Small-angle neutron scattering (SANS)

SANS studies were conducted at the extended Q-range small-angle neutron scattering diffractometer line (EQ-SANS BL-6) at the Spallation Neutron Source (SNS) at Oak Ridge National Laboratory (ORNL). Samples were prepared at a concentration of 20 mg mL^{-1} in deuterated solvents (ACN-*d*3, THF-*d*8, ACE-*d*6, DMF-*d*7) to enhance contrast between the polypeptoids and the solvents. Solutions were sonicated for 30 min and sit overnight to allow sufficient dissolution. Quartz banjo cells with a path length of 2 mm were used in a multiple position sample holder with temperature set to 20 °C. 3 different configurations of sample-to-detector distance and neutron wavelength (4 m-2.5 Å, 1.3 m-2.5 Å, and 1.3 m-1 Å) were used. Data reduction followed standard procedures implemented in MantidPlot.[99] The measured

intensity was corrected for detector sensitivity and the scattering contributions from the solvent and empty cells, and calibrated to an absolute scale using a Porasil B standard.[100]

2.3.7 SANS data fitting

SANS data fitting was carried out in the SasView software, using the flexible cylinder model with excluded volume. The chain model is a parametrization of simulations of discrete representation of the wormlike chain model of Kratky and Porod applied in the pseudocontinuous limit with original equations developed by Pedersen and Schurtenberger and the corrected formula was used.[101-102]

The total scattering function of a wormlike chain is given by

$$I_{WLC}(q, L_C, b, R) = \frac{cM}{\rho N_{Av}} \Delta\rho^2 S_{WLC}(q, L_C, b) P_{CS}(q, R) + I_{inc}$$

where c is the concentration, M is the molecular weight of the polymer, ρ is the mass density, N_{av} is Avogadro's number, Δρ is the scattering length density difference between the polymer and the solvent, L_C is the contour length, b is the Kuhn length, R is the radius of the cylinder, I_{inc} is the incoherent background scattering. The scattering function from the cross section of a rigid rod is given by

$$P_{CS}(q, R) = \left(\frac{2J_1(qR)}{qR}\right)^2$$

where $J_1(x)$ denotes the Bessel function of the first kind. S_{WLC} (q, L_C, b) is the scattering function of single semiflexible chain with excluded volume effects and is given by

$$S_{WLC}(q, L_C, b) = \left[1 - w\left(qR_g\right)\right] S_{Debye}(q, L_C, b)$$
$$+ w\left(qR_g\right)\left[1.22\left(qR_g\right)^{-1/0.585} + 0.4288\left(qR_g\right)^{-2/0.585}\right.$$
$$\left. - 1.651\left(qR_g\right)^{-3/0.585}\right]$$
$$+ \frac{C(n_b)}{n_b}\left\{\frac{4}{15} + \frac{7}{15u} - \left(\frac{11}{15} + \frac{7}{15u}\right) \times exp[-u(q, L_C, b)]\right\}$$

where

$$S_{Debye}(q, L_C, b) = \frac{2}{u(q, L_C, b)}\{exp[-u(q, L_C, b)] + u(q, L_C, b) - 1\}$$

$$u(q, L_C, b) = \frac{L_C b}{6}\left\{1 - \frac{3}{2n_b} + \frac{3}{2{n_b}^2} - \frac{3}{4{n_b}^3}[1 - exp(-2n_b)]\right\} q^2$$

$$n_b = \frac{L_C}{b}$$

$$w(x) = \frac{\{1 + tanh[(x - 1.523)/0.1477]\}}{2}$$

$$\langle {R_g}^2 \rangle = \alpha(n_b)^2 \frac{L_C b}{6}$$

$$u(q, L_C, b) = \alpha(n_b)^2 q^2 \frac{L_C b}{6}$$

$$\alpha(x) = \sqrt{\left[1 + \left(\frac{x}{3.12}\right)^2 + \left(\frac{x}{8.67}\right)^3\right]^{0.176/3}}$$

$$C(n_b) = \begin{cases} 3.06{n_b}^{-0.44} & for\ L_C > 10b \\ 1 & for\ L_C \leq 10b \end{cases}$$

Fitting parameters include scale, background, contour length (L_C), Kuhn length (b) and radius (R). In particular, the contour lengths were estimated based on the *cis/trans* ratio of polypeptoid backbone configurations, where an all *trans* polypeptoid 36-mer will have a contour length of ~13.9 nm, and an all *cis* polypeptoid 36-mer will have a contour length of

~11 nm.[103] For the helical polypeptoids, the backbone preferentially adopts *cis* configuration in the helical geometry with 3 residues per turn and a helical pitch ~ 6 Å, and the overall *cis/trans* ration is ~ 3.3.[56, 59-60] This gives a helix contour length for the helical polypeptoids ($L_{C,\text{helix}}$) of ~ 8.7 nm and the fitting range for $L_{C,\text{helix}}$ is set to 7.2–10.5 nm. For the coil polypeptoids, a 1:1 *cis*/*trans* ratio is estimated as the isomerization energy is relatively low for residues with these types of side chains,[104] which then gives a chain contour length ($L_{C,\text{coil}}$) of ~ 12.4 nm and the fitting range for $L_{C,\text{coil}}$ is set to 11–13.9 nm. The fitting range for Kuhn length (b) is set to 1–3 nm. Fitting results are presented in Figure 2.5 and Table 2.2.

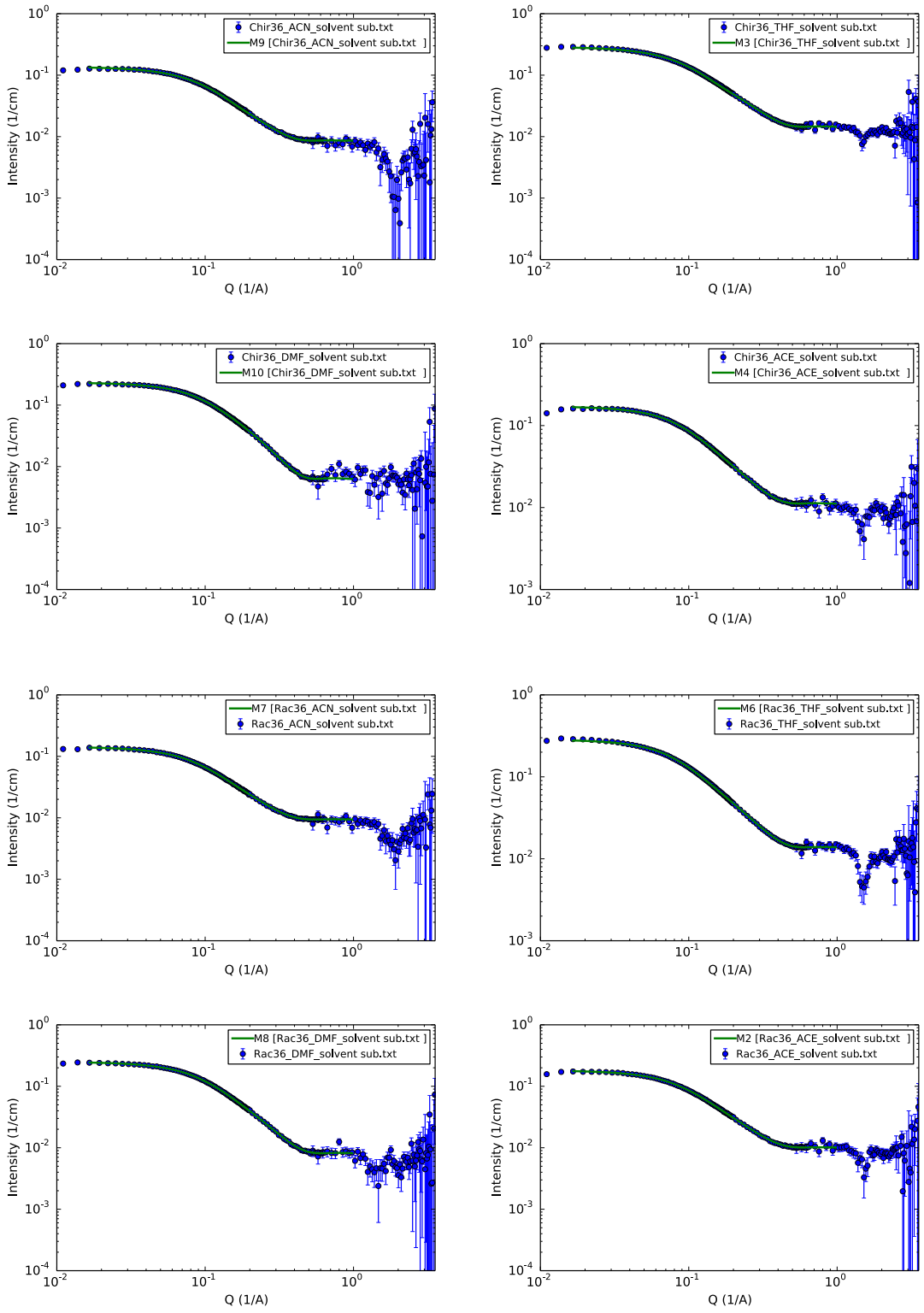

Figure 2.5 SANS data fitting in SasView
SANS data were fit to the flexible cylinder model with excluded volume in SasView.

Table 2.2 Fitting results (L_C, b, R, chi^2) and calculated radius of gyration, R_g

	Solvent	L_C (nm)	b (nm)	R^* (nm)	Chi^2	R_g (nm)
Chir36	ACN	8.75 ± 0.24	2.27 ± 0.12	0.73	1.45	1.14 ± 0.04
	THF	8.72 ± 0.08	2.57 ± 0.05	0.65	6.80	1.20 ± 0.02
	ACE	8.86 ± 0.33	1.89 ± 0.13	0.70	1.17	1.07 ± 0.05
	DMF	8.68 ± 0.25	1.79 ± 0.10	0.69	1.19	1.04 ± 0.04
Rac36	ACN	12.81 ± 0.59	1.21 ± 0.09	0.70	0.99	1.17 ± 0.06
	THF	9.78 ± 0.18	2.00 ± 0.07	0.65	5.83	1.17 ± 0.03
	ACE	12.30 ± 0.15	1.23 ± 0.00	0.65	1.44	1.15 ± 0.01
	DMF	11.80 ± 0.11	1.18 ± 0.00	0.64	1.22	1.10 ± 0.01

*Radius (R) has negligible errors from the fitting, therefore errors of R are not listed.

2.4 Polypeptoid helical conformation persists across different solvents

The polypeptoids with chiral, bulky side chains of identical chirality (Chir36) display characteristic circular dichroism (CD) spectra that correspond to the repeating helical secondary structure adopted by the polypeptoid chains in solution. A distinct peak at 220–225 nm (from the $n \rightarrow \pi^*$ amplification[43, 55]) is observed in the range of solvents–tetrahydrofuran (THF), acetone (ACE), acetonitrile (ACN) examined, while the coil polypeptoids (Rac36) do not give any peaks associated with a secondary structure (Figure 2.6a). For the fourth solvent used in this study, dimethylformamide (DMF), the wavelength range of interest (180–220 nm) is below the solvent cutoff (DMF absorbance cutoff: ~267 nm), thus no characteristic peaks could be observed in the CD spectrum to confirm the helical conformations of Chir36 in DMF. Nevertheless, these polypeptoid helices are designed to be stable with a length of 36 residues and 50 % of α-chiral, aromatic side chains, including one placed at the C-terminus. The helical secondary structure has been shown to be stable across a wide range of solvents and at elevated temperatures.[55, 60, 105] In the present

system, there is no obvious interactions associating the solvent molecules with the polypeptoid chains in dilute solution. Further, with molecular volumes of solvents (diameter ~ 5.5–6.3 Å) comparable to the helical pitch of Chir36 (~ 6 Å), the solvent molecules are unlikely to reside in between helical turns. Therefore, the local conformation on the length scale within a helix segment is defined by the chemical structure of the polypeptoids and is unlikely to vary with solvent conditions, while the conformation on the whole-chain length scale can still vary with solvent conditions.

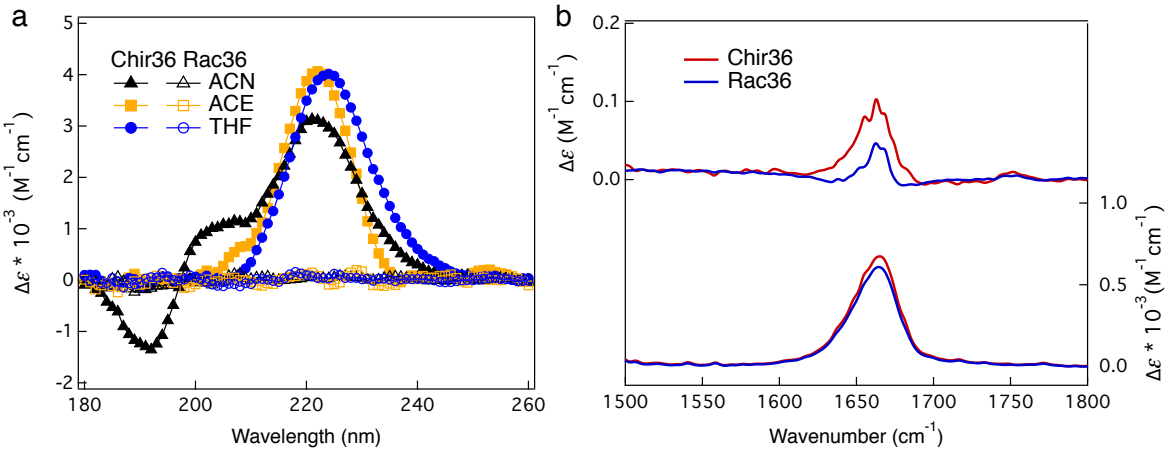

Figure 2.6 CD and VCD spectra of helical and coil polypeptoids in solution
a) Circular dichroism (CD) spectra of helical (Chir36) and coil (Rac36) polypeptoids in tetrahydrofuran (THF), acetone (ACE) and acetonitrile (ACN). The peak around 220–225 nm from $n \rightarrow \pi^*$ amplification is observed for the helical polypeptoids in all three solvents, indicating the existence of a helical secondary structure. The coil polypeptoids do not show characteristic peaks associated with a secondary structure. b) Vibrational circular dichroism (VCD) spectra and corresponding FT-IR absorption spectra of Chir36 and Rac36 in dilute solution of *d*-chloroform. The positive VCD signal at 1665 cm^{-1} (C=O stretching motions, perpendicular to the main-chain) indicates a helical conformation adopted by the polypeptoid backbone.

Polypeptoid backbone helical conformation is further confirmed with vibrational circular dichroism (VCD), which probes the vibrational coupling between two chromophores.[106] Cotton effects with a positive VCD band at 1665 cm^{-1} are found, corresponding to the

characteristic absorption of the C=O stretching motions, which are perpendicular to the main-chain and can be used to represent a helical conformation adopted by the polypeptoid backbone (Figure 2.6b). Furthermore, the coil polypeptoids (Rac36) also show similar positive Cotton effects, but with much lower intensity. This slight positive VCD signal is attributed to the non-equal population between *cis* and *trans* backbone configurations, where neighboring glycine units both adopting *cis* configuration will have a rotation angle between neighboring C=O bonds, leading to a net VCD signal. The stronger signal at 1665 cm^{-1} observed for Chir36 indicates a preferential helical conformation adopted by the polypeptoid backbone, in consistent with previous studies on this type of polypeptoids.[55, 60]

2.5 Chain conformation response to solvent quality variations

For sterically defined helical polypeptoids, the helical secondary structure changes chain trajectory, chain stretching penalty, and the joints/defects between helix segments can also be stabilized differently depending on solvent conditions. With these possible energetic contributions from the helical secondary structure, we further examine the chain conformation change of chemically identically helical and coil polypeptoids as a function of solvent quality on the whole-chain length scale, where the chain conformations are parameterized by radius of gyration (R_g, measured *via* small-angle neutron scattering, SANS) and solvent quality is parameterized by the second virial coefficient (A_2, determined *via* static light scattering, SLS).

Both helical and coil polypeptoids show a polymer coil characteristic of the scattering intensity $I(q)$, without features present from the helical secondary structure due to the small characteristic length scales of the helix segment (i.e., helical pitch, radius) expected only at

higher q, where the incoherent scattering dominates (Figure 2.7a). In each solvent, the absolute intensity in the low-q region of the helical polypeptoids is consistently lower than that of the coil polypeptoids. Recall that both polypeptoids should have the same scattering length density (SLD) since they are chemically identical; therefore, the smaller low-q intensity of the helical polypeptoids indicates a higher density than the coil analogue, which likely results from a more compact packing of monomers imposed by the helical secondary structure (Figure 2.8). In the Guinier regime, the radius of gyration, R_g, of polypeptoids in different solvents can be extracted without *a priori* knowledge of chain shapes (Figure 2.7b, results are summarized in Table 2.3).

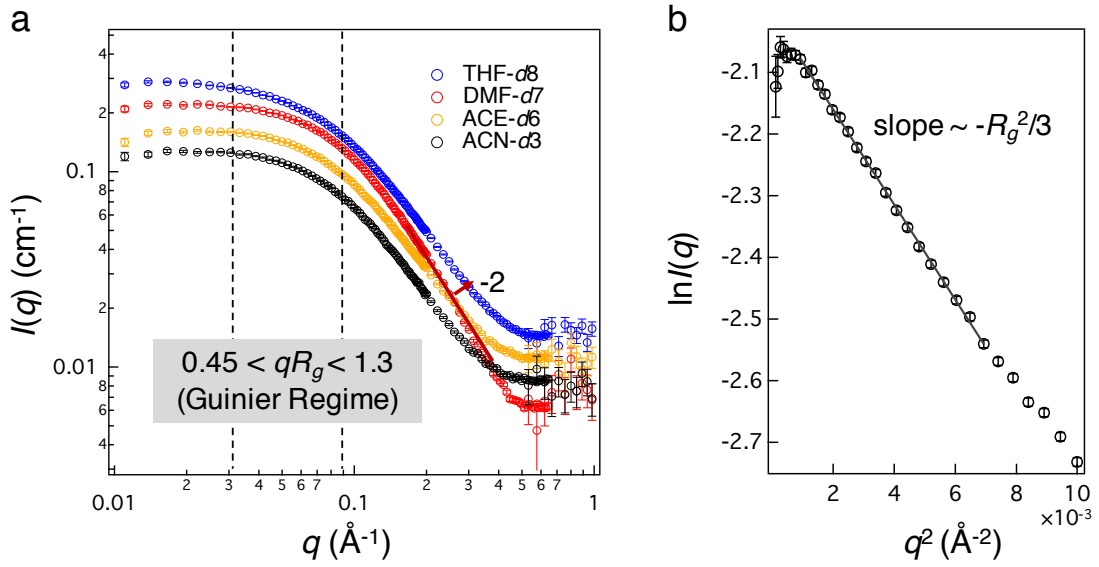

Figure 2.7 SANS of helical polypeptoids in dilute solution and R_g determination
a) Representative SANS data (solvent background subtracted) of the helical polypeptoids (Chir36) in dilute solutions of tetrahydrofuran-*d*8 (THF-*d*8), dimethylformamide-*d*7 (DMF-*d*7), acetone-*d*6 (ACE-*d*6), and acetonitrile-*d*3 (ACN-*d*3). The region between dashed vertical lines at low q is the Guinier regime where the size of polymer chains can be obtained without any assumption of the chain shape. b) An example of the Guinier plot of Chir36 in ACN-*d*3. The radius of gyration, R_g, is determined from the slope of ln $I(q)$ *vs.* q^2.

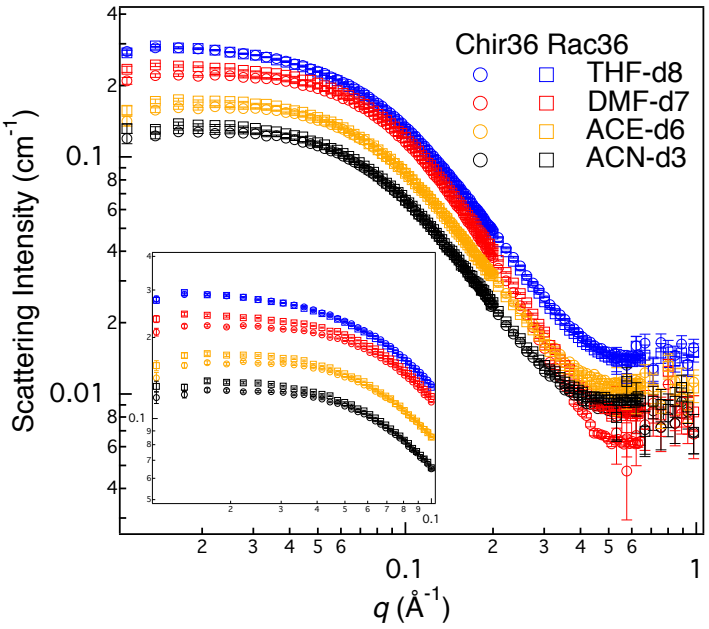

Figure 2.8 Scattering intensity comparison of helical and coil polypeptoids
The inset shows the low q region comparison, where the scattering intensity of the helical polypeptoids (Chir36) is consistently lower than the chemically identical coil polypeptoids (Rac36) under the same dilute solution conditions, indicating the helical polypeptoids have a higher density.

Table 2.3 A_2 and R_g of the polypeptoids in dilute solutions

	Chir36 (helical)	Rac36 (coil)	Achir36 (coil)
	$A_2 \times 10^3$ (cm^3 mol g^{-2})		
ACN	0.29 ± 0.09	0.20 ± 0.09	0.16 ± 0.12
THF	0.39 ± 0.07	0.43 ± 0.17	0.26 ± 0.06
ACE	0.55 ± 0.08	0.65 ± 0.30	0.57 ± 0.13
DMF	1.83 ± 0.21	1.46 ± 0.22	1.43 ± 0.31
	R_g (Å)		
ACN	15.22 ± 0.08	15.76 ± 0.07	15.75 ± 0.08
THF	16.07 ± 0.05	16.43 ± 0.05	16.63 ± 0.05
ACE	14.94 ± 0.06	15.63 ± 0.06	15.38 ± 0.06
DMF	14.79 ± 0.05	15.02 ± 0.05	14.79 ± 0.05

Second virial coefficient, A_2, of different polypeptoid–solvent pairs, determined by static light scattering (SLS), and radius of gyration, R_g, of the polypeptoids in the corresponding deuterated solvents, determined by small-angle neutron scattering (SANS), at 20 °C.

In all cases, the polypeptoids consisting of chiral monomers with the same chirality (which show CD spectra indicating helicity) have a more compact chain conformation (smaller R_g) than the racemic analogue in any given solvent (Table 2.3). Although solvent quality, which reflects excluded volume interactions in dilute solution, is expected to depend on polymer chain shapes,[107] here the solvent quality (as indicated by A_2) does not show explicit chain shape dependence. When accounting for the difference in A_2 between the analogues, both polypeptoids show only a very weak dependence of R_g on A_2 (Figure 2.9a), in contrast to the usual swelling of flexible unstructured polymers in dilute solution with a better solvent. R_g of these polypeptoids is also insensitive to temperature in the range from 10 °C to 40 °C. The relative constant chain size of the coil polypeptoids (Rac36) can be rationalized that the overall chain size is approximately equal or smaller than the thermal blob size ξ_T (Table 2.4), therefore the excluded volume interactions are weaker than the thermal energy k_BT and the changes in the excluded volume induced by solvent condition variations have negligible effects on chain size. However, even with the helical secondary structure imposed along the chain, the helical polypeptoids do not show obvious chain conformation dependence on solvent quality and behave similarly to the coil polypeptoids in terms of R_g, which indicates the contributions from the helical secondary structure to chain conformation are negligible or do not depend strongly on solvent quality.

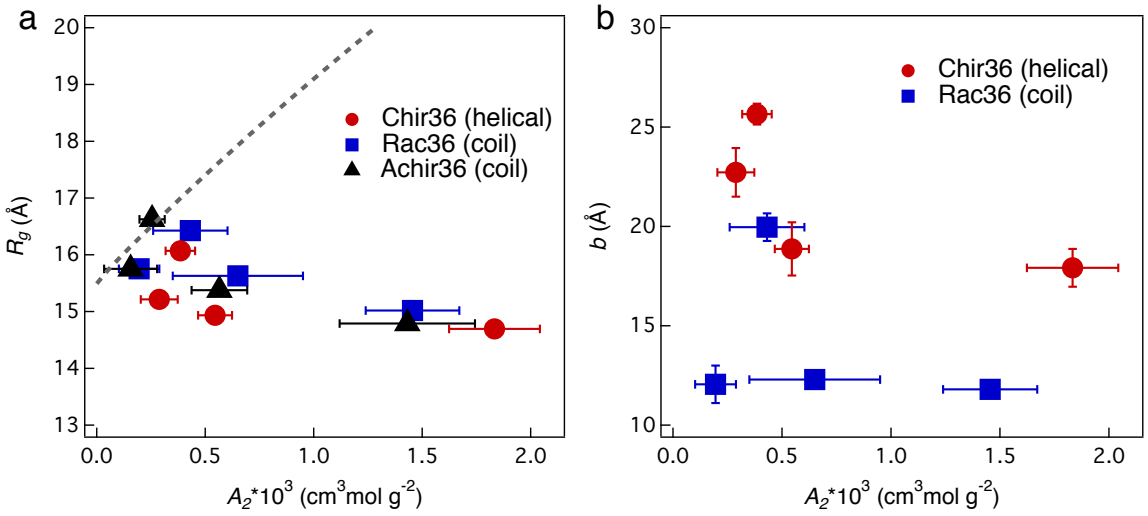

Figure 2.9 Overall chain size and local chain stiffness as a function of solvent quality a) Chain conformation variations of the helical (Chir36) and coil polypeptoids (Rac36 and Achir36) in dilute solution shown in terms of radius of gyration, R_g, as a function of solvent quality, parameterized by the second virial coefficient, A_2. The dashed line represents the swelling of a polymer chain with similar flexibility and molecular weight if it follows the universal swelling behavior.[108-109] All polypeptoids show a very weak dependence of R_g on A_2. b) Kuhn lengths of the helical (b_{helix}) and coil (b_{coil}) polypeptoids in dilute solution as a function of A_2.

Table 2.4 Thermal blob calculations

	Solvent	$A_2 \times 10^3$ (cm^3 mol g^{-2})	z	v (nm^3)	ξ_T (nm)	g_T
Chir36	ACN	0.288	0.142	1.69	15.68	47.7
	THF	0.385	0.159	2.92	14.93	33.8
	ACE	0.545	0.347	2.17	5.89	9.7
	DMF	1.833	1.307	6.81	1.51	0.7
Rac36	ACN	0.195	0.140	0.15	14.10	135.8
	THF	0.431	0.218	1.57	10.16	25.8
	ACE	0.650	0.483	0.57	4.03	10.7
	DMF	1.455	1.223	1.27	1.53	1.7

Calculations are based on scaling approaches in Rubinstein and Colby's.[35] z, chain interaction parameter, v, excluded volume of a Kuhn monomer, ξ_T, thermal blob size, g_T, number of monomers in a thermal blob.

Considering both polypeptoids have chiral centers in their side chains (Chir36 with chiral side chains of identical chirality, Rac36 with racemic side chains), the bulky side chains may make the polymer chains less susceptible to solvent conditions and therefore lead to the observed consistent trend of chain size as a function of solvent quality. To test the potential effects due to monomer chirality, another unstructured coil polypeptoid (Achir36) is examined, which lacks side chain chirality but has otherwise identical composition to the Chir36 and Rac36 materials. The coil polypeptoids (Achir36) in the above solvents also show similar trend of R_g as a function of solvent quality A_2 (Figure 2.9a). Therefore, potential effects from solvents impacting the chiral centers in the side chains and thus dominating chain conformation changes are excluded in this case. Nevertheless, it is obvious that the chain conformations of polypeptoids with chiral centers are different in DMF than in other solvents, which are more coil-like, as indicated by the porod scaling exponent (close to -2, whereas -1 corresponds to a rod-like chain). However, this change in chain shape in DMF only occurs for polypeptoids with a chiral center (Chir36 and Rac36) while not in the case of the achiral polypeptoids, Achir36 (Figure 2.10). The relationship between solvent quality for the copolypeptoids studied above (recall Chir36, Rac36 and Achir36 consist of two types of monomers with a specific sequence) and the corresponding homopolypeptoids (Nme36 and Npe36) is further investigated. The calculated second virial coefficient ($A_{2,\text{calc}}$) based on $A_{2,\text{homo}}$s ($A_{2,\text{Nme36}}$, $A_{2,\text{Npe36}}$) and the weight fractions of monomers does not match the measured solvent quality ($A_{2,\text{measured}}$) for the copolypeptoids (Table 2.5). This discrepancy observed in A_2s implies that by having two different components, there likely exist extra attractive/repulsive interactions between the unlike monomers, but the expected changes

from these extra interactions (i.e., more swelled chains in DMF than in THF) are not observed.

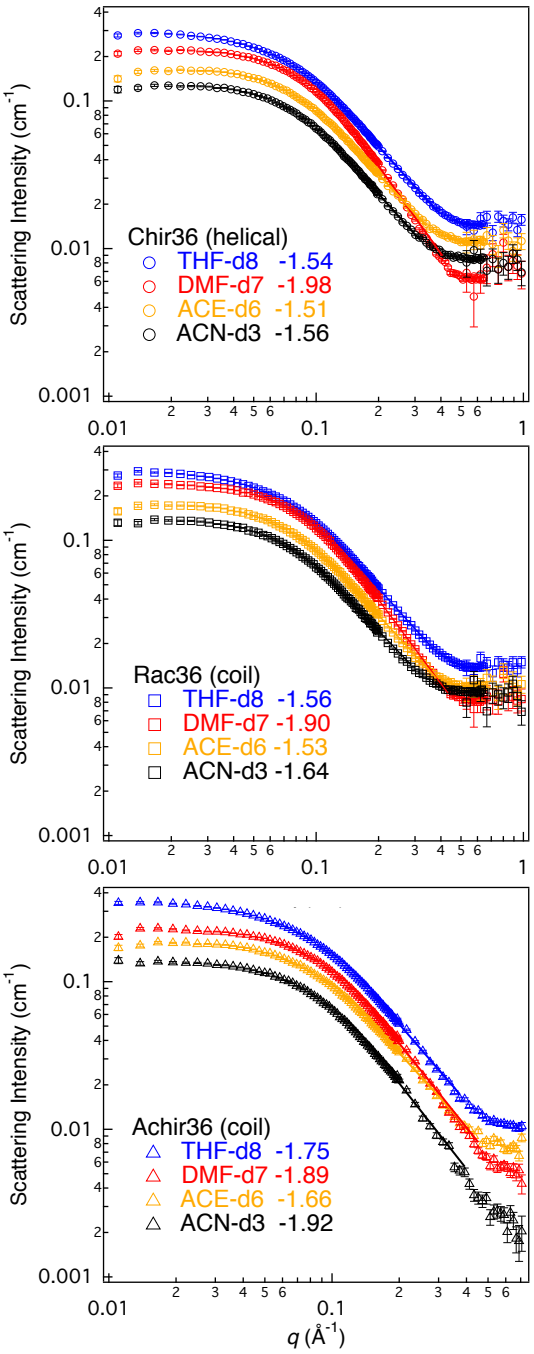

Figure 2.10 Porod scaling exponents of polypeptoids in dilute solutions

Table 2.5 A_2 of Achir36 and its corresponding homopolypeptoids (Nme36, Npe36)

Solvent	Second virial coefficient, $A_2 \times 10^3$ (cm^3 mol g^{-2})			
	$A_{2,\text{Nme36}}$	$A_{2,\text{Npe36}}$	$A_{2,\text{Achir36\_calc}}$	$A_{2,\text{Achir36\_measured}}$
ACN	1.68 ± 0.72	Insoluble	/	0.16 ± 0.12
THF	1.62 ± 0.48	0.58 ± 0.21	1.02 ± 0.52	0.26 ± 0.06
ACE	1.20 ± 0.22	Insoluble	/	0.57 ± 0.13
DMF	1.40 ± 0.48	1.27 ± 0.34	1.32 ± 0.59	1.43 ± 0.31

The homopolypeptoids with all chiral/racemic side chains are not synthetically accessible. Here, solvent quality for corresponding homopolypeptoids of Achir36 (i.e., Nme36 and Npe36) were examined. The calculated second virial coefficient assumes a linear dependence of A_2 on monomer weight fractions.

Recall that the helical polypeptoids are made of jointed helices, where the defects make the joints between helix segments, imparting flexibility of the helical chains. The Kuhn lengths of helical and coil chains (b_{helix} and b_{coil}, where the former characterizes the distance over which the helical contour loses persistence) were extracted by fitting a flexible cylinder model with excluded volume interactions to the SANS data, using Kuhn length b as one of the fitting parameters.[101-102] Local chain stiffness of the helical chains (b_{helix}) appears to have a stronger dependence on the solvent quality–more defective helical chains (i.e., smaller b_{helix}) in a better solvent (larger A_2). However, the local chain stiffness of the coil chains (b_{coil}) does not show explicit dependence on solvent quality (Figure 2.9b). The radius of gyration, R_g, calculated based on the wormlike chain model fits is nearly constant as A_2 changes (Table 2.2), which is in consistent with the results obtained from the Guinier analysis. This in turn, indicates that, defect stabilization is not likely the major contributing factor to the overall chain size change of the helical polypeptoids in dilute solution, as both helical and coil polypeptoids show very weak R_g dependence on A_2.

2.6 Conclusions

In this work, comparison between chemically identical helical and coil polypeptoids in dilute solution demonstrates that the helical chains (with secondary structure driven by steric interactions from chiral, bulky side chains) are locally stiffer, but have more compact chain conformations than the coil chains formed from the racemic or achiral analogues. Nevertheless, for all polypeptoids in dilute solution, solvent quality does not show dominant effects on the chain conformations in terms of radius of gyration, R_g, which is almost constant as solvent quality (A_2) changes. For the sterically defined helical chains, there is no specific interactions associating solvent molecules with the polymer chains, and the solvent molecule sizes are comparable to the helical pitch; thus, the local conformation on the length scale within a helix segment is unlikely to change, while the conformation on the whole-chain length scale can still vary with solvent conditions. These helical chains, with local chain trajectories defined by helical turns but overall random walk statistics of the jointed helix segments, are an intermediate scenario of polymers with completely random to entirely dictated chain trajectories. From this study, the contributions from the sterically defined helical secondary structure to polymer chain conformations appear to be either negligible or do not depend strongly on solvent quality. We suspect that the consistent trend of chain size dependence on solvent quality is due to the dominating interactions between polypeptoid segments as opposed to interactions imposed by the helical secondary structure or polymer–solvent interactions. These sterically defined helical chains also provide insights on the rational design of polymer chains with stable secondary structures that are insensitive to the surrounding environments.

2.7 Acknowledgements

The authors gratefully acknowledge funding from the National Science Foundation (NSF) Division of Materials Research (DMR) Polymers program (DMR-1608297). This research used resources at the Spallation Neutron Source, a DOE Office of Science User Facility operated by the Oak Ridge National Laboratory. Polymer characterization was performed with support from the MRL Shared Experimental Facilities (supported by the MRSEC Program of the NSF under Award DMR-1720256; a member of the NSF-funded Materials Research Facilities Network). The authors thank Dr. Changwoo Do at the Spallation Neutron Source for assistance with SANS experiments, Dr. Tuan Nguyen at UCSB for assistance with static light scattering measurements, Dr. Rachel Behrens at the UCSB MRL for help with polymer characterization, and Dr. Ron Zuckermann for helpful discussions regarding polypeptoid synthesis.

Chapter 3

Effects of Helical Chain Shape on Lamellae-Forming Block Copolymer Self-Assembly

3.1 Abstract

Understanding the effects of non-ideal polymer chain shapes on block copolymer self-assembly is important for designing functional materials, such as biopolymers or conjugated polymers, with controlled self-assembly behavior. While helical chain shapes in block copolymers have been shown to produce unique morphologies, the details of how chain helicity influences the thermodynamics of self-assembly are still unclear. Here, we utilize model coil–coil and coil–helix block copolymers based on polypeptoids, for which the chain

shape can be tuned from helix to coil via monomer chirality with otherwise constant chemistry. This model block copolymer system is used to probe the effects of chain helicity on the thermodynamics of block copolymer self-assembly. Small-angle X-ray scattering of the bulk materials shows that the block copolymers form well-ordered lamellar structures. While having identical domain spacing, the coil–helix block copolymer displays a lower order–disorder transition temperature (T_{ODT}) than its coil–coil analogue. The coil–helix block copolymer is found to have a smaller enthalpic contribution to mixing, supported by a smaller effective Flory–Huggins interaction parameter (χ_{eff}) determined in the disordered state. Furthermore, the helical block of the coil–helix block copolymer experiences larger chain stretching penalties in the lamellar morphology, which leads to a larger entropic gain upon disordering. The combined effects of the enthalpic and entropic contributions are likely to have lowered the T_{ODT} of the coil–helix block copolymer, yielding insight into the importance of different thermodynamic contributions that arise from polymer chains with non-ideal shapes in block copolymer self-assembly.

3.2 Introduction

In the canonical case of coil–coil block copolymers, the self-assembly behavior can be captured by the relatively simple trade-off between chain stretching and mixing at the interface.[1-2, 6, 82] In rod–coil block copolymers, the liquid crystalline interactions and geometric asymmetry significantly impact the self-assembly behavior.[19-20, 110-111] In both cases, space-filling characteristics and local stiffness of the chain impact the self-assembly. The intermediate regime—semiflexible polymers and chains with complex structures—is practically important, as many newly developed block copolymers have variation in local

chain stiffness and/or secondary structures that are central for their use as functional materials. However, understanding the deviations from ideal coil–coil block copolymer self-assembly behavior imposed by secondary chain structures can be challenging, because these complex chain shapes usually require particular chemistries and thus are unlikely to have a chemically analogous coil chain for comparison. Moreover, the frequent inclusion of multiple complicating factors (e.g., liquid crystalline interactions, hydrogen bonding, charge–charge interactions, etc.) adds even more complexity to deconvoluting the chain shape effects on self-assembly.

Among different chain shapes, helices are a particularly common shape in biopolymers and serve as an important structural motif for molecular functions.[112-114] Helices have also been formed in synthetic polymers through the introduction of chiral or steric interactions,[41, 92, 115-117] or isotacticity in semi-crystalline polymers such as isotactic polypropylene and isotactic poly(1-butene).[118-119] Synthetic helices are often used as model systems to understand the role of polymer helical chain shape in hierarchical systems; a few have been readily incorporated into block copolymers, where the helical chain shape was shown to significantly impact the self-assembled structures.[120-123] For example, polystyrene–poly(L-lactide) block copolymers with a helical poly(L-lactide) block self-assemble into a hexagonally-packed helical phase that is not observed in the corresponding achiral system in bulk.[32-33] However, with synthetic helical polymers that display crystallinity, crystallization can be a competing factor with the self-assembly process,[124] potentially concealing effects from the helical chain shape. Block copolymer systems that contain a helical block, but lack other complicating factors, are desirable to study effects of polymer helical chain shape on the self-assembly behavior.

Polypeptoids (*N*-substituted polyglycines) are a class of sequence defined materials, capable of folding to well-defined, repetitive secondary structures including helices.[56, 58-59] Polypeptoids have recently been shown to form highly ordered crystals; however, if appropriate monomers and monomer sequences are chosen, polypeptoids can be completely amorphous.[26, 125] The polypeptoid block used in this work is designed to be non-crystalline and forms either a helical secondary structure with homochiral, aromatic side chains, or an unstructured coil if a racemic mixture of the same side chains is incorporated (Figure 3.1).[55, 60] This polypeptoid helix is a polyproline I-type helix with *cis* bond conformations preferred by the backbone, confirmed via a combination of circular dichroism and 2D NMR.[56, 94] There are several important features to consider regarding the effects of this helical chain shape on the self-assembly of block copolymers: (1) The helical chain is locally stiffer, but overall is flexible rather than rod-like. It has a helical persistence length ($l_{p,\text{helix}}$, the distance over which the helical contour loses persistence–as opposed to chain persistence length) of approximately 1 nm in solution,[24, 26] which is much smaller than that of other synthetic polymer helices.[92] (2) When incorporated into block copolymers, the helical and coil polypeptoids will not contribute differently to the interaction parameter (χ) in terms of chemical identity. Nevertheless, the variations in local chain structure of the polypeptoids could cause changes to the interactions between dissimilar blocks, where the locally stiffer and more condensed helices are likely to prevent contacts between chains, potentially leading to a small decrease in the segregation strength (χN). (3) The polypeptoid helical chain is made of jointed helix segments: for a polypeptoid 60mer, there are approximately 12 helical segments (estimated based on $L_{C,\text{helix}}/l_{p,\text{helix}}$, $L_{C,\text{helix}}$ is the length of the helical contour); due to this jointed nature, the helical chain stretching is not like the longitudinal stretching of a

spring, but rather the helix segments rearranging to adopt extended configurations (it is speculated that the helical pitch and number of residues per turn stay constant). (4) The polypeptoids here do not crystallize so there is no competition between crystalline interactions and block copolymer interactions during self-assembly. This polypeptoid system also affords high synthetic yields at large scale via highly efficient solid-phase synthesis,[52] enabling bulk studies to probe the helical chain shape contributions to block copolymer self-assembly.

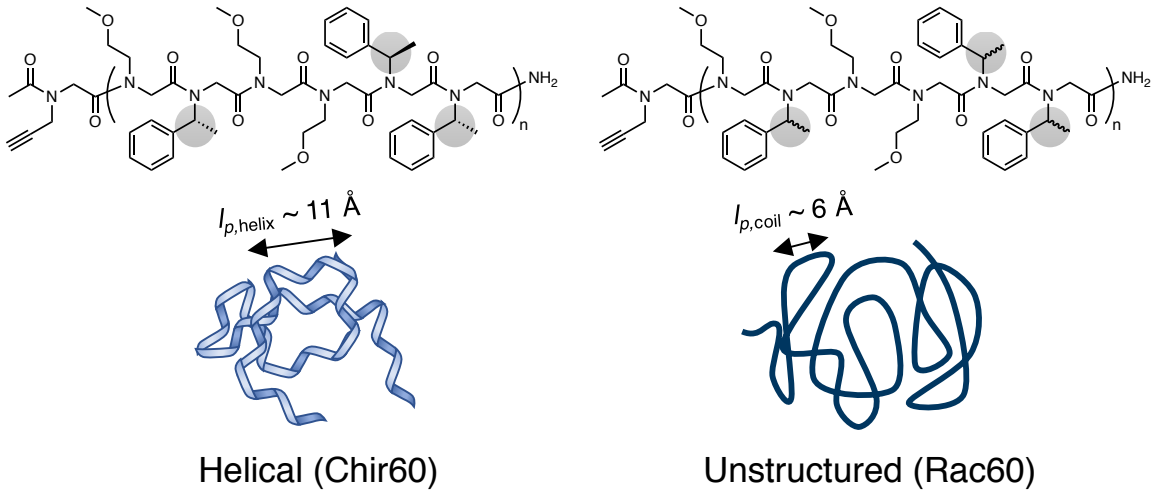

Figure 3.1. Molecular structure and chain shape of polypeptoid 60-mers
Incorporating homochiral, aromatic side chains with identical *R*-chirality induces helix formation (Chir60), while a racemic mixture of the same side groups generates an unstructured coil chain (Rac60). The helical chain has a helical persistence length ~ 11 Å, which is much longer than that of the coil chain ($l_{p,\text{coil}}$ ~ 6 Å). However, these two persistence lengths are qualitatively different as $l_{p,\text{helix}}$ is a correlation distance along the helical contour and $l_{p,\text{coil}}$ is a correlation distance along the polymer chain contour. Number of repeat units, n = 10, number of residues, m = 60.

This work demonstrates that polypeptoid-containing block copolymers, with tunable chain shape but lacking backbone chirality, hydrogen bonding and crystallinity, are an ideal system to probe the effects of chain helicity on block copolymer self-assembly. The poly(*n*-butyl acrylate)–polypeptoid (coil–coil and coil–helix) block copolymers display identical domain

spacings in the lamellar morphology, while the coil–helix block copolymer has a lower order–disorder transition temperature (T_{ODT}) than its coil–coil analogue. The coil–helix block copolymer is found to have a smaller enthalpic contribution to mixing, supported by a smaller effective Flory–Huggins interaction parameter (χ_{eff}), which is determined in the disordered state using a newly-derived correlation function for the helical chain. Furthermore, the helical block of the coil–helix block copolymer experiences larger chain stretching penalties in the lamellar morphology, which leads to a larger entropic gain upon disordering. Both the enthalpic and entropic factors contribute to lowering the T_{ODT} of the coil–helix block copolymer.

3.3 Experimental section

3.3.1 Materials

Solvents and reagents were purchased from commercial suppliers and used without further purification, unless otherwise noted. Anhydrous anisole, dimethylformamide (DMF), and *N*,*N*-diisopropylethylamine (DIPEA) were used for synthesis of poly(*n*-butyl acrylate) and block copolymers. HPLC-grade tetrahydrofuran (THF), acetonitrile (ACN), and water (H_2O) were used for precipitations and lyophilization.

3.3.2 Synthesis and purification of alkyne-terminated polypeptoids

Polypeptoids were synthesized on a custom robotic synthesizer using commercially available amine submonomers as described in 2.3.2. Rink amide resin (300 μm scale, Novabiochem) with 0.50 mmol g^{-1} loading was used. Bromoacetylation steps were performed twice to enable high yields of the desired product. An additional unit was added in

the same method with propargylamine to give the alkyne end group after the desired sequence. The chain end was finally acetylated as previously described. Polypeptoids were cleaved from the resin and purified as described in 2.3.2. Polypeptoid mass and purity were determined by UPLC-MS.

3.3.3 Synthesis of azide-terminated poly(n-butyl acrylate)

Bromine-terminated poly(*n*-butyl acrylate) was first synthesized via atom-transfer radical polymerization (ATRP). The initiator (methyl 2-bromo-propionate), solvent (anhydrous anisole), and catalyst (copper(I) bromide, Cu(I)Br) were used as received. Butyl acrylate monomer and ligand *N,N,N′,N′,N″*-pentamethyldiethylenetriamine (PMDETA) were filtered through basic alumina before use. In an oven-dried Schlenk flask, 0.128 mmol initiator, 0.048 mmol PMDETA, 0.048 mmol Cu(I)Br, 34.7 mmol butyl acrylate, and 2 mL anisole were combined. The reaction mixture was degassed by three freeze–pump–thaw cycles (to pressure < 100 mTorr) and reacted for 6 h at 80 °C under nitrogen. The viscous reaction mixture was diluted with THF, filtered through basic alumina to remove copper compounds, and then precipitated into cold methanol. The collected polymer was dried *in vacuo* overnight. The bromine-terminated poly(*n*-butyl acrylate) was dissolved in DMF (0.05 M concentration), and 1.5 molar equivalents of sodium azide was added. The reaction mixture was stirred for 24 h at room temperature. Three chloroform : water (1:1, v/v) extractions were performed for the reaction mixture to remove residual sodium azide. The organic layer was collected and dried *in vacuo* to yield a highly viscous liquid.

3.3.4 Synthesis of poly(n-butyl acrylate)–polypeptoid block copolymers

Alkyne-terminated polypeptoid (~130 mg, 2 equiv.) was combined with azide-terminated poly(*n*-butyl acrylate) (1 equiv.) and 2 mL anhydrous DMF in a capped vial. *N*,*N*-Diisopropylethylamine (DIPEA, 10 equiv.), PMDETA (5 equiv.), and ascorbic acid (6 equiv.) were added. The reaction mixture was sparged with nitrogen for 45 min. In an oven-dried Schlenk flask, Cu(I)Br (5 equiv.) was added, and the flask was evacuated and backfilled with nitrogen three times. The sparged reaction mixture was added to the Schlenk flask with a degassed syringe, and then further degassed with three freeze–pump–thaw cycles (to pressure < 100 mTorr). The reaction was allowed to react under static vacuum at 50 °C for approximately 40 h. The solution was then diluted with DMF and filtered through basic alumina to remove copper compounds. The solution was dried *in vacuo*, dissolved in THF (100 mg mL^{-1}), and precipitated twice into an ACN : H_2O (1:1, v/v) mixture to remove excess polypeptoid. The precipitate was isolated by centrifugation and dried *in vacuo* at 40 °C overnight.

3.3.5 Ultrahigh-pressure liquid chromatography mass spectrometry (UPLC-MS).

UPLC-MS was performed on a Waters Xevo G2-XS, equipped with a time-of-flight mass spectrometer. Polypeptoid samples were dissolved at ~ 0.5 mg mL^{-1} in ACN : H_2O (1:1, v/v) mixtures (with 0.1 % formic acid). Separation was achieved on a Waters BEH C18 column with eluent gradients changing from 50 % ACN/50 % H_2O to 100 % ACN over 10 min. Polypeptoid materials were detected by UV absorption at 214 nm. Charged polypeptoid species were detected in the mass spectrometer (Figure 3.2).

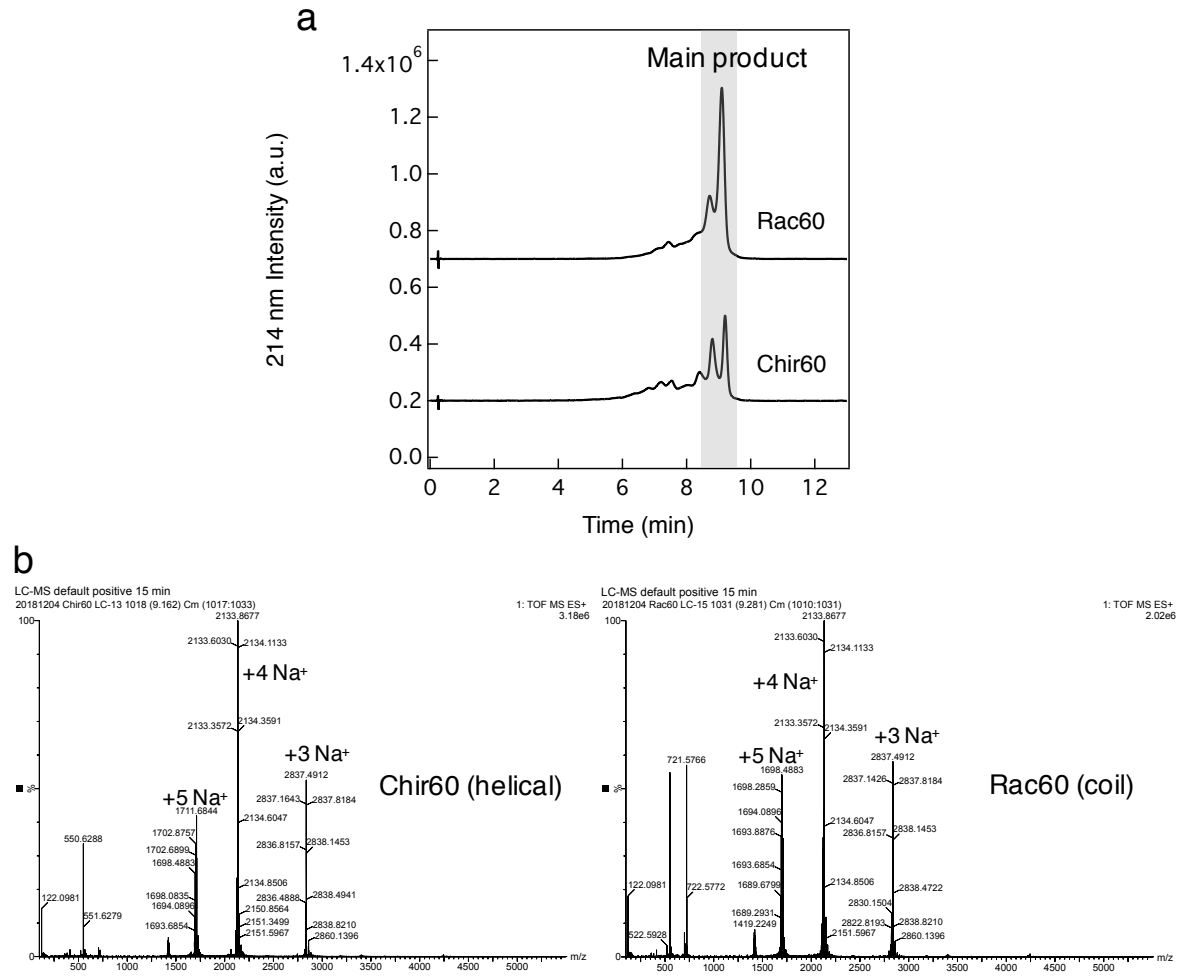

Figure 3.2 UPLC-MS of polypeptoids
a) Polypeptoids were detected by UV absorption at 214 nm. The first peak in the major product region is polypeptoid 60-mers with one methylbenzyl side chain cleaved off (Mw: 8338.6, full 60-mer Mw: 8443.5). The molar ratio of chains affected this way is 1 : 1 for Chir60 and 0.6 : 1 for Rac60. This defect does not appear to change the conformation of the polypeptoid chains nor the self-assembly behavior. Other minor impurities are shorter polypeptoid chains. b) Triply, quadruply, and quintuply charged polypeptoid species were detected in the mass spectrometer.

3.3.6 Gel permeation chromatography (GPC)

The molecular weight of poly(*n*-butyl acrylate) was measured on a Waters Alliance HPLC System with an e2695 Separation Module using an Agilent PLgel 5 μm MiniMIX-D column with THF as the eluent. Refractive index traces from a Waters 2414 differential

refractive index detector were used for molecular weight determination using polystyrene calibration standards (Agilent Technologies). GPC traces of poly(*n*-butyl acrylate), polypeptoids, and block copolymers were obtained in the same way and compared in Figure 3.3.

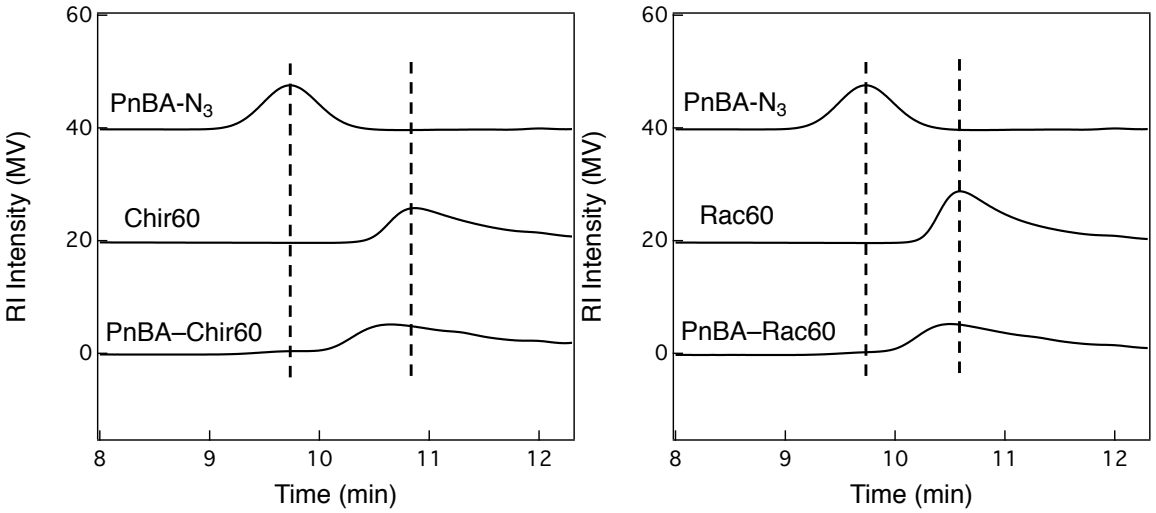

Figure 3.3 GPC of poly(*n*-butyl acrylate), polypeptoids, and block copolymers
The polypeptoids are monodisperse (as shown via UPLC-MS), but have broad peaks in GPC likely due to interactions with the column and therefore have a large and broadened retention time range. As a result, the block copolymers also have broadened GPC peaks due to the polypeptoid block interactions and the retention times of the block copolymers are in between PnBA and polypeptoid.

3.3.7 Circular Dichroism (CD)

CD measurements were performed on a J-1500 CD spectrometer. Polypeptoid and block copolymer solutions were prepared at a concentration of 0.1 mg mL^{-1} and 0.2 mg mL^{-1} in ACN, and CD spectra of the solutions were collected using quartz cells (Starna Cells) with a 1 mm path length. Solid-state samples for CD measurements were prepared by drop-casting polypeptoids and polypeptoid-containing block copolymers from THF solutions onto quartz

discs, dried in air, and then dried *in vacuo* overnight to remove residual solvent. A scan speed of 200 nm min^{-1} was used, and 5 measurements were averaged for each sample (Figure 3.4).

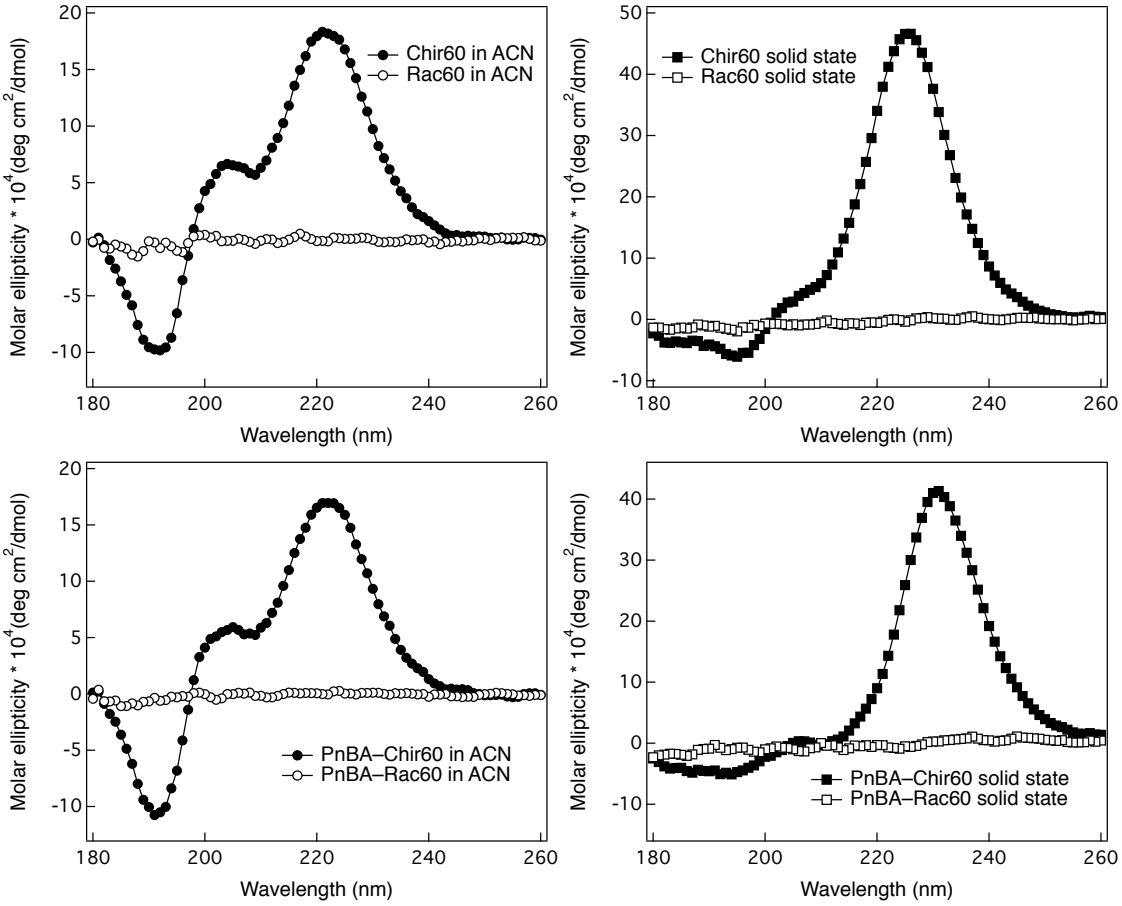

Figure 3.4 CD of polypeptoids and block copolymers in solution and in bulk
CD of polypeptoids (top row) and block copolymers (bottom row) in solution (acetonitrile) and in bulk (drop-casted film on quartz). The characteristic peaks at 190 nm, 205 nm, and 220 nm indicate the helical conformation adopted by polypeptoid chains.[60] Both polypeptoid (Chir60) and block copolymer (PnBA–Chir60) in solution and in bulk show corresponding characteristic peaks, indicating helical chain conformation persists in the solid state.

3.3.8 Small-angle X-ray scattering (SAXS)

Dry block copolymers were loaded into a Kapton lined aluminum washer. Samples were annealed at reduced pressure (4×10^{-8} Torr) at 170 °C for 24 h, slowly cooled to 110 °C, and

annealed at 110 °C for another 24 h. After cooling to room temperature under reduced pressure, the washers were sealed with Kapton under ambient conditions.

SAXS was performed at the Stanford Synchrotron Radiation Lightsource (SSRL, beamline 1-5, SLAC National Accelerator Laboratory) with an X-ray energy of 10 keV, and the National Synchrotron Light Source II (NSLS-II, beamline 11-BM, Brookhaven National Laboratory) with an X-ray energy of 13.5 keV. Peak positions and errors were determined by Gaussian-peak fitting. Order–disorder transitions (ODTs) of block copolymer materials were determined at SSRL, using a custom-built heat stage with temperatures measured at the sample positions to ensure accuracy. Samples were equilibrated for 5–10 min at each temperature (to an accuracy of $\pm$ 0.3 °C) before collecting exposures. Calibration using a silver behenate standard, circular averaging of the 2D scattering pattern, and correction for empty cell scattering were performed using the Nika package for Igor Pro.[126]

3.3.9 Random phase approximation (RPA) structure factors

In the disordered state of block copolymers, the connectivity of the two dissimilar blocks leads to a correlation hole effect that manifests as a broad peak proportional to the structure factor in scattering measurements.[2-3] The peak position and peak shape correspond to a fluctuation length scale related to the copolymer radius of gyration and the magnitude of the interaction parameter χ. The RPA structure factor for an incompressible melt of diblock copolymers is[3]

$$S(q) = \frac{N}{F(q) - 2\chi N} \tag{1}$$

with

$$F(q) = \frac{\hat{g}_{\mathrm{AA}} + 2\hat{g}_{\mathrm{AB}} + \hat{g}_{\mathrm{BB}}}{\hat{g}_{\mathrm{AA}}\hat{g}_{\mathrm{BB}} - \hat{g}_{\mathrm{AB}}{}^{2}} \tag{2}$$

where $\hat{g}_{\mathrm{AA}}, \hat{g}_{\mathrm{BB}}$ and $\hat{g}_{\mathrm{AB}}$ are the intra-block and inter-block correlation functions, respectively. The different chain shapes are incorporated into these correlation functions. Within each helical segment, the correlation is carefully captured by taking into account the details of the helical chain geometry, while the correlations on the length scale larger than a helical segment are calculated based on freely jointed chains (Figure 3.5). This model based on freely jointed chains is appropriate for these block copolymers because each block has an overall contour length much longer than the corresponding persistence length.

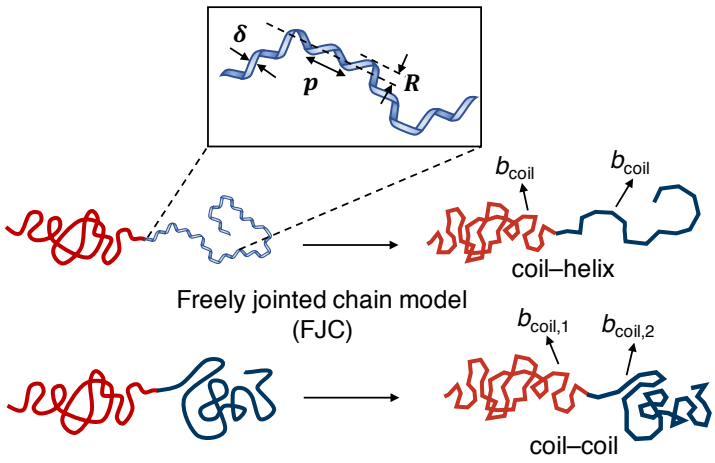

Figure 3.5 Schematic of chain models for coil–helix and coil–coil block copolymers
Chain models are based on the freely jointed chain model of *N* statistical segments of rod length *b*. The helical chain geometry is captured as freely jointed helix segments with radius, *R*, ribbon width, δ, and helical pitch, *p*.

The helical chain geometry is modeled as a freely jointed chain of helical ribbons,[127] where the helical segments have radius, *R*, ribbon width, δ, and helical pitch, *p*; the overall

chain is then composed of N helical segments of length b. The correlation function of this freely jointed chain of helical ribbons is

$$\hat{g}_{\mathrm{hFJC}} = \frac{1}{N\left[N + \frac{b}{p}\left(\frac{\delta}{2}\right)^2 - 1\right]}\left\{2\left[\frac{N-1}{1-j_0(bq)} - \frac{j_0(bq)\left(1-j_0^{N-1}(bq)\right)}{[1-j_0(bq)]^2}\right]\left(\frac{Si(bq)}{bq}\right)^2 + N\frac{b}{p}\sum_{-\infty}^{\infty} i^{2n}\int_0^{\pi/2} d\beta\, \frac{\sin^2\left(\frac{\delta}{2}q_z'\right)}{{q_z'}^2} J_n^2(q_\perp' R\sin\beta)\sin\beta\right\} \tag{3}$$

where $Si(x) = \int_0^x \frac{\sin t}{t} dt$ is the integral sine function, $j_0(x)$ is the zeroth-order spherical Bessel function of the first kind, $J_n(x)$ is the Bessel function of the first kind of order n, $q_z' = q_\perp \sin\beta + q_z \cos\beta = \sqrt{q^2 - n^2\pi^2/p^2}\sin\beta + (n\pi/p)\cos\beta$, and $q_\perp' = q_\perp \cos\beta - q_z \sin\beta = \sqrt{q^2 - n^2\pi^2/p^2}\cos\beta - (n\pi/p)\sin\beta$.

The coil blocks are modeled as freely jointed chains with the mass centered on the rods connecting the beads with an intra-block Debye-like correlator:[18]

$$\hat{g}_{\mathrm{FJC}} = \frac{1}{N} + \frac{2}{N^2}\sum_{i=1}^{N-1}(N-i)\,[j_0(bq)]^i\left(\frac{Si(bq)}{bq}\right) \tag{4}$$

where N is the number of statistical segments of length b in that block. Finally, the inter-block correlation function between two blocks of freely jointed chains, used for both coil–coil and coil–helix block copolymers, is

$$\hat{g}_{\mathrm{AB}} = \frac{1}{N_{\mathrm{A}}N_{\mathrm{B}}} \sum_{i=1}^{N_{\mathrm{A}}-1} \sum_{j=1}^{N_{\mathrm{B}}-1} [j_0(b_{\mathrm{A}}q)]^i j_0(\bar{b}q)[j_0(b_{\mathrm{B}}q)]^j \left(\frac{Si(b_{\mathrm{A}}q)}{b_{\mathrm{A}}q}\right)\left(\frac{Si(b_{\mathrm{B}}q)}{b_{\mathrm{B}}q}\right)$$

$$= \frac{j_0(\bar{b}q)}{N_{\mathrm{A}}N_{\mathrm{B}}} \left(\frac{[j_0(b_{\mathrm{A}}q)]^{N_{\mathrm{A}}} - 1}{j_0(b_{\mathrm{A}}q) - 1}\right)\left(\frac{[j_0(b_{\mathrm{B}}q)]^{N_{\mathrm{B}}} - 1}{j_0(b_{\mathrm{B}}q) - 1}\right)\left(\frac{Si(b_{\mathrm{A}}q)}{b_{\mathrm{A}}q}\right)\left(\frac{Si(b_{\mathrm{B}}q)}{b_{\mathrm{B}}q}\right) \quad (5)$$

where b_k is the statistical segment length of block k, and $\bar{b}$ is the length of the statistical segment connecting the A and B blocks, assumed to be the linear average of b_{A} and b_{B}. It should be noted that this neglects the local helical monomer arrangement when calculating inter-block correlations for simplicity; an assumption that is expected to be valid in this case of large N and $b >> R$.

This results in the RPA expressions for the Helical FJC (hFJC)–FJC and FJC–FJC structure factors applicable to the coil–helix and coil–coil block copolymers in the disordered state,

$$S_{\mathrm{hFJC\text{-}FJC}}(q) = \frac{N_{\mathrm{A}} + N_{\mathrm{B}}}{\left(\frac{\hat{g}_{\mathrm{hFJC}} + 2\hat{g}_{\mathrm{AB}} + \hat{g}_{\mathrm{FJC}}}{\hat{g}_{\mathrm{hFJC}}\hat{g}_{\mathrm{FJC}} - \hat{g}_{\mathrm{AB}}{}^2}\right) - 2\chi(N_{\mathrm{A}} + N_{\mathrm{B}})} \quad (6)$$

and

$$S_{\mathrm{FJC\text{-}FJC}}(q) = \frac{N_{\mathrm{A}} + N_{\mathrm{B}}}{\left(\frac{2\hat{g}_{\mathrm{FJC}} + 2\hat{g}_{\mathrm{AB}}}{\hat{g}_{\mathrm{FJC}}{}^2 - \hat{g}_{\mathrm{AB}}{}^2}\right) - 2\chi(N_{\mathrm{A}} + N_{\mathrm{B}})} \quad (7)$$

with block correlation functions as defined in Equations 3–5.

3.3.10 SAXS profile fitting to RPA structure factors

The SAXS profiles of the block copolymers at different temperatures above ODT were fit to the RPA structure factors incorporating the chain shape details (Equations 6–7). The number of statistical segments N for each block was calculated based on the molecular weights, densities of the poly(*n*-butyl acrylate) and polypeptoids, and a reference volume of 0.1 nm^3 (Table 3.1). The SAXS profile of the coil–coil block copolymer was first fit to the standard RPA diblock copolymer structure factor of Gaussian coils with asymmetric statistical segment lengths,[128] which gives b_{PnBA}, b_{Rac60}. The same SAXS profile of the coil–coil block copolymer was then fit to the FJC–FJC structure factor in Equation 7 using χ as an adjustable parameter—the peak position was fit exactly when the b_{PnBA} and b_{Rac60} values obtained from the continuous Gaussian chain version of the RPA structure factor fit were used. For the coil–helix block copolymer, the corresponding SAXS profile was fit to the helical FJC–FJC structure factor in Equation 6, where N_{PnBA} and N_{Chir60} used values as calculated, b_{PnBA} used the same value from the coil–coil analogue, $\delta \approx 6$ Å and $R \approx 2$ Å were estimated from the molecular structures,[56] p was set to the value of the helical pitch of a similar peptoid determined in solution,[94] and b_{Chir60} and χ were used as adjustable parameters to fit for the peak position and peak shape. The same fitting process was performed for the SAXS profiles of block copolymers at different temperatures (Figure 3.6). Statistical uncertainty of the fitted χ_{eff} was estimated by a sensitivity analysis of the fit (Table 3.2).

Table 3.1 Number of statistical segments *N* for each block

	M_n (g mol^{-1})	ρ (g cm^{-3})	N
poly(*n*-butyl acrylate)	8913	1.08	137
polypeptoid (Chir60/Rac60)	6444	1.18	119

Calculation is based on a reference volume of $v_0 = 0.1$ nm^3.

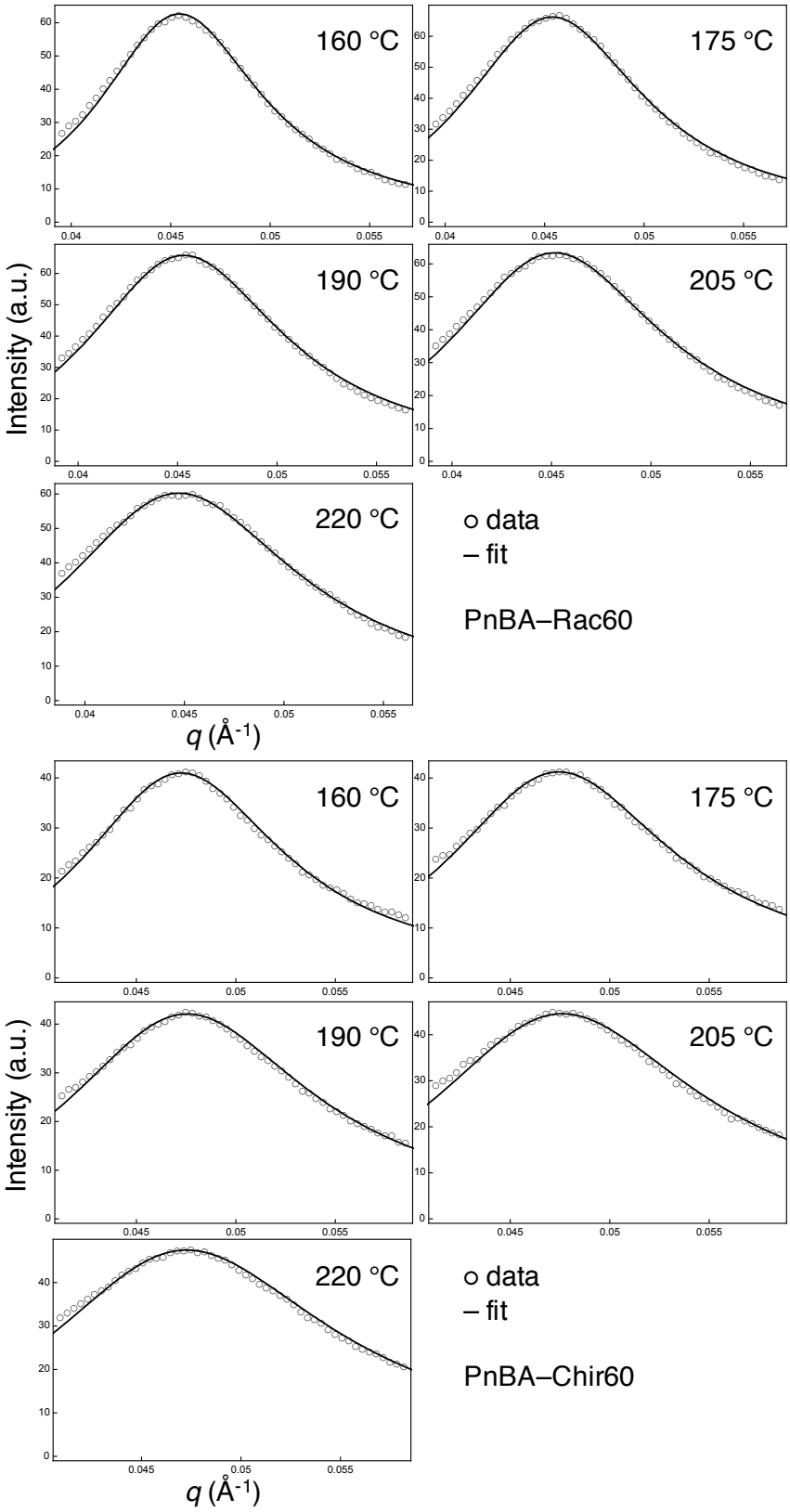

Figure 3.6 Fitting of SAXS profiles to RPA structure factors

Table 3.2 Summary of fitting results

Temp (°C)	PnBA–Chir60			PnBA–Rac60		
	b_{PnBA} (Å)	b_{Chir60} (Å)	χ_{eff}	b_{PnBA} (Å)	b_{Rac60} (Å)	χ_{eff}
160	6.41	6.37	0.00960 ± 0.00002/3	6.41	6.72	0.00996 ± 0.00001
175	6.42	6.30	0.00956 ± 0.00003/5	6.42	6.73	0.00992 ± 0.00001
190	6.43	6.25	0.00952 ± 0.00004	6.43	6.74	0.00988 ± 0.00002/1
205	6.45	6.20	0.00947 ± 0.00005/3	6.45	6.76	0.00984 ± 0.00001/2
220	6.51	6.23	0.00942 ± 0.00004/6	6.51	6.83	0.00978 ± 0.00002/3

To investigate the impact of helical chain shape on the thermodynamics of block copolymer self-assembly, model coil–helix and coil–coil block copolymers with identical monomer chemistries but different chain shapes were synthesized. With identical domain spacings in the lamellar morphology, the coil–helix block copolymer has a lower order–disorder transition temperature (T_{ODT}) than its coil–coil analogue. We examine the thermodynamic origins of the difference in the order–disorder transition (ODT) from two aspects—first, via the effects of the helical chain shape on the enthalpic contribution from contacts between dissimilar blocks, and second, the entropic contribution from chain stretching in the lamellar morphology. Both are found to be contributing factors to the difference in T_{ODT}.

3.4 Lamellar domain spacing and order–disorder transition (ODT)

To investigate how the helical chain shape impacts the thermodynamics driving segregation, we synthesized lamellar-forming coil–helix and coil–coil (poly(*n*-butyl acrylate)–polypeptoid) block copolymers with the same monomer chemistries. The lamellar morphology is targeted to eliminate packing frustrations, which were hypothesized to cause

the larger domain spacings of coil–helix block copolymers over coil–coil block copolymers in hexagonally-packed cylinders.[26] The model coil–helix and coil–coil block copolymers were synthesized with one block composed of a polypeptoid, for which the chain shape is tuned between helix and coil by altering the side chain chirality (Figure 3.1).[55, 60] The polypeptoids containing a precise number of monomers (m = 60) were incorporated into block copolymers with identical poly(n-butyl acrylate) blocks via an azide–alkyne cycloaddition reaction (Scheme 3.1). Thus, the obtained coil–helix and coil–coil block copolymers differ *only* in the shape of the polypeptoid block.

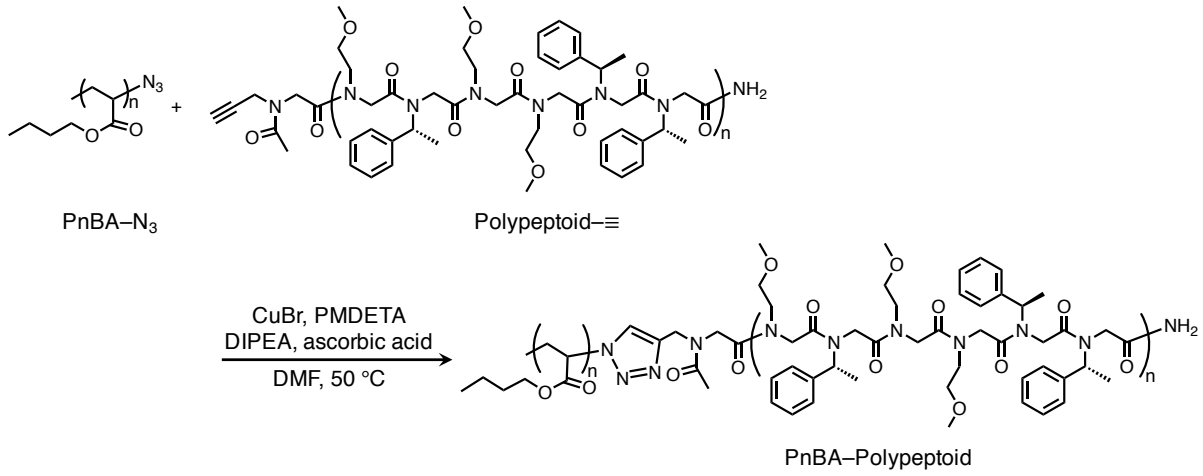

Scheme 3.1 Synthesis of poly(*n*-butyl acrylate)–polypeptoid block copolymers.

Both block copolymers ($f_{peptoid}$ = 0.46) formed well-ordered lamellar structures, indicated by the appearance of a sharp primary peak (q^*) and higher order reflections at $2q^*$ and $3q^*$ in SAXS patterns (Figure 3.7). The block copolymers display identical domain spacings of (13.5 ± 0.1) nm (Table 3.3), in contrast to the larger domain spacings observed in the coil–helix block copolymers ($f_{peptoid}$ ~ 0.3) adopting a hexagonally-packed cylinder morphology (~25 % larger than those of the coil–coil block copolymers).[26] Previously, the larger domain

spacings of the coil–helix block copolymers were attributed to the unfavorable packing interactions from the helical polypeptoid block in the confined cylindrical core. Packing frustrations are expected to be eliminated or minimized in the lamellar morphology; the identical domain spacing observed in the lamellar structures here (1) affirms that packing frustrations were the origin of the different domain spacings observed in the hexagonally-packed cylindrical morphology and (2) removes the role of packing frustrations from impacting the self-assembly of the coil–helix block copolymers.

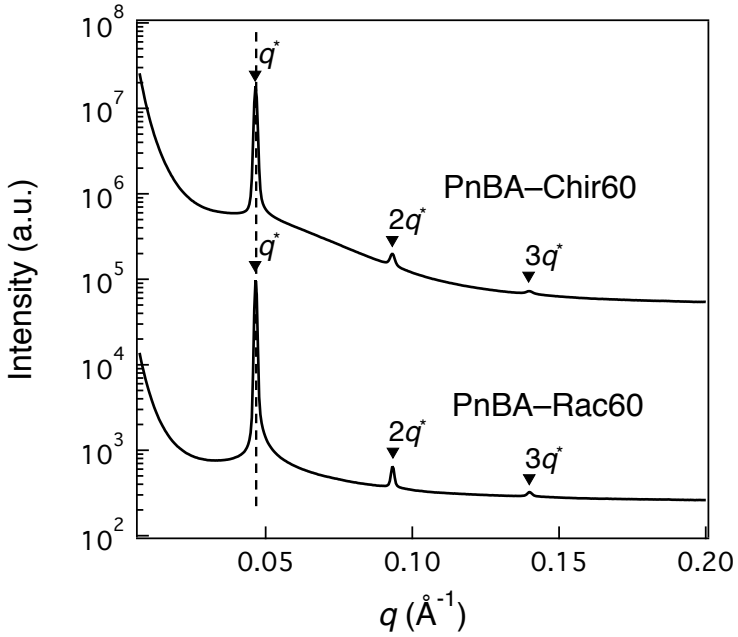

Figure 3.7 SAXS of coil–helix and coil–coil block copolymers
Small-angle X-ray scattering (SAXS) patterns of bulk coil–helix (PnBA–Chir60) and coil–coil (PnBA–Rac60) block copolymer samples at 45 °C. Both block copolymers formed well-ordered lamellar structures and display identical domain spacings of (13.5 ± 0.1) nm, despite differences in the shape of their polypeptoid block.

Table 3.3 Summary of block copolymers synthesized and their characteristics.

Block copolymers	$M_{n,PnBA}$	$Đ_{PnBA}$	$M_{peptoid}$ measured/theoretical	f_{pep}	D (nm)
PnBA–Chir60 (coil–helix)	8913	1.12	8443.5/8444.2	0.46	13.5 ± 0.1
PnBA–Rac60 (coil–coil)	8913	1.12	8443.5/8444.2	0.46	13.5 ± 0.1

The order–disorder transition temperature (T_{ODT}) of the coil–helix block copolymer is lower than that of the coil–coil analogue despite adopting identical domain spacings. Naïvely, block copolymers of identical chemical composition and molecular weight would be expected to have the same forces driving segregation. In symmetric diblock copolymers that form lamellar structures, the domain spacing d can be related to the segregation strength χN by a mean-field form: $d = R_g F(\chi N)$, where R_g is the radius of gyration in the disordered state, and F is a dimensionless function of χN.[1-2, 129] However, with a helical chain shape, the block copolymer could have a different segregation strength χN, and/or a different scaling between chain dimension in the disordered state and domain spacing relative to the coil–coil analogue.

Here we examine the ODTs of these block copolymers to probe the balance of enthalpic penalties from dissimilar segments mixing and entropic penalties from chains stretching to adopt extended configurations. The coil–helix and coil–coil block copolymers display T_{ODT}s of (146.7 ± 0.2) °C and (150.6 ± 0.3) °C, respectively (Figure 3.8). Despite identical domain spacings, the coil–helix block copolymer showed a 3.9 °C lower T_{ODT}. This trend was also observed in another set of block copolymers with a different volume fraction (Figure 3.9). The lamellar morphology readily minimizes the possibility of packing frustration as an entropic contribution that can affect the ODTs of these materials; the ODT differences must arise from a combination of enthalpic and other entropic contributions. Enthalpic contributions may arise because the helical chain shape induces changes in the spatial

arrangement of the polymer chain, leading to differences in the number of contacts with its neighboring chains. Entropically, the helical chain geometry of jointed helices also potentially stretches differently compared to an unstructured coil chain. Further, the fact that the helical chain has a lower effective number of segments could also impact the fluctuation effects near ODT and the translational entropy gain upon disordering, leading to a different ODT from the coil–coil block copolymer. Here we systematically investigate the interactions in the disordered state and the chain stretching in the lamellar structures to probe the relative contributions of these forces to block copolymer self-assembly.

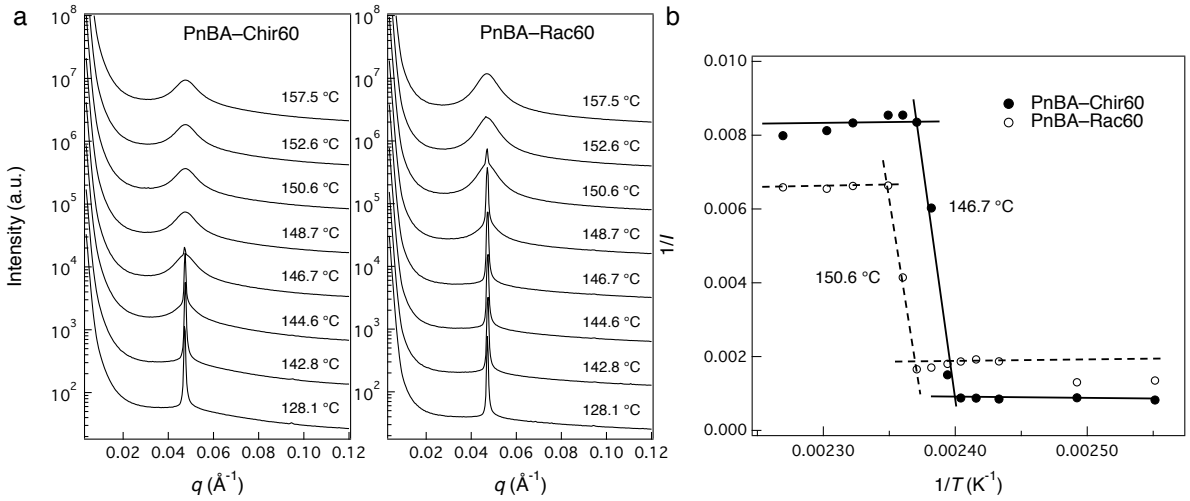

Figure 3.8 Order–disorder transitions of coil–helix and coil–coil block copolymers
a) SAXS patterns of the block copolymers show ODTs at different temperatures; b) Order–disorder transition temperatures (T_{ODT}s) of the coil–helix (PnBA–Chir60) and coil–coil (PnBA–Rac60) block copolymers were determined by plotting $1/I$ vs. $1/T$ to find the discontinuous change (lines in b) are guides to the eye to show the discontinuous change in $1/I$).[130] The coil–helix block copolymer showed a 3.9 °C lower T_{ODT} than the coil–coil analogue despite identical domain spacings. Possible thermodynamic origins are either different enthalpic penalties from a different number of contacts with neighboring chains, or different entropic penalties from chain stretching of the helical polypeptoid block.

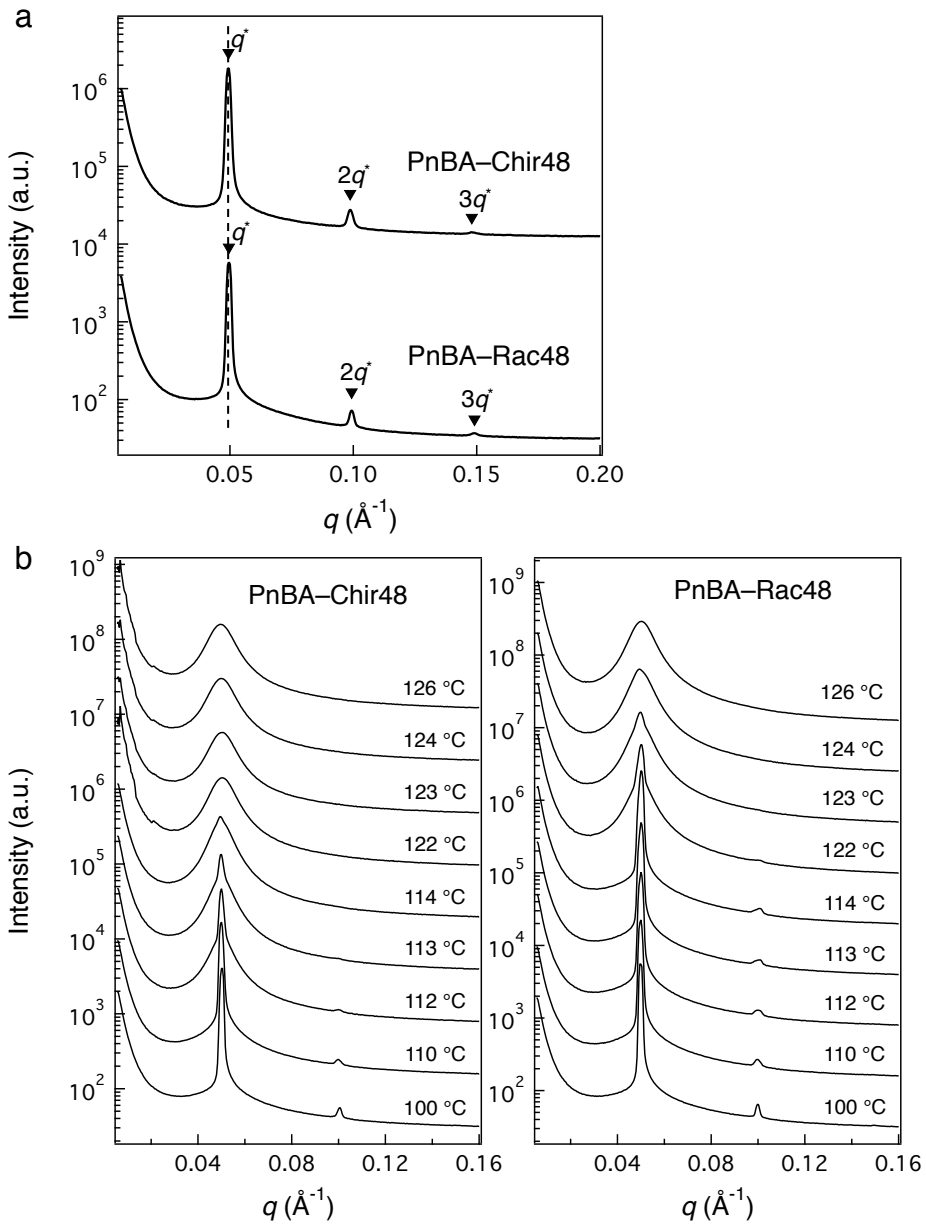

Figure 3.9 Domain spacing and ODT compare of block copolymers with $f_{peptoid}$ ~ 0.42
a) Small-angle X-ray Scattering (SAXS) patterns of another set of coil–helix (PnBA–Chir48) and coil–coil (PnBA–Rac48) block copolymer samples ($f_{peptoid}$ ~ 0.42) at room temperature. Both block copolymers formed well-ordered lamellar structures with an identical domain spacing of (12.8 ± 0.1) nm. b) The coil–helix (PnBA–Chir48) block copolymer showed a lower order–disorder transition temperature (T_{ODT}) than the coil–coil (PnBA–Rac48) block copolymer.

3.5 Enthalpic interactions between dissimilar blocks in the disordered state

To compare the enthalpic contribution to disordering of the coil–helix and coil–coil block copolymers, the effective interaction parameter, χ_{eff}, between poly(*n*-butyl acrylate) and polypeptoid (coil or helical) in the disordered state is measured; the coil–helix block copolymer has a smaller χ_{eff}, indicating smaller enthalpic penalties from the mixing of dissimilar segments than the coil–coil block copolymer. The mixing free energy is commonly described by a Flory–Huggins interaction parameter: $\chi = \frac{z\Delta w}{k_B T} = \frac{z}{k_B T}(\epsilon_{12} - \frac{\epsilon_{11}+\epsilon_{22}}{2})$, which captures the energetic penalty associated with breaking pure component contacts ($\epsilon_{11}, \epsilon_{22}$) and forming cross contacts (ϵ_{12}).[1, 14] Here the pairwise mixing energy, Δw, is equivalent because the chemical compositions of these block copolymers are identical. However, different chain geometries (i.e., helical *vs.* coil) fill space differently, which can cause a different number of chain contacts (z), and therefore, change the enthalpic interactions between the constituent blocks.[14]

To quantify the enthalpic interactions between the two blocks, we fit the SAXS profiles of the block copolymers in the disordered state to the RPA structure factors to extract an effective interaction parameter, χ_{eff} (recall, the polypeptoid block is made of two distinct monomers). The chiral polypeptoid-containing block copolymer fit is based on a model of a freely jointed chain of helical ribbons (Equations 3–6) to capture the helical chain geometry in the correlation functions, as the commonly used RPA structure factor assumes continuous Gaussian chains of equal statistical segment length.[3]

The coil–helix block copolymer has smaller χ_{eff} values than the coil–coil analogue at all temperatures (Figure 3.10), indicating smaller enthalpic penalties from dissimilar segments mixing. When fitting SAXS profiles to RPA structure factors, the peak shape is most

sensitive to the interaction parameter, compared to other parameters including statistical segment lengths and geometric parameters (δ, p, R) of the helical segments. There is significant difference between the χ_{eff} values of the coil–coil and coil–helix block copolymers based on the errors, which are obtained from sensitivity analysis of the effective interaction parameter on the fits. This leads to a difference of $\chi_{eff}N \approx 0.1$, which likely contributed to the observed difference in T_{ODT} between the two block copolymers.

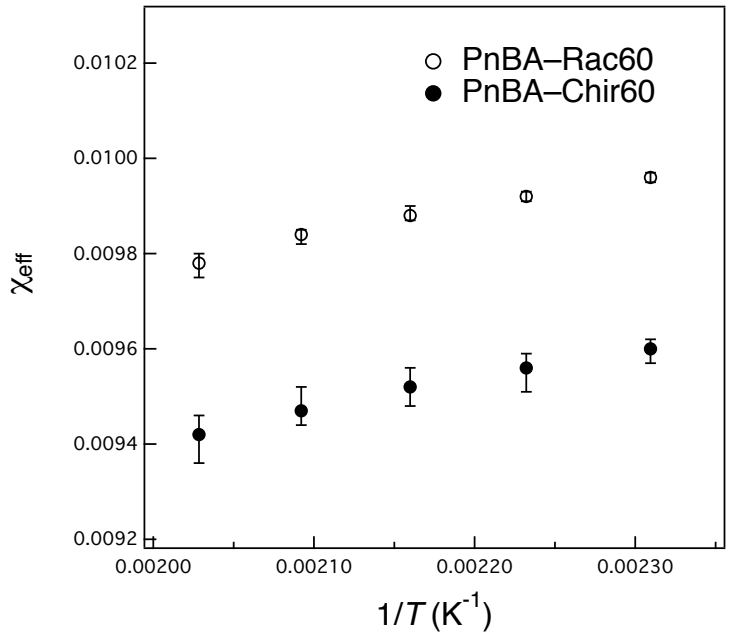

Figure 3.10 Effective interaction parameters of coil–helix and coil–coil block copolymers
χ_{eff}s of PnBA–Rac60 (coil–coil) and PnBA–Chir60 (coil–helix) in the disordered state are determined by fitting to the FJC–FJC structure factor and helical FJC–FJC structure factor, respectively. The coil–helix block copolymer shows a smaller χ_{eff}, indicating that the enthalpic contributions from monomer contacts are smaller for the coil–helix block copolymer.

Variations in local chain structure affect the segment–segment interaction parameter.[14] Thus, the helical chain is expected to interact with neighboring chains differently than the coil chain. We speculate that, with monomers confined within helical turns, the intrinsically

less flexible helices lower the chances of mixing between the polypeptoid and the poly(*n*-butyl acrylate) blocks. Therefore, the coil–helix block copolymer has a smaller number of contacts (z) per reference volume that contributes toward the smaller χ_{eff}. Besides enthalpic effects, entropic effects from chain stretching may also contribute to the observed differences in ODT, which is discussed in the following section.

3.6 Entropic contributions from chain stretching in the lamellar structures

When block copolymers microphase separate, the reduction in free energy cost from minimizing interaction between dissimilar segments is balanced with entropy loss from ordering and chains adopting extended configurations at the interface. Different chain shapes (helical *vs.* coil) may have different entropic penalties from chain stretching, which will impact the thermodynamic balance of self-assembly. The coil–helix block copolymer appears to have experienced more chain stretching/deformation in the ordered lamellar structures, which can contribute to lowering the T_{ODT} because the helical chain gains more configurational freedom upon disordering.

We compare the overall chain stretching by examining the chain dimensions in the disordered state and extended chain configurations in the lamellae. The coil–helix block copolymer experiences a larger chain deformation as it starts with a smaller radius of gyration in the disordered phase, but stretches to form lamellar domains of the same size ((13.5 ± 0.1) nm) as the coil–coil block copolymer. The coil–helix block copolymer has a 3.4 % smaller overall $R_{g,BCP}$ relative to the coil–coil block copolymer. If we assume the difference in $R_{g,BCP}$ comes mainly from chain shape differences in the polypeptoid block (i.e., the PnBA block is assumed to be of similar size in these block copolymers), the helical

polypeptoid has a ~7 % smaller R_g than the coil polypeptoid (Figure 3.11). With an identical domain spacing observed for these block copolymers, the chain stretching penalties are then inversely related to the chain dimensions in the disordered state. Therefore, the helical polypeptoid chain with a smaller dimension must stretch more (losing more configurational freedom) to fill up the same domain area as the coil polypeptoid chain does in the lamellar structures, which will drive the ODT to lower temperatures (Figure 3.12).

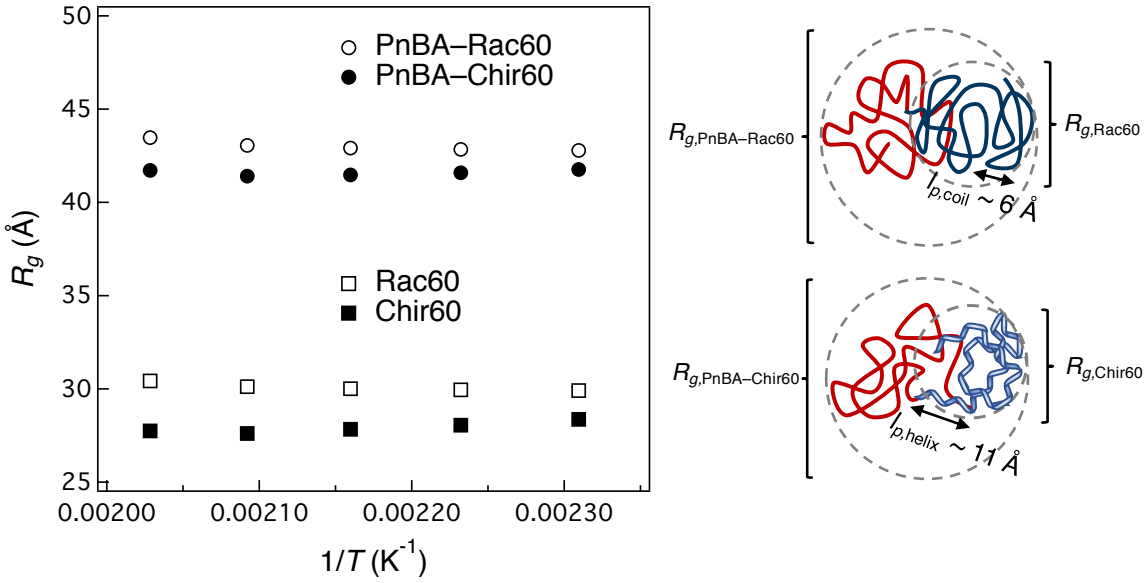

Figure 3.11 Radius of gyration of block copolymers and polypeptoid blocks in the disordered state from RPA fits
R_g is calculated based on N and b (v_0 = 0.1 nm^3) of each block from fitting obtained SAXS patterns in the disordered state to the corresponding RPA structure factor. The coil–helix (PnBA–Chir60) block copolymer has a smaller chain dimension than its coil–coil analogue (PnBA–Rac60). The helical chain is around 7 % smaller than the coil chain in size in the disordered state, if the R_g difference comes mainly from the polypeptoid block.

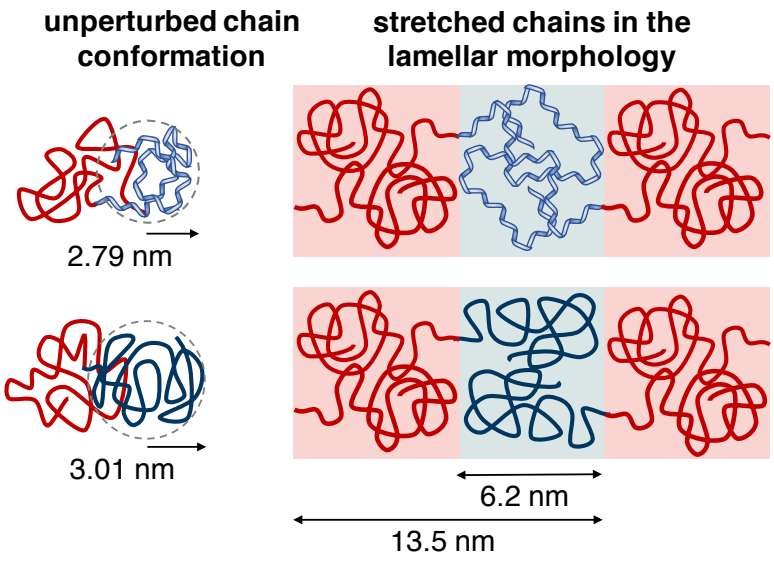

Figure 3.12 Schematic drawing of chain stretching of block copolymers in lamellae Comparing the relatively unperturbed conformation of the polypeptoid chains above ODT and their stretched chain conformation in the self-assembled lamellar structures, the helical polypeptoid chain experiences more chain stretching, losing more configurational freedom from the disordered state than the coil polypeptoid.

Besides the configurational entropy difference between the helical and coil polypeptoid chains, the difference in the way the same number of monomers fill space results in an overall difference in entropy. In fact, since the helical chain (in a moderately good solvent) has a larger helical persistence length ($l_{p,\text{helix}} \sim 11$ Å) but a significantly smaller contour length ($L_{C,\text{helix}} \sim 88$ Å) relative to the coil chain ($l_{p,\text{coil}} \sim 6$ Å, $L_{C,\text{helix}} \sim 128$ Å),[24, 131] it occupies a smaller number of segments (effective N), which may also cause differences in translational entropy upon disordering and fluctuation effects near the ODT.[69, 132-134] While the precise chain dimensions of these block copolymers in the bulk have not been directly measured, the polypeptoid chain conformations will be similar from a marginal solvent to the bulk state according to the Flory theory. Further, if the trend is maintained for these polypeptoid chains incorporated into block copolymers, then the helical block has only about half of the number of segments as the equivalent coil block. As a result, the coil–helix block copolymer chains

will gain more translational entropy by going from the ordered lamellar structure to the disordered state. Moreover, the helical chain with fewer effective segments also has larger fluctuation effects near the ODT. For diblock copolymers of equal volume fraction, the segregation strength at the transition has the form: $(\chi N)_t = 10.495 + 41.022N^{-1/3}$, which shows that the coil–helix block copolymer with a smaller effective N will have a larger $(\chi N)_t$.[69] Both factors arising from the smaller effective N of the helical polypeptoid chain are expected to contribute to the lower T_{ODT} of the coil–helix block copolymer.

3.7 Conclusions

In this work, we examine the impact of polymer helical chain shape on the thermodynamics of block copolymer self-assembly. The strategy of leveraging sequence-defined polypeptoids to tune chain shape by varying only the side chain chirality allows the chain shape effects to be decoupled from chemical effects. The model coil–helix and coil–coil block copolymers with the same chemistry and molecular weight display different ODTs despite identical domain spacings of the lamellar structure formed. In this system, enthalpic penalties from contacts of dissimilar segments mixing in the coil–helix block copolymer is found to be smaller, supported by the smaller effective interaction parameters (χ_{eff}s) of the coil–helix block copolymer in the disordered state. Besides enthalpic effects, entropic effects from greater chain stretching penalties of the helical polypeptoid chain also likely contribute to lowering the T_{ODT} of the coil–helix block copolymer, where the coil–helix block copolymer is found to experience a larger chain dimension change from the disordered state to the ordered lamellar structure. The helical chain studied in this work is relatively flexible, and therefore in many cases, behaves similarly to its coil counterpart (e.g., same morphology

and equivalent domain spacings of the self-assembled structures). However, the helical chain geometry decreases the number of contacts between neighboring chains and increases chain stretching penalties, which alters the thermodynamic balance of enthalpic and entropic contributions to the free energy of block copolymer self-assembly.

Here, we demonstrate that chain shape can be a potential tool to tune block copolymer self-assembly at constant chemical composition and molecular weight. The combined effects from space-filling characteristics and local "stiffness" of the helical chain lead to different enthalpic and entropic interactions in block copolymer self-assembly. We expect similar types of sterically induced helices will have similar effects in block copolymers (i.e., larger chain stretching penalties and smaller number of contacts compared to a chemically identical coil). However, it is important to emphasize that these effects will only be observable in only well-controlled systems. Polymers with crystallinity or stiffer helices will have crystallization or alignment interactions from rod-like helices competing with the self-assembly process, potentially concealing the pure chain shape effects. The compact and locally stiffer helical chain may offer opportunities for accessing complicated morphologies or broadening complex phase windows. This polypeptoid based system can also incorporate different functional groups precisely along the chain, which in combination with the tunable chain shape, will be a powerful tool to further manipulate the chain conformation near the domain interface.

3.8 Acknowledgements

The authors gratefully acknowledge funding from the National Science Foundation (NSF) Division of Materials Research (DMR) Polymers program (DMR-1608297). Polymer

characterization was performed with guidance from Dr. Rachel Behrens and with support from the MRL Shared Experimental Facilities (supported by the MRSEC Program of the NSF under Award No. DMR-1720256; a member of the NSF-funded Materials Research Facilities Network). X-ray scattering experiments utilized resources of the Stanford Synchrotron Radiation Lightsource, SLAC National Accelerator Laboratory (supported by the U.S. Department of Energy, Office of Science, Office of Basic Energy Sciences under Contract No. DE-AC02-76SF00515), and the National Synchrotron Light Source II (a U.S. Department of Energy (DOE) Office of Science User Facility operated for the DOE Office of Science by Brookhaven National Laboratory under Contract No. DE-SC0012704). The authors thank Dr. Ron Zuckermann at the Molecular Foundry of the Lawrence Berkeley National Lab for helpful discussions regarding polypeptoid synthesis.

Chapter 4

Tuning the Double Gyroid Phase Window in Block Copolymers via Polymer Chain Conformation Near the Interface

4.1 Abstract

While block copolymer network morphologies have been proven interesting for applications ranging from mechanical to transport and optical properties, these structures occupy a very narrow window of phase space. Polymer chain conformation plays an important role in determining self-assembly behavior and could be used as an additional handle to target these network morphologies in block copolymers. Here, we utilize poly(styrene-*b*-peptoid) block copolymers, for which the polypeptoid block chain

conformation can be tuned via side chain chirality and steric hindrance. In this model system, a small segment of 6 peptoid units in the immediate vicinity of the block junction is designed to adopt either a helical or a coil conformation (PS–($Chir_6Nme_y$) vs. PS–($Achir_6Nme_y$)), allowing us to probe the role of chain conformation near the interface on double gyroid (G) phase formation. The G phase is accessed in both block copolymer series, while the boundaries are shifted towards larger polypeptoid volume fractions in the PS–($Chir_6Nme_y$) series, due to the less space-filling feature of the compact helix segment. The space-filling difference between the helix and coil segment is further corroborated by the smaller d_{211} spacing of PS–($Chir_6Nme_{39}$) compared to PS–($Achir_6Nme_{36}$) (13.9 nm vs. 14.3 nm). Furthermore, a broadened G phase window is accessed in the PS–($Achir_6Nme_y$) series that has a flexible coil segment near the interface. Our results demonstrate the possibility of tuning the G phase in linear block copolymers by chain conformation near the interface alone, highlighting chain conformation as a versatile handle in block copolymer design.

4.2 Introduction

Materials with network mesostructures exhibit unique mechanical,[135-137] transport,[138-140] and optical[141-145] properties due to their multiply continuous, percolating domain structures with high interfacial areas. Block copolymers can produce such network structures with features on the order of tens of nanometers via self-assembly, with the process governed by thermodynamic contributions from dissimilar blocks mixing and chain stretching.[1-2] The double gyroid (G) phase is identified as a thermodynamically equilibrium network morphology (the orthorhombic *Fddd* network phase is also thermodynamically stable, but only in an extremely small phase window).[4, 134, 146] Nevertheless, the G phase region is much

smaller than other ordered morphologies in the diblock copolymer phase diagram, making it hard to access.[4, 134, 147] The competition between minimizing interfacial area, which favors forming constant mean curvature (CMC) interfaces, and chain stretching that favors domains of uniform thickness, drives the phase selection in block copolymers. While the classical morphologies (lamellae, cylinders, spheres) allow both simultaneously, network phases like the G phase do not–they suffer from high degrees of packing frustration as some regions require excessive chain stretching to fill space uniformly,[148-150] making them only stable in a very limited volume fraction range.

Driven by the mechanism of network phase formation and stabilization, numerous strategies have been employed to stabilize network phases. Homopolymers in block copolymer/homopolymer blends fill interstitial spaces reducing the degree of chain stretching in the block copolymer and thereby stabilizing the network phases.[151-154] Similarly, increasing chain length dispersity helps relieve packing frustration because longer chains preferentially arrange at thicker regions in the domain (e.g., connectors as opposed to network struts).[70, 152, 155-156] Other strategies involve changing chain architecture/connectivity (e.g., multiblock or star-block architectures) to expand parameter space and broaden network phase windows.[77, 157-159] While most focus has been on eliminating the packing frustration, the interfacial region plays a critical role as most segmental mixing happens near the interface and the interfacial curvature dictates chain packing in the domains. In particular, network phases have a high interfacial area per unit volume and require a delicate balance between enthalpic and entropic contributions;[150] therefore, significant changes are expected if polymer chain conformation near the interface is manipulated around the network phase

window, as the free energy minimum can be overturned easily if the contributions are altered, which could lead to morphological changes.

While chain conformation has been shown to play a role in lamellar, cylindrical, and spherical morphologies in linear diblock copolymers,[17, 26, 96, 160] few studies have considered chain conformation effects in network phases. Compare to other parameters (e.g., chemical composition, chain length), chain conformation is not straightforward to tune. Leveraging the sequence precision and monodispersity of polypeptoids, polypeptoid-containing block copolymers and block copolypeptoids have been demonstrated as ideal systems to study monomer architecture and sequence, polydispersity, and polymer chain conformation effects on block copolymer self-assembly.[26, 83-86, 96, 161] In this work, we utilize poly(styrene-*b*-peptoid) block copolymers, where the polypeptoid block has a segment near the block junction of tunable chain shape (Figure 4.1). We show the double gyroid (G) phase boundary and window width can be tuned by chain conformation near the interface alone. By having a compact helix segment near the interface, the phase boundaries are shifted towards larger polypeptoid volume fractions, due to the less space-filling feature of the helix segment. Further, the block copolymer series with a flexible coil segment near the interface displays a broadened G phase window relative to the series with a helix segment near the interface.

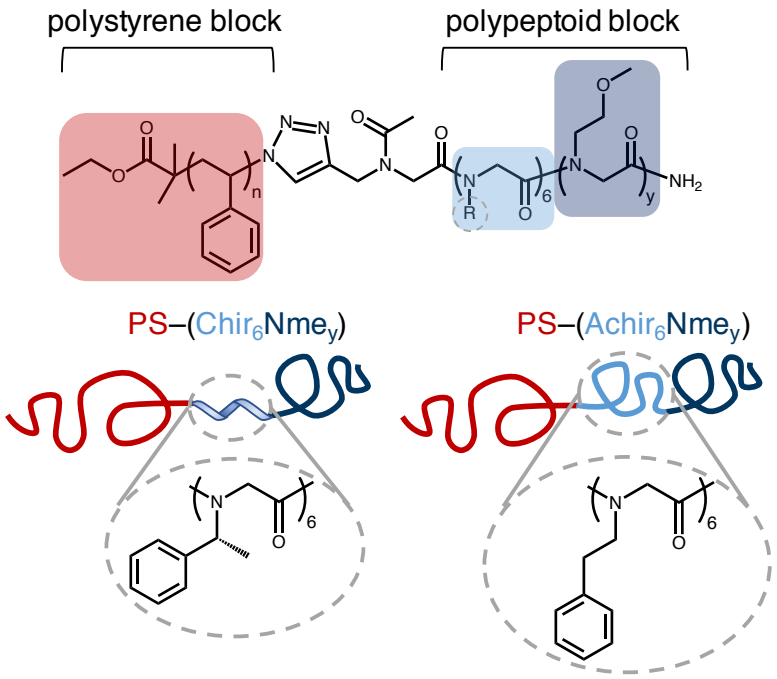

Figure 4.1 System design of poly(styrene-*b*-peptoid) block copolymers
The chain conformation of the polypeptoid segment near the block junction is either helical ($Chir_6$) or coil ($Achir_6$), tuned by side chain chirality and steric hindrance. The long tail of the polypeptoid block consists of Nme units and is coil-like.

4.3 Experimental section

4.3.1 Materials

Solvents and reagents were purchased from commercial suppliers and used without further purification, unless otherwise noted. Anhydrous dimethylformamide (DMF), and *N*,*N*-diisopropylethylamine (DIPEA) were used for synthesis block copolymers.

4.3.2 Synthesis of alkyne-terminated polypeptoids

Polypeptoids were synthesized on a custom robotic synthesizer using commercially available amine submonomers as described in 2.3.2 and 3.3.2. Rink amide resin (100-200 mesh, Novabiochem) with intermediate loading (~ 0.50 mmol g^{-1}) was used. For the chiral

units, *N*-((*R*)-(+)-α-methylbenzyl)glycine (N*R*pe), bromoacetylation steps were performed twice to improve efficiency after a bulky side chain. An additional unit was added in the same method with propargylamine to give the alkyne end group after the desired sequence. The chain end was finally acetylated using a mixture of 0.4 M acetic anhydride and 0.4 M pyridine in DMF (3.5 mL for 100 μmol scale) for 30 min. Polypeptoids were cleaved from the resin as described in 2.3.2. Polypeptoid mass were determined by MALDI and UPLC-MS.

4.3.2 Synthesis of azide-terminated polystyrene

Bromine-terminated polystyrene was first synthesized via atom-transfer radical polymerization (ATRP). Styrene monomer and ligand, *N,N,N',N',N''*-pentamethyldiethylenetriamine (PMDETA), were filtered through basic alumina before use. The initiator, ethyl α-bromoisobutyrate, and catalyst, copper-(I) bromide (Cu(I)Br), were used as received. 48 mmol of styrene (112.1 equiv.), 0.43 mmol of initiator (1 equiv.), 0.085 mmol PMDETA (0.2 equiv.) were combined in a scintillation vial and sparged with nitrogen for 45 min. In an oven-dried Schlenk flask, 0.085 mmol of Cu(I)Br (0.2 equiv.) was added. Then the flask was evacuated and refilled with nitrogen three times, before the sparged liquid mixture was transferred in with a degassed syringe. The reaction mixture was degassed by three freeze–pump–thaw cycles, and reacted at 100 °C under nitrogen for ~40 h (until the mixture solidified). The solid mixture was dissolved in tetrahydrofuran (THF), then filtered through basic alumina to remove copper compounds. The collected solution was dried *in vacuo* to get a slightly viscous solution and precipitated into methanol. The collected polymer was dried *in vacuo* at 50 °C overnight. The bromine-terminated polystyrene was dissolved in

DMF (0.05 M concentration), and 1.5 equiv. of sodium azide was added. The reaction mixture was stirred for 24 h at room temperature, then precipitated into methanol twice to remove residue sodium azide. The collected polymer was dried *in vacuo* at 50 °C overnight.

4.3.4 Synthesis of poly(styrene-b-peptoid) block copolymers

Alkyne-terminated polypeptoid (60–70 mg, 1 equiv.) and azide-terminated polystyrene (2 equiv.) were dissolved in 2 mL of anhydrous DMF in a scintillation vial. DIPEA (10 equiv.) and PMDETA (5 equiv.) were added, and the reaction mixture was sparged with nitrogen for 45 min. In an oven-dried Schlenk flask, Cu(I)Br (5 equiv.) and ascorbic acid (6 equiv.) were added, and the flask was evacuated and refilled with nitrogen three times. The sparged reaction mixture was added to the Schlenk flask with a degassed syringe and then further degassed with three freeze–pump–thaw cycles. The reaction was allowed to react under static vacuum at 50 °C for ~ 40 h. The solution was then diluted with DMF and filtered through basic alumina to remove copper compounds. The collected solution was dried *in vacuo*, dissolved in THF (~ 125 mg mL^{-1}), and precipitated into a hexane : cyclohexane (3:2, v/v) mixture to remove excess polystyrene. The precipitate was isolated by centrifugation and dried *in vacuo* at 50 °C overnight.

4.3.5 Matrix-assisted laser desorption/ionization with time-of-flight (MALDI-TOF) mass spectrometry

MALDI-TOF MS was performed on a Bruker Microflex LRF MALDI TOF mass spectrometer. Sample solutions were prepared by dissolving polypeptoids in ACN : H_2O (1:1, v/v) at ~ 1 mg mL^{-1} concentration, or directly used Prep GPC fractions of the block

copolymers in THF. α-Cyano-4-hydroxycinnamic acid in ACN : H_2O (1:2, v/v) (~ 10 mg mL^{-1}, saturated) was used as matrix for polypeptoid samples, and 20 mg mL^{-1} *trans*-2-[3-(4-*tert*-butylpheny)-2-methyl-2-propenylidene]malonitrile (DCTB) in THF with silver trifluoroacetate (AgTFA) added at ~ 1 mg mL^{-1} was used for polystyrene-containing materials. 5 μL sample solution was combined with 5 μL matrix and matrix–sample mixtures were spotted onto a polished steel MALDI target plate (Bruker). Mass spectra were collected in either reflectron or linear mode with appropriate mass ranges. Mass peaks were calibrated against peptide and protein standards (Bruker). MALDI-TOF spectra of polypeptoids are shown in Figure 4.2.

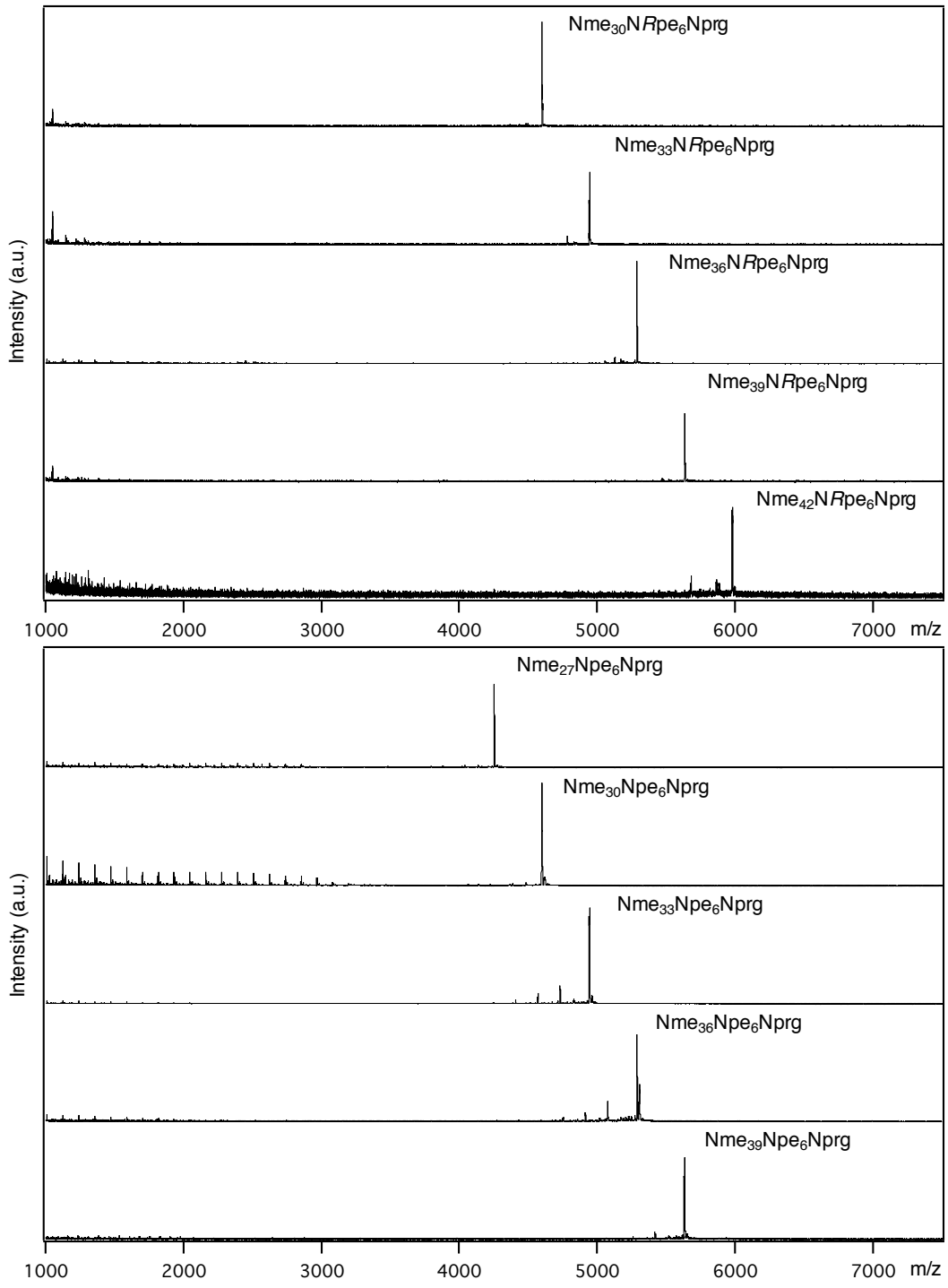

Figure 4.2 MALDI spectra of polypeptoids
For the Nme_xNRpe_6Nprg and Nme_xNpe_6Nprg series, Δm is ~ 345 between adjacent polypeptoids, corresponding to the mass of 3 Nme units. N*R*pe: *N*-((*R*)-(+)-α-methylbenzyl)glycine, corresponds to the chiral, aromatic unit "Chir", Npe: *N*-(2-phenylethyl)glycine, corresponds to the achiral, aromatic unit "Achir", Nme: *N*-(2-methoxyethyl)glycine, Nprg: *N*-(2-propargyl)glycine, gives the alkyne end.

4.3.6 Ultrahigh-pressure liquid chromatography mass spectrometry (UPLC-MS)

UPLC-MS was performed on a Waters Xevo G2-XS equipped with a time-of-flight mass spectrometer. Polypeptoid samples were dissolved at ~ 0.5 mg mL^{-1} in MS grade ACN : H_2O (1:1, v/v) mixtures. Separations was achieved on a Waters BEH C18 column with eluent gradients from 5% ACN/95% H_2O to 100% ACN (with 0.1% formic acid) over 10 min. Polypeptoid materials were detected by UV absorption at 214 nm. Charged polypeptoid species were detected in the mass spectrometer. Molar masses of polypeptoids used in this study are summarized in Table 4.1.

Table 4.1 Theoretical and LC-MS measured molar mass of polypeptoids used in this study

Polypeptoids	Theoretical (m/z)	Measured (m/z)
$Nme_{30}N\mathit{R}pe_6Nprg$	4574.5	4574.4
$Nme_{33}N\mathit{R}pe_6Nprg$	4919.7	4919.6
$Nme_{36}N\mathit{R}pe_6Nprg$	5264.9	5265.7
$Nme_{39}N\mathit{R}pe_6Nprg$	5610.1	5611.0
$Nme_{42}N\mathit{R}pe_6Nprg$	5955.2	5955.2
$Nme_{27}Npe_6Nprg$	4229.3	4229.3
$Nme_{30}Npe_6Nprg$	4574.5	4574.4
$Nme_{32}Npe_6Nprg$	4804.6	4804.5
$Nme_{33}Npe_6Nprg$	4919.7	4919.6
$Nme_{36}Npe_6Nprg$	5264.9	5264.6
$Nme_{39}Npe_6Nprg$	5610.1	5611.0
$Nme_{36}Npe_3N\mathit{R}pe_3Nprg$	5264.9	5265.7
Nme_{36} $N\mathit{R}pe_3Npe_3Nprg$	5264.9	5265.7

4.3.7 Gel permeation chromatography (GPC)

The molecular weight of polystyrene was measured on a Waters Alliance HPLC system with an e2695 separation module using an Agilent PLgel 5 μm MiniMIX-D column with THF as the eluent. Refractive index traces from a Waters 2414 differential refractive index detector were used for molecular weight determination using polystyrene calibration standards (Agilent Technologies).

4.3.8 Preparative gel permeation chromatography (Prep GPC)

The precipitated raw product (PS–Polypeptoid block copolymer and unreacted polypeptoid homopolymer) was further purified via Prep GPC. The raw product was dissolved in 2 mL HPLC grade THF (one injection volume, 30–50 mg mL^{-1}) and separated on a Waters system with a Waters 1525 Binary HPLC Pump and an Agilent PLgel Prep 10 μm, 100000 Å column, with THF as the eluent at a flow rate of 4 mL min^{-1}. Refractive index traces from a Waters 2414 differential refractive index detector were used for detecting different species eluting at different times. Fractions were collected with 30 s intervals and later characterized with MALDI-TOF (Figure 4.3).

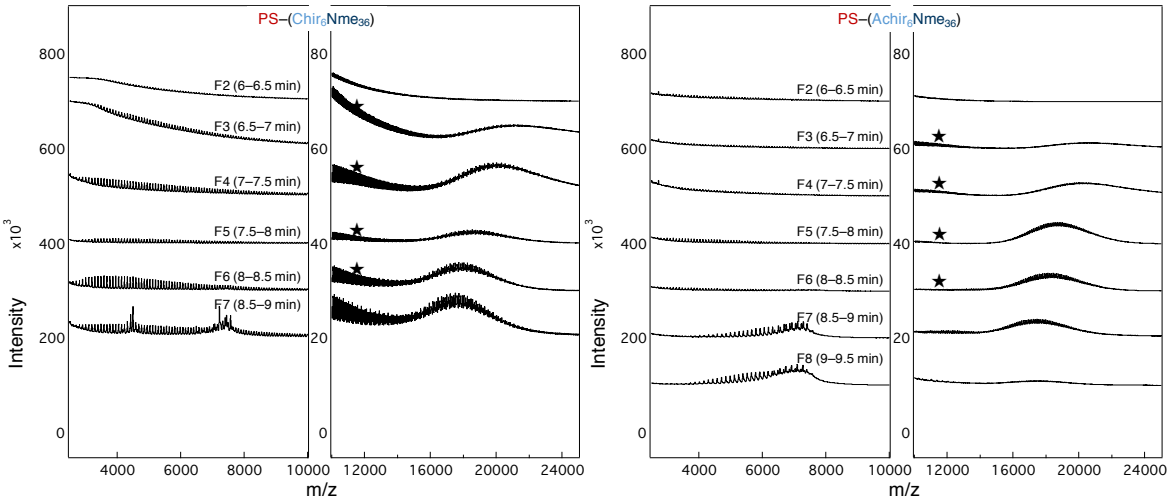

Figure 4.3 MALDI spectra of collected Prep GPC fractions
Two examples of PS–($Chir_6Nme_{36}$) and PS–($Achir_6Nme_{36}$). Fractions labelled with ★ are combined and used for subsequent SAXS characterization.

4.3.9 Small-angle X-ray scattering (SAXS)

Dry block copolymers were loaded into a Kapton-lined aluminum washer. Samples were annealed at reduced pressure (3×10^{-8} Torr) at 180 °C for ~12 h, then annealed at 150 °C for 24 h and at 130 °C for another 24 h. After slowly cooling to room temperature, the washers were sealed with Kapton under ambient conditions.

SAXS measurements were performed at the National Synchrotron Light Source II (NSLS II, beamline 11-BM, Brookhaven National Laboratory) with an X-ray energy of 13.5 keV and at the Advanced Light Source (ALS, beamline 7.3.3, Lawrence Berkeley National Laboratory) with an X-ray energy of 10 keV. *In-situ* temperature studies were conducted at 11-BM using the beamline-developed heat stage. The samples were equilibrated for 5 min at each temperature before collecting exposures, and longer annealing time at 220 °C. The exposure time was 30 s for measurements at room temperature and 10 s for measurements at elevated temperatures. The scattering data were calibrated with silver behenate standards, reduced using circular averaging of the 2D scattering pattern.

To investigate the impact of polymer chain conformation near the interface on the phase boundary and window width of the double gyroid (G) phase, model poly(styrene-*b*-peptoid) block copolymers were synthesized, where the polypeptoid block conformation in the immediate vicinity of the interface is tuned by side chain chirality and steric hindrance.[24, 26, 60, 96] In this study, two series of block copolymers in the polypeptoid volume fraction (f_{pep}) range between 0.268 and 0.34 were examined. These two series differ from each other in terms of chain conformation of the polypeptoid segment near the block junction, with either a compact and stiff helix segment or a flexible coil segment (Figure 4.1, Table 4.2). When tuning the polypeptoid segment conformation near the interface, the phase boundaries are shifted such that the block copolymer series with a flexible coil segment near the interface shows a broadened G phase window compared to that with a helix segment near the interface.

Table 4.2 Characteristics of block copolymer materials used in the study

Sample ID[a]	$M_{n,PS}$ (g/mol)[b]	$M_{n,pep}$ (g/mol)	f_{pep}[c]	Morphology[d]
PS–($Chir_6Nme_{30}$)	10202	4574	0.285	HEX
PS–($Chir_6Nme_{33}$)	10282	4919	0.299	DIS
PS–($Chir_6Nme_{36}$)	10282	5264	0.313	DIS/G
PS–($Chir_6Nme_{39}$)	10282	5609	0.327	G
PS–($Chir_6Nme_{42}$)	10282	5954	0.340	LAM
PS–($Achir_6Nme_{27}$)	10282	4229	0.268	DIS
PS–($Achir_6Nme_{30}$)	10282	4574	0.284	DIS/G
PS–($Achir_6Nme_{32}$)	10282	4804	0.294	G
PS–($Achir_6Nme_{33}$)	10282	4919	0.299	G
PS–($Achir_6Nme_{36}$)	10282	5264	0.313	G
PS–($Achir_6Nme_{39}$)	10282	5609	0.327	LAM
PS–($Chir_3Achir_3Nme_{36}$)	10986	5264	0.299	HEX
PS–($Achir_3Chir_3Nme_{36}$)	10986	5264	0.299	G

[a]"Chir" corresponds to the chiral, aromatic unit N*R*pe, "Achir" corresponds to the achiral, aromatic unit Npe.
[b]PS blocks: M_n = 10202 g mol^{-1}, Đ = 1.17; M_n = 10282 g mol^{-1}, Đ = 1.15; M_n = 10986 g mol^{-1}, Đ = 1.11. M_n and Đ are determined by gel permeation chromatograph against PS standards using tetrahydrofuran as eluent.
[c]The volume fraction of the polypeptoid block, f_{pep}, is calculated based on densities of each block, ρ_{PS} = 1.05 g cm^{-3}, ρ_{pep} = 1.18 g cm^{-3}.
[d]Morphologies: DIS-disordered, HEX-hexagonally packed cylinders, G-double gyroid, LAM-lamellae.

4.4 Chain conformation of a small segment near the interface shifts phase boundaries

The chain segment near the block junction largely impacts segmental mixing between dissimilar blocks near the interface, as well as the preferred interfacial curvature of the dividing interface between the blocks.[162-166] For the two series of poly(styrene-*b*-peptoid) block copolymers in this study, the helix and coil polypeptoid segments differ in space-filling characteristics as well as local stiffness, while having identical chemistry. Overall, the

boundaries of the double gyroid (G) phase in the PS–(Chir$_6$Nme$_y$) series containing a helix segment are shifted towards larger polypeptoid volume fractions (f_{pep}), relative to the PS–(Achir$_6$Nme$_y$) series, which has a more flexible coil segment near the block junction (Figure 4.4). The phase diagram at room temperature directly shows the phase boundary shift between the two series of block copolymers (Figure 4.5).

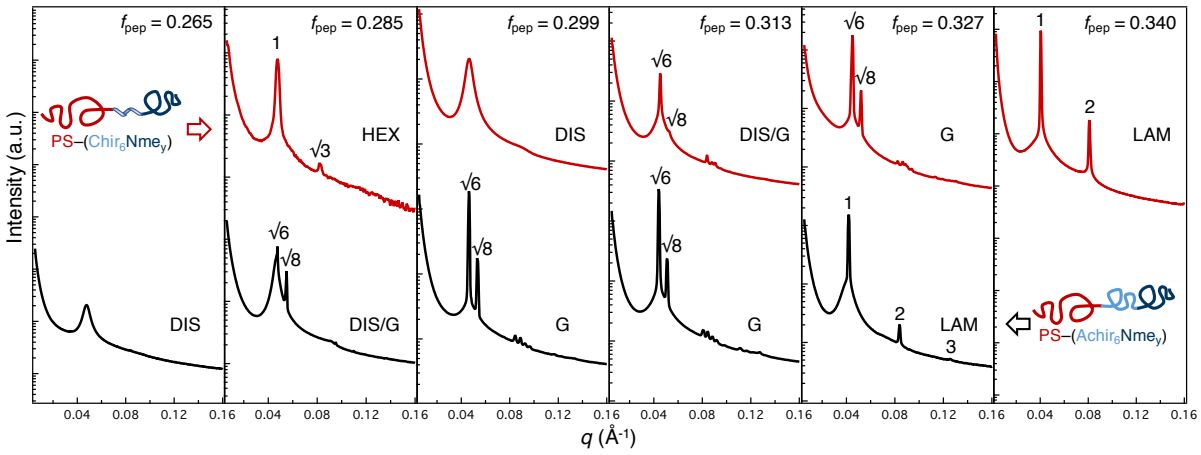

Figure 4.4 SAXS of PS–(Chir$_6$Nme$_y$) and PS–(Achir$_6$Nme$_y$) series at room temperature
PS–(Chir$_6$Nme$_y$) (red, top) and PS–(Ahir$_6$Nme$_y$) (black, bottom), polypeptoid volume fraction (f_{pep}) range: 0.265–0.340.

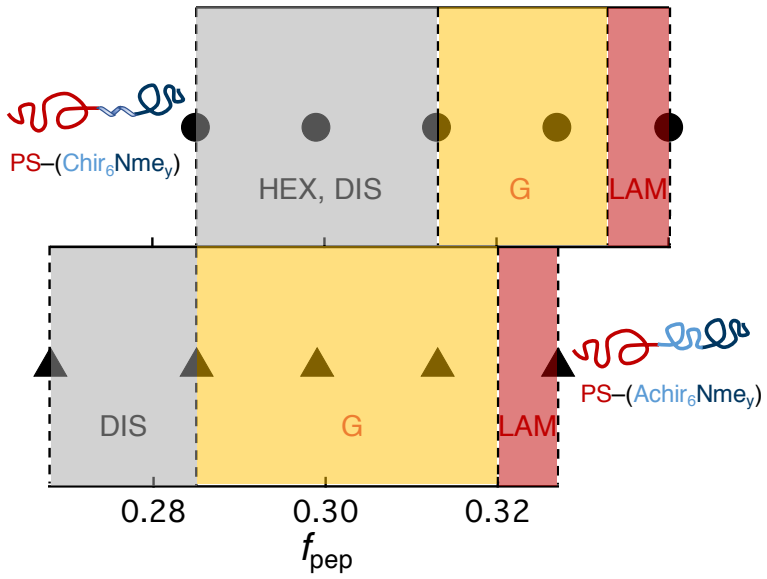

Figure 4.5 Phase diagrams of PS–(Chir$_6$Nme$_y$) and PS–(Achir$_6$Nme$_y$) series at room temperature
The double gyroid (G) morphology occupies a smaller slice of the phase diagram for the block copolymer with a compact and stiff interfacial helix segment (PS–(Chir$_6$Nme$_y$)).

While the classical block copolymer phase diagram is defined with the bulk chain volume fraction as the x axis, the difference in space-filling characteristics of chains contributes to phase boundary shifts due to local effects.[6, 14] Conventionally, the space-filling of polymer chains can be parameterized by the conformational symmetry parameter β^2 ($\beta^2 = R_g^2/V$, where R_g is radius of gyration, V is chain volume).[6] The densities of the two polypeptoid blocks are nearly identical according to previous measurements on materials with the same monomers, leading to identical chain volumes.[26, 83] Therefore, in this system, differences in conformational symmetry (β^2) can be entirely attributed to differences in R_g. Here, the interfacial helix segment consists of 6 chiral units (N*R*pe), which will form two helical turns with a helix pitch ~ 6 Å,[56, 94] leading to a short rod-like segment of length ~ 1.2 nm. While the second series of block copolymers has an interfacial coil segment that consists of 6 achiral units (Npe) with a persistence length around 6 Å (contour length ~ 21 Å).[24, 131] It is

intuitive that a polymer chain filling up space more efficiently will shift the G phase boundary towards a larger volume fraction. Comparing PS–($Chir_6Nme_{36}$) and PS–($Achir_6Nme_{36}$) as an example, the volume (4/3 R_g^3) occupied by the interfacial helix segment (0.042 nm^3) is 67% less than the volume occupied by the interfacial coil segment (0.127 nm^3) (Table 4.3). The locally denser helix segment will drive the PS block and the $(Nme)_y$ tail pack more compactly as chains need to fill space at uniform density. It can be further corroborated by comparing the lattice parameter of the G phase-forming PS–($Chir_6Nme_{39}$) and PS–($Achir_6Nme_{36}$), where the former has a smaller d_{211} spacing than the latter (13.9 nm vs. 14.3 nm), despite the former having a longer polypeptoid block (i.e., 3 more Nme units) (Figure 4.6). This also demonstrates that the helix segment fills less space than the equivalent coil segment (both consist of 6 peptoid units) in the ordered double gyroid mesostructure.

Table 4.3 Calculation of space occupied by the interfacial polypeptoid segment

	$Chir_6$	$Achir_6$
L_C (nm)	1.2	2.1
l_p (nm)	1.2	0.6
R_g^2 (nm^2)	0.099	0.209
4/3 R_g^3 (nm^3)	0.042	0.127

The radius of gyration (R_g) is calculated using the wormlike chain model[10], with the contour length, L_C, and the persistence length, l_p, estimated based on results from Chapter 2.

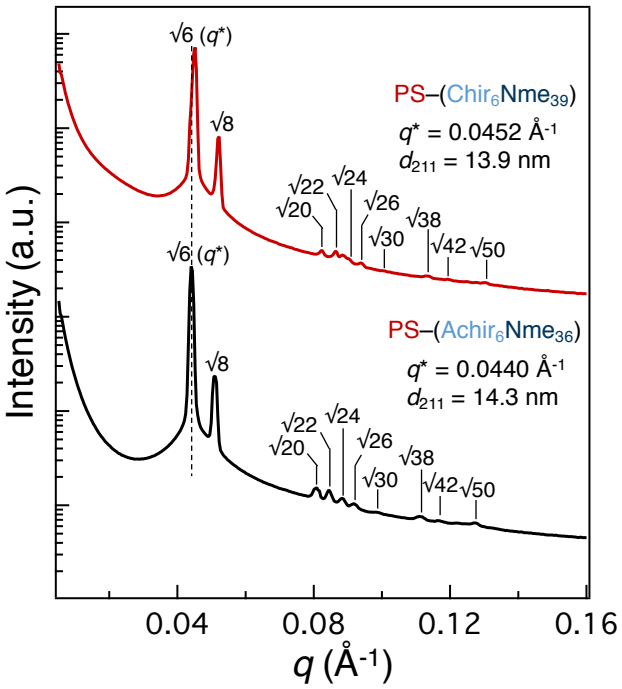

Figure 4.6 Domain spacing compare of two double gyroid-forming block copolymers Two double gyroid-forming block copolymers: PS–(Chir$_6$Nme$_{39}$) and PS–(Achir$_6$Nme$_{36}$). The primary peak position (q^*) corresponds to the d_{211} spacing and PS–(Chir$_6$Nme$_{39}$) has a smaller d_{211} spacing than PS–(Achir$_6$Nme$_{36}$) (13.9 nm vs. 14.3 nm), despite the former having a longer polypeptoid block (i.e., 3 more Nme units).

4.5 Having a flexible coil segment near the interface broadens the double gyroid (G) phase window

While both sides of the double gyroid (G) phase window shifted in the same direction, the block copolymer with a coil segment (Achir$_6$) near the interface shows a broader G phase window, spanning from f_{pep} = 0.285 to f_{pep} ~ 0.32 (Figure 4.5). The formation of network phases is commonly recognized as a result of the competing minimization between interfacial tension and packing frustration, where packing frustration refers to polymer chains experiencing excessive stretching to fill the thicker domain regions (e.g., the center of the connectors).[147-149, 152, 167] In this model system, the two series of block copolymers have the

same polystyrene block and both have the coil-like Nme_y polypeptoid tail; therefore, the packing frustration in the domain centers is expected to be similar. Instead, we focus on the space-filling characteristics of the polypeptoid segment (mediated by different chain shapes) in the immediate vicinity of the interface, which are expected to play a vital role in determining self-assembly through impacting segmental mixing and dictating chain packing in the domains.

The space-filling characteristics of the polymer segment near the interface impacts the interaction energy between the dissimilar blocks via the effective interaction parameter, χ_{eff}. Since the chemistries are identical the differences in χ_{eff} are attributed to conformational effects.[11, 14, 96] A lower χ_{eff} is expected for the block copolymer, PS–($Chir_6Nme_y$): a compact helical chain conformation leads to fewer contacts with neighboring chains, resulting in a smaller χ_{eff}.[96] Therefore, with a smaller χ_{eff}, having a helix segment near the interface will preferentially lower the interaction energy, which is also reflected by the lower transition temperatures observed for the block copolymers with a helix segment near the interface (Figure 4.7). However, it should be noted that entropic contributions from chain stretching also affect transitions.[168] Considering the chain conformation difference of the interfacial segments, there is likely a difference in the entropic component between the two block copolymers, which either facilitate or prohibit the transitions, while the enthalpic component in PS–($Chir_6Nme_y$) favors more demixing than that in PS–($Achir_6Nme_y$).

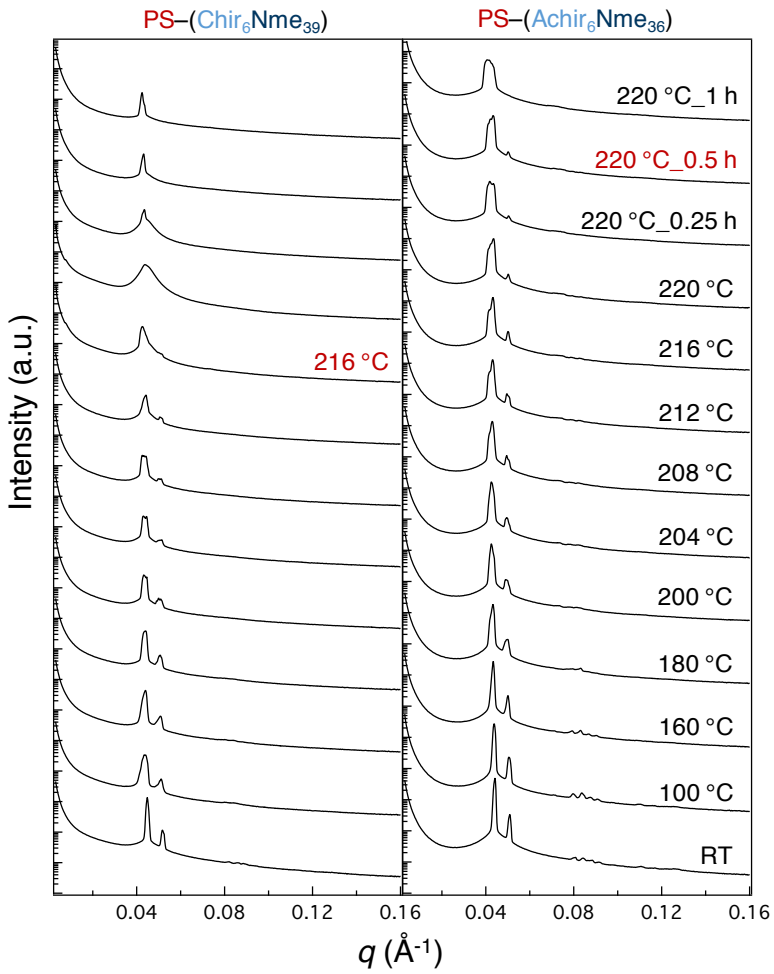

Figure 4.7 Transitions from the double gyroid (G) phase at elevated temperatures *In-situ* temperature SAXS studies of PS–($Chir_6Nme_{39}$) and PS–($Achir_6Nme_{36}$). PS–($Chir_6Nme_{39}$) transits at a lower temperature at 216 °C than PS–($Achir_6Nme_{36}$) at 220 °C, despite having a longer polypeptoid block.

However, the lower χ_{eff} of the PS–($Chir_6Nme_y$) series did not lead to a broadened G phase window, which was previously considered to be a contributing factor to access G phase for block copolymers with tapered interfaces. Previous experimental and theoretical studies have shown that a tapered interface favors the formation the G phase (broader phase window), while having decreased order–disorder transitions due to a lowered χ_{eff}.[165, 169-170] In this study, however, the PS–($Achir_6Nme_y$) block copolymer series has a broadened G phase window, in both the f_{pep} axis and T axis (Figure 4.8). While transitions along the T axis trends

with the χ_{eff} relation, the broadening of G phase along the f_{pep} axis was unexpected. We suspect the flexibility of the segment (ability to rearrange repeat units) near the interface impacts the G phase formation. The dividing interface between dissimilar blocks in the double gyroid mesostructure has been shown not to adopt a constant mean curvature (CMC), nor do the struts (consist of the minority block) have constant length, all of which are manifestation of relieving packing frustration to minimize the overall free energy.[148, 150, 167, 171] Here, the coil segment ($Achir_6$) is more flexible compared to the helix segment ($Chir_6$), which has monomers arranged along the helical turns (with the backbone preferentially adopting a *cis* configuration[56, 60, 131]) and has much less configurational freedom. With the coil segment being more flexible near the interface and contributing to the overall configurational freedom of the polypeptoid block, it is favorable for relieving packing frustration despite having a slightly higher interaction parameter, χ_{eff}. Moreover, the fact that the polypeptoid block is monodisperse means that chain flexibility is even more critical because while packing frustration can partially be relieved by dispersed chain lengths in traditional synthetic polymers, this is not possible in completely monodisperse block domains.

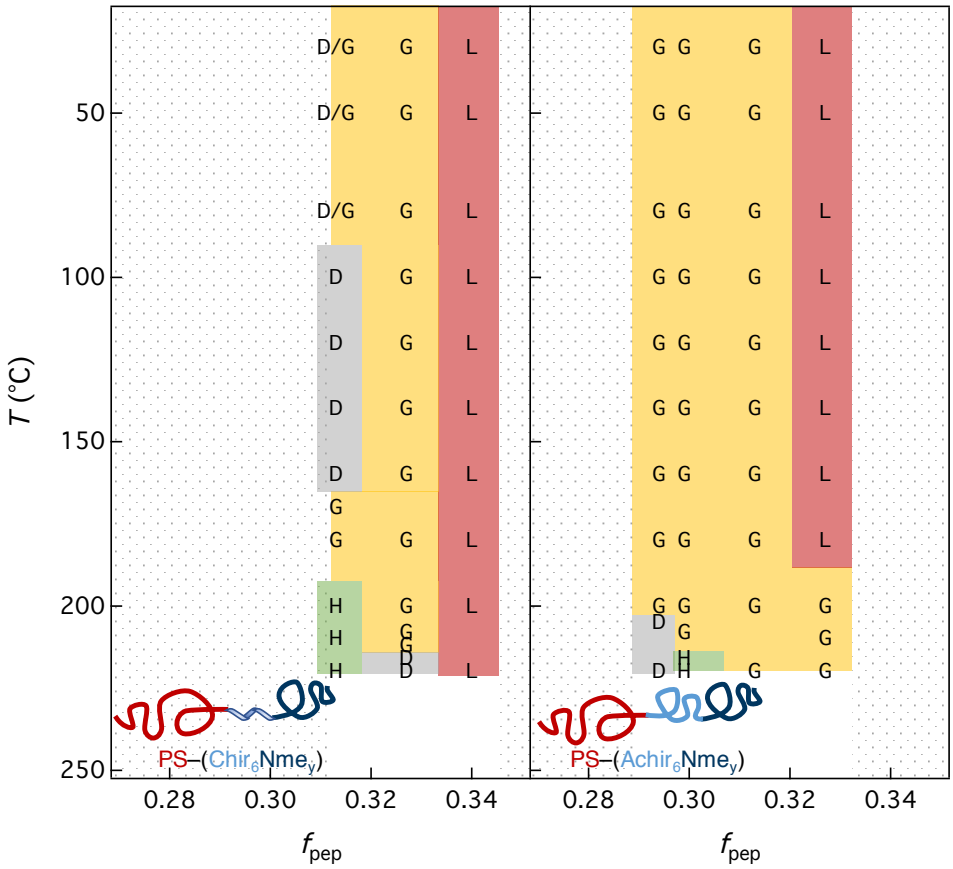

Figure 4.8 *T*–f_{pep} phase diagrams of PS–(Chir$_6$Nme$_y$) and PS–(Achir$_6$Nme$_y$) series
Overall, the PS–(Chir$_6$Nme$_y$) block copolymers have lower transition temperatures than the PS–(Achir$_6$Nme$_y$) series, with an overall smaller double gyroid (G) phase window.

4.6 The interfacial region critical to self-assembled structure is minimal

To further investigate the range of the interfacial region that is critical in determining the self-assembled structure, we modified the interfacial region and synthesized two new block copolymers with the same f_{pep} = 0.299, PS–(Chir$_3$Achir$_3$Nme$_{36}$) and PS–(Achir$_3$Chir$_3$Nme$_{36}$), by flipping the conformation of the two segments (each consists of 3 peptoid units) near the interface. The previous phase diagram for PS–(Chir$_6$Nme$_y$) and PS–(Achir$_6$Nme$_y$), presents HEX/DIS and the G phase at f_{pep} = 0.299, respectively. Here, the G phase forms only in PS–(Achir$_3$Chir$_3$Nme$_{36}$) with a 3-unit coil segment placed immediately next to the interface,

while the PS–(Chir$_3$Achir$_3$Nme$_{36}$) adopts the HEX morphology with a 3-unit helix segment immediately near the interface (Figure 4.9). The overall chain space-filling characteristic is identical within this block copolymer pair, suggesting that the chain conformation right next to the interface is critical to drive the G phase. Meanwhile, it demonstrates that even the conformation change of a smaller segment (of 3 units) is sufficient to drive the morphological change in these block copolymers.

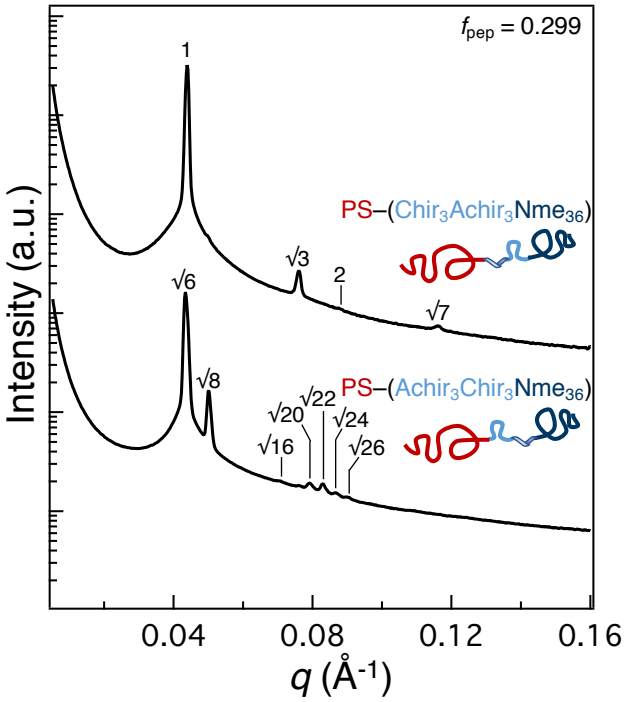

Figure 4.9 Morphology compare of PS–(Chir$_3$Achir$_3$Nme$_{36}$) and PS–(Achir$_3$Chir$_3$Nme$_{36}$) PS–(Chir$_3$Achir$_3$Nme$_{36}$) adopts a hexagonally packed cylinders (HEX) morphology, and PS–(Achir$_3$Chir$_3$Nme$_{36}$) adopts a double gyroid (G) morphology. The two block copolymers have overall identical types and numbers of peptoid units.

4.7 Conclusions

In this work, we demonstrate the role of chain conformation near the interface on the double gyroid (G) phase formation in block copolymers. The differences in space-filling

characteristics and chain flexibility of the interfacial segment, which are mediated via a polypeptoid segment adopting either a helical or coil conformation, impact chain packing in the domains that leads to phase boundary shifts, as well as the configuration freedom of chains that is critical for stabilizing the G phase. Here in the model poly(styrene-*b*-peptoid) block copolymers, the G phase boundaries are shifted towards larger polypeptoid volume fractions (f_{pep}) when a helix segment is placed near the interface, due to the less space-filling feature of the compact helix segment, compared to the chemically analogous coil segment. This space-filling difference between the helix and coil segment is further reflected by the smaller d_{211} spacing formed in block copolymers with a helix segment. More importantly, in the block copolymer series, PS–(Achir$_6$Nme$_y$), with a coil segment near the interface, a broadened G phase window could be accessed compared to the PS–(Chir$_6$Nme$_y$) series, which has a helix segment near the interface. Despite having a larger interaction parameter (χ_{eff}) expected for PS–(Achir$_6$Nme$_y$), which is presumably unfavorable for network phase formation, its broadened G phase window points to the importance of having a flexible segment near the interface. Our results highlight the possibility of tuning and accessing network phases by manipulating chain conformation near the domain interface without chemistry or composition changes, which could be potentially useful to guide block copolymer design with complex mesostructures.

4.8 Acknowledgements

The authors gratefully acknowledge funding from the National Science Foundation (NSF) Division of Materials Research (DMR) Polymers Program (DMR-1608297, Special Creativity Award). This research used resources at the National Synchrotron Light Source II

(a U.S. Department of Energy (DOE) Office of Science User Facility operated for the DOE Office of Science by Brookhaven National Laboratory under Contract DE-SC0012704), and the Advanced Light Source (a U.S. DOE Office of Science User Facility under Contract DE-AC02-05CH11231). We acknowledge the use of shared facilities of the NSF Materials Research Science and Engineering Center (MRSEC) at UC Santa Barbara, DMR-1720256. The UC Santa Barbara MRSEC is a member of the Materials Research Facilities Network. The authors thank Dr. Rachel Behrens (Materials Research Laboratory, UC Santa Barbara) for help with polymer characterization, Dr. Masafumi Fukuto (11-BM, NSLS II, Brookhaven National Laboratory) for assistance with SAXS measurements, and Dr. Ron Zuckermann (Molecular Foundry, Lawrence Berkeley National Laboratory) for discussions regarding polypeptoid synthesis.

Chapter 5

Conclusions and Outlook

This dissertation leverages sequence-defined polypeptoids as a block of tunable chain conformation via controlling the secondary structure, to understand the helical chain conformation and its role in block copolymer self-assembly. We first show polypeptoid helical chains are locally stiffer but more compact than the chemically analogous coil chains. When incorporated into block copolymers, these helical chains alter self-assembly thermodynamics via impacting the free energy contributions from both enthalpic mixing and entropic chain stretching. With the understanding, we further demonstrate chain conformation near the interface could be manipulated to access network morphologies, which are of interest to many technological applications.

Polymer chain conformation underlies most polymer physical properties and impacts a number of polymer functionalities. Therefore, we started with a close look at the chain

conformation of the sequence-defined polypeptoids first. In Chapter 2, comparison between chemically identical helical and coil polypeptoids in dilute solution shows that the helical chains, with the secondary structure driven by steric interactions from the chiral, bulky side chains, are locally stiffer but adopt more compact chain conformations. Further examination of chain conformation response to solvent condition variations indicates this type of sterically defined helical chains is relatively insensitive to solvent quality. This is in drastic contrast to other helical chains (e.g., most helical biopolymers and some synthetic helical polymers), whose conformations are typically sensitive to their surrounding environments including pH, temperature etc. The chain conformation dependence on external conditions could trace back to the driving forces of the secondary structures, as the stabilization mechanism predicts how and how much external conditions will disrupt or facilitate the formation of these secondary structures. In our model system, the nature of the stabilizing interactions (i.e., steric interactions from side chains) likely makes the polymer chains less susceptible to solvent conditions, unless there are factors changing the optimized side chain packing.

Nevertheless, it should be noted that the information on chain conformation so far is from solution studies, while we are hoping to interpret chain conformation effects in bulk polymeric systems. From a polymer physics point of view, chain conformation in dilute solution informs bulk chain conformation to some degree–for example, chain conformation in a θ-solvent is equivalent to that in the melt state. It is most desirable to extract chain conformation in the state of interest, especially for polymer chains with complex structures, as additional intermolecular interactions and particular chain packing may arise when chains come close with each other in the melt state (e.g., change of hydrogen bond from intra-molecular to inter-molecular for polylactide in bulk[25]). The associated challenge lies in

experimental feasibility and/or technique capability to study chain conformation in the melt state. Small-angle neutron scattering is likely the most appropriate technique to probe the relevant length scales of polymer chain conformation, as has been demonstrated in numerous bulk chain conformation studies. However, getting sufficient neutron scattering contrast, typically by deuterium labelling, is still synthetically challenging in our system. Furthermore, the possibility of local alignment of these locally stiff chains in the melt state could lead to low q upturns that will add complexity to data interpretation.

The model systems based on sequence-defined polypeptoids enjoy couple advantages compared to traditional synthetic polymer systems, which allow tunable chain shape by varying only the side chain chirality, making it possible to tease out conformational effects from other complicating factors that are commonly seen in traditional polymers, such as chain length and polydispersity variations between synthesis batches. Chapter 3 establishes model coil–helix and coil–coil block copolymers based on poly(*n*-butyl acrylate-*b*-peptoid) to examine the impact of helical chain conformation on the thermodynamics of self-assembly. We show the helical chain conformation alters order–disorder transitions (ODTs) of these lamellae-forming diblock copolymers (with the coil–helix block copolymers showing lower T_{ODT}s), through two contribution aspects: 1) A smaller enthalpic contribution from the helical block to mixing, supported by a smaller effective Flory–Huggins interaction parameter (χ_{eff}) determined in the disordered state by random phase approximation (RPA); 2) The helical block of the coil–helix block copolymer experiencing larger chain stretching in the lamellar morphology, leading to a larger entropic gain upon disordering. These changes to free energy are closely related to the conformational properties of the helical chains, because adopting a helical secondary structure essentially changes the correlation between

monomers, i.e., from random-walk statistics to local contours defined by helical turns. Consistent with results from solution studies, these helical chains appear to be more compact (smaller R_g) than their coil analogues based on RPA fitting results in the disordered state. Together with the increased local stiffness, the number of contacts between neighboring chains decreases and larger chain stretching is required in order to fill space at constant density within the domains for the coil–helix block copolymer. It is easier to stretch stiffer chains, but only with the prerequisite that the objects of comparison have the same number of segments; here, the helical block has the same number of monomers as the coil counterpart but has fewer segments.

The knowledge of how helical chain conformation impacts self-assembly thermodynamics from the relatively simple lamellar geometry provides insights to design block copolymers using chain conformation as a tool to tune self-assembly. In Chapter 4, we highlight the feasibility of tuning and accessing network phases by manipulating chain conformation near the interface, a region carefully chosen because it hosts most segmental mixing between dissimilar blocks and the geometric feature of the interface impacts the overall free energy. We show that by having a small helix segment (of 6 peptoid units) near the interface, the double gyroid network phase boundaries are shifted towards larger polypeptoid volume fractions due to the less space-filling feature of the compact helix segment, and the double gyroid phase occupies a smaller window in the phase diagram. Despite a smaller interaction parameter (χ_{eff}) expected by having a helix segment near the interface, which is presumably favorable for network phase formation, it points to the importance of having a flexible interfacial segment to stabilize the double gyroid phase that requires a delicate balance between interfacial tension and chain packing.

An important question is the universality of the conclusions and design rules learned in these studies. It is important to note that the helical chains here are highly flexible with persistence lengths ~ 1 nm, which are nowhere near rod-like. Yet many commonly seen helical chains are much stiffer (e.g., peptide α-helix, poly(*n*-hexyl isocyanate)) and almost certainly have alignment interactions in bulk. We expect similar types of sterically induced helices that do not involve specific interactions such as hydrogen-bonding and crystallinity, and are only locally stiff to have similar behaviors in impacting block copolymer self-assembly. There are also questions yet to be answered: When does a polymer chain is categorized as flexible, semiflexible, or rod-like? When do alignment interactions start to appear or dominate the phase behaviors? The ratio of contour length (L_C) to persistence length (l_p) is useful to define whether a polymer chain is flexible (typically flexible polymer chains are expected to have $L_C/l_p > 10$), while alignment interactions may directly correlate with the absolute value of l_p–a very long DNA molecule can be categorized as a flexible chain overall, but local alignment interactions will likely still present considering its large l_p ~ 60 nm, and the boundary between flexible and semiflexible is blurred at this point.

One obvious limitation of sequence-defined polypeptoids is the relatively short chain lengths accessible. Direct synthesis of long polypeptoids is limited by the reaction efficiency of each step in the solid-phase synthesis, and has been limited to below 100-mers (~ 15 kDa). The molecular weight limitation largely prohibited studies to look at scaling behaviors with respect to chain length in these sequence-defined polypeptoids. It also limited studies on self-assembly of block copolypeptoids in bulk (though not without examples[86, 161]) since the chemical incompatibilities come only from side chains and therefore longer chains are needed to get sufficient segregation strength (χN). Yet polypeptoids, as highly-controlled

polymer blocks and when conjugated with traditional synthetic polymers, provide unique opportunities to answer some of the fundamental questions in block copolymer self-assembly.

There is still unexplored space in melt self-assembly of block copolymers using sequence-defined polypeptoids. First, polypeptoid-containing block copolymers are systems that could probably enable continuous tuning of flexibility. Side chains with different architectures, e.g., linear, branched, and multiple branched, could be incorporated with designated sequences to tune chain stiffness, while keeping chemistry constant and avoiding polydispersity effects. The helical secondary structure could also be further tuned through monomer sequence, as the stabilization of helical conformations, which correlates with local chain stiffness, has been shown to depend on specific sequences.[60] There are also different types of side chains that promote the formation of helical secondary structures in polypeptoids, with the *cis*/*trans* ratio of backbone configurations dictating the relative stiffness.[59] While this involves changes in side chain chemistry, it may be possible to capture the transition point where alignment interactions start to appear as stiffer helices are induced in the polypeptoid block. Furthermore, polypeptoids may provide opportunities to investigate the formation mechanism of symmetry-breaking sphere phases (e.g., Frank–Kasper phases). Conformational asymmetry, chain length dispersity, which are proposed as stabilizing factors, could be systematically examined using polypeptoid blocks with precisely tuned space-filling features and chain length dispersity.

Beyond the arena of block copolymer melt self-assembly, polypeptoids are potentially useful in addressing questions in a number of other fields. Solution self-assembly of block copolymers is another major research direction as the hierarchical structures formed could

find a variety of applications. The hierarchically self-assembled structures are determined via the interplay between multiple interactions (e.g., polymer–solvent interactions, electrostatics, hydrogen-bonding, aromatic interactions, and geometric factors) across different length scales. Various types of structures have been readily reported from solution self-assembly in polypeptoid systems[172-175] and we anticipate polypeptoids to be ideal candidates to systematically study the mechanisms and establish rules to guide the design of polymer materials with well-controlled structures in solution. While natural peptides/proteins are limited to the 20 naturally occurring amino acids, polypeptoids possess a larger library of submonomers, with available side chains ranging from aliphatic, aromatic, to ionic, heterocyclic, and chiral. The variety of functionalities available makes polypeptoids attractive in exploring designs for other material applications such as using polypeptoids as binding ligands to separate out heavy metal contaminants,[176] employing polypeptoids as polyelectrolytes to study structure–conductivity relationships,[177] for which a study has been initiated under the frame of this dissertation to look at precise ion placement on the morphology of ion aggregates, block copolymers, and the corresponding ionic conductivities (see Appendix).

We provide the final perspective by considering polypeptoids as bioinspired macromolecules that bridge between biology and polymer science. While a major challenge in synthetic polymer design is to replicate the complexity of biopolymers, and to hierarchically control structures across length scales starting from the primary monomer sequence, appropriate simplification of such complexity or encoding more structural information in originally simple polymers, is likely the correct direction to elucidate some of the common principles shared by biological and synthetic systems. Polypeptoids appear to be

at the right position, which retain the precision, perfection and well-controlled features of biopolymers, and are devoid of complicating factors like backbone chirality and hydrogen-bonding. One of the intriguing problems is the chirality transfer across length scales in both chiral and achiral, biological and synthetic systems,[178-179] and there are opportunities with carefully designed polypeptoids to address questions including homochiral evolution and breaking of symmetry that lies at the mechanistic origin of life.

Overall, we have made significant advances in fundamentally understanding chain conformation effects on the self-assembly thermodynamics of block copolymers. By precisely manipulating chain conformation through sequence-defined polypeptoids, we decoupled chain conformation effects from other contributing factors, and achieved tuning the self-assembled structures via chain conformation. We hope this dissertation provides insights on block copolymer self-assembly from a molecular level understanding of polymer chain conformation, and establish some design rules between primary and secondary structures to mesoscale structures in polymer materials.

Appendix

A Model Block Copolymer System for Precise Ion Placement

A1. Introduction

Solid polymer electrolytes are promising alternatives to organic liquid electrolytes in battery applications with its safety, mechanical and chemical stability, and broader tunability. Since the discovery of ion conduction in polymers, there are numerous studies looking at ion conduction mechanism in polymer electrolytes, which is primarily governed by ion concentration and ion mobility–factors that are impacted by the highly convoluted interactions between cation, anion, and the polymer.[180-183]

One important property for electrochemical devices is the mechanical robustness, of which homopolymers only have a limited range to tune. A new category of polymeric

materials therefore has evolved as ion-containing block copolymers, which allow tuning orthogonal properties to achieve both high mechanical strength and high ionic conductivity with careful design of the consisting blocks. With the capability of block copolymers to microphase separate, the self-assembly thermodynamics, morphology and ionic conductivity become interconnected factors, and unique structure–conductivity relationships exist in ion-containing block copolymers. For example, the ionic conductivity has been shown to have a distinct molecular weight dependence in block copolymers, which is related to the conductive domain thickness.[184-186] Incorporation of ions (tethered ions or salt doped) also modifies the Flory–Huggins interaction parameter (χ), which is shown to be related to the effective charge carrier concentration.[187-189] Furthermore, the particular morphology adopted by the block copolymer also impacts ion transport through modulating the conductive pathway.[138, 140, 190]

Ion diffusivity in ion-containing block copolymers is closely related to the interfacial zone, and the local connectivity of ions.[186, 191] Further interesting topics arise such as how the charged block location (in multi-block copolymers), or how the exact ion placement within the ion-containing block, impacts ionic conductivity in block copolymers. In this study, we aim to establish a model block copolymer system utilizing sequence-defined polypeptoids, which will enable the ions to be precisely located on the designated monomers (either as single-ion conductors or with salt-doping, Figure A1). Upon the successful establishment of the model block copolymer system, we propose to examine how precise ion placement impacts ion aggregates morphology, block copolymer self-assembly, and ionic conductivities. In conjunction with theoretic studies, we hope to reveal the structure–property relationship in ion-containing block copolymers starting from the monomer length scale.

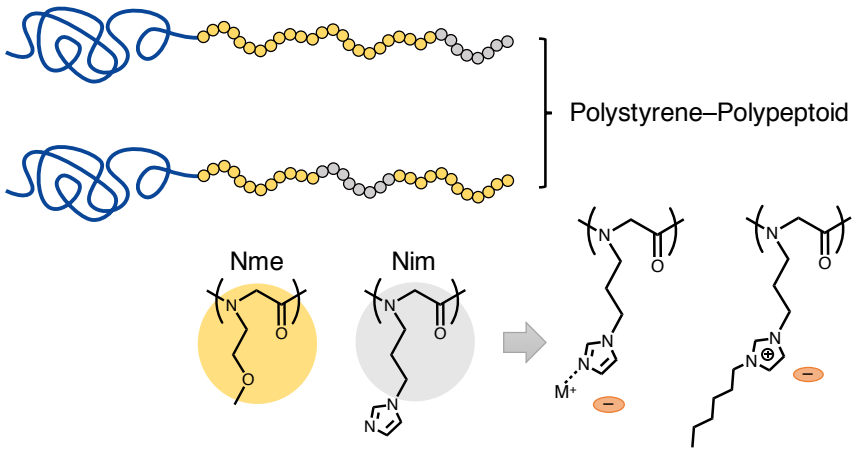

Figure A1. Proposed model system with an imidazole-containing polypeptoid block
The pendant imidazole side chains can be quaternized to act as cations, or coordinate with metal ions as ligands when doped with salt.

A2. Experiment Methods

A2.1 Materials

Solvents and reagents were purchased from commercial suppliers and used without further purification, unless otherwise noted. Styrene monomer and ligand *N,N,N′,N′,N″*-pentamethyldiethylenetriamine (PMDETA) were filtered through basic alumina before use. Anhydrous dimethylformamide (DMF), and *N*,*N*-diisopropylethylamine (DIPEA) were used for synthesis of block copolymers.

A2.2 Synthesis of polypeptoids with unprotected heterocyclic side chains

Polypeptoids were synthesized on a custom robotic synthesizer using commercially available amine submonomers. Rink amide resin (100-200 mesh, Novabiochem) with intermediate loading (~ 0.50 mmol g^{-1}) was used. Synthesis steps are the same as described in previous chapters, with the following modifications of synthesis conditions: Acylation:

chloroacetic acid (7.5 equiv., 0.375 M in DMF) and diisopropylcarbodiimide (DIC, 9.1 equiv., 43 % v/v in DMF) were added and mixed for 5 min. Nucleophilic displacement: Amine (2-methoxyethylamine or 1-(3-aminopropyl)imidazole, 38 equiv., 2 M in N-methyl-2-pyrrolidone (NMP)) was added and mixed for 1 h. An additional unit was added in the same method with propargylamine to give the alkyne end group after the desired sequence. The chain end was finally acetylated using a mixture of 0.4 M acetic anhydride and 0.4 M pyridine in DMF (3.5 mL for 100 μmol scale) for 30 min.

Polypeptoids were cleaved from the resin using a cleavage cocktail of trifluoroacetic acid (TFA) in dichloromethane (DCM) (1:1 v/v with another 2.5 % HPLC grade water) for 10 min. The resin was filtered and rinsed with more cleavage cocktail. The collected solution was dried *in vacuo* and lyophilized from acetonitrile (ACN) : water (H_2O) (1:1 v/v) to yield the dried product.

A2.3 Synthesis of poly(styrene-b-peptoid) block copolymers

Azide-terminated polystyrene was synthesized as described in 4.3.3. Alkyne-terminated polypeptoid (60–70 mg, 1 equiv.) and azide-terminated polystyrene (2 equiv.) were dissolved in 2 mL of anhydrous DMF in a scintillation vial. *N,N*-diisopropylethylamine (DIPEA, 10 equiv.) and PMDETA (5 equiv.) were added, and the reaction mixture was sparged with nitrogen for 45 min. In an oven-dried Schlenk flask, Cu(I)Br (5 equiv.) and ascorbic acid (6 equiv.) were added, and the flask was evacuated and refilled with nitrogen three times. The sparged reaction mixture was added to the Schlenk flask with a degassed syringe and then further degassed with three freeze–pump–thaw cycles. The reaction was allowed to react under static vacuum at 50 °C for ~ 40 h. Upon completion of the reaction, the solution was

diluted with DMF. Basic alumina was added to the solution and stirred for 15 min. The mixture was then filtered to remove most of the copper compounds. More basic alumina was added to the filtered solution and stirred for 3–4 h before the second filtration to remove the residue copper compounds. The collected solution was dried *in vacuo*, dissolved in THF (~ 125 mg mL^{-1}), and precipitated into a hexane : cyclohexane (3:2, v/v) mixture to remove excess polystyrene. The precipitate was isolated by centrifugation and dried *in vacuo* at 50 °C overnight.

A2.4 Gel permeation chromatography (GPC)

The molecular weight of polystyrene was measured on a Waters Alliance HPLC system with an e2695 separation module using an Agilent PLgel 5 μm MiniMIX-D column with tetrahydrofuran (THF) as the eluent. Refractive index traces from a Waters 2414 differential refractive index detector were used for molecular weight determination using polystyrene calibration standards (Agilent Technologies).

A2.5 Matrix-assisted laser desorption/ionization with time-of-flight (MALDI-TOF) mass spectrometry

MALDI-TOF MS was performed on a Bruker Microflex LRF MALDI TOF mass spectrometer. Sample solutions were prepared by dissolving polypeptoids in ACN : H_2O (1:1, v/v) at ~ 1 mg mL^{-1} concentration, click reaction products in THF at ~ 1 mg mL^{-1} concentration. α-Cyano-4-hydroxycinnamic acid in ACN : H_2O (1:2, v/v) (~ 10 mg mL^{-1}, saturated) was used as matrix for polypeptoid samples, and 20 mg mL^{-1} *trans*-2-[3-(4-*tert*-butylpheny)-2-methyl-2-propenylidene]malonitrile (DCTB) in THF with silver

trifluoroacetate (AgTFA) added at ~ 1 mg mL^{-1} was used for polystyrene-containing materials. 5 μL sample solution was combined with 5 μL matrix and matrix–sample mixtures were spotted onto a polished steel MALDI target plate (Bruker). Mass spectra were collected in either reflectron or linear mode with appropriate mass ranges. Mass peaks were calibrated against peptide and protein standards (Bruker).

A2.6 Small-Angle X-ray Scattering (SAXS)

Dry block copolymers were loaded into a Kapton-lined aluminum washer. Samples were annealed at reduced pressure (3×10^{-8} Torr) at 150 °C for ~12 h, then annealed at 130 °C for 24 h. After slowly cooling to room temperature, the washers were sealed with Kapton under ambient conditions. SAXS measurements were performed at the National Synchrotron Light Source II (NSLS II, beamline 11-BM, Brookhaven National Laboratory) with an X-ray energy of 13.5 keV. Exposure time was 30 s. The scattering data were calibrated with silver behenate standards, reduced using circular averaging of the 2D scattering pattern.

A3. Preliminary Results and Discussion

In solid polymer electrolytes, cations that form labile bonds with a polymer can have significant contributions to the ionic conductivity through the ion–polymer association, and kinetically labile metal–ligand coordination is one of the examples.[192] Imidazole and histidine moieties are of particular interest due to their ability to interact with transition metal ions,[193] and have been readily incorporated into polymers either as ligands or as backbone components.[194-196] Here we seek to incorporate imidazole moieties into polypeptoids as

pendant side chains, and subsequently into block copolymers to study the precise placement of metal–ligand coordination sites on ion transport in block copolymer electrolytes.

While solid-phase submonomer method has been successful to incorporate a variety of side chains into polypeptoids, unprotected heterocyclic nitrogen-containing side chains usually lead to side product formation and poor synthetic yields. In this study, we followed the reported modifications to the solid-phase synthesis conditions: bromoacetic acid was replaced with the less labile chloroacetic acid, and acylation reagent concentration and acylation time were reduced, to increase the selectivity between the acylation and the unwanted alkylation of the heterocyclic side chains. Further, to compensate for the lower reactivity of the less labile chloride, amine concentration was increased to 2 M in NMP in the displacement step.[197] Polypeptoids with 25 % of the repeat units bearing imidazole side chains (8 consecutive Nim units in 32-mers) at different locations were synthesized with reasonably good purity (Figure A2).

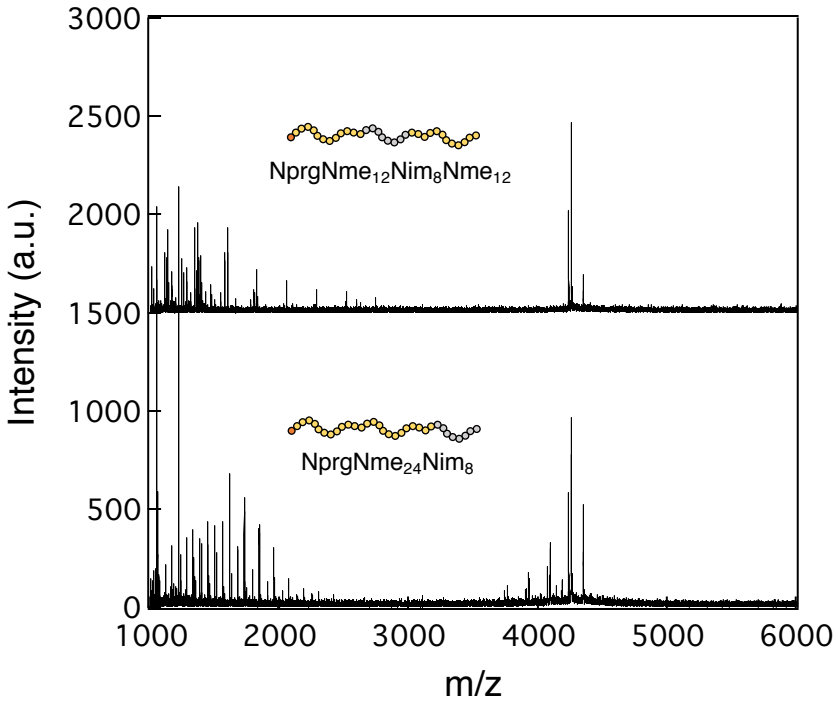

Figure A2. MALDI-TOF of imidazole-containing polypeptoids
Nprg: *N*-(propargyl)glycine, Nme: *N*-(2-methoxyethyl)glycine, Nim: *N*-(1H-imidazole-1-propan)glycine

The presence of imidazole side chains (and their relative location from the alkyne end of polypeptoids) was shown to affect the azide–alkyne click reaction, leading to low reaction efficiencies compared to previous click reactions with polypeptoids that are devoid of heterocyclic side chains (~ 10 % vs. ~ 56 % yield based on the product mass after precipitation). Block copolymer species were detected in MALDI, together with unreacted homopolymer species after preliminary purifications (Figure A3). It is likely the imidazole side chains of polypeptoids are coordinating with the catalyst, Cu^{+} (although Cu(I)Br was added in excess), and therefore lowered the click reaction efficiency. Other types of click chemistries, or synthetic strategies such as esterification, are worth exploring for these imidazole-containing polypeptoids.[198-200]

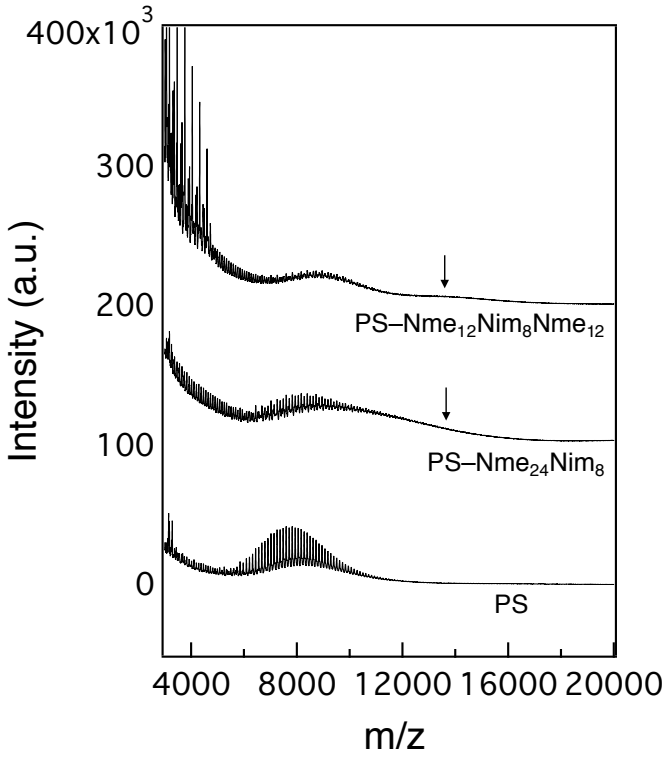

Figure A3. MALDI-TOF of products from click reactions of polystyrene and polypeptoids
The major peaks in click reaction products shifted to slightly larger masses compared to the polystyrene homopolymer, which are likely polystyrene residue from the first precipitation step. The broad shoulders (indicated by arrows) in the higher mass range are likely block copolymers, which are poorly ionized due to the presence of the polypeptoid block.

The amount of block copolymers (f_{pep} ~ 0.4) presented in the preliminarily purified products still induced self-assembly, with PS–$Nme_{12}Nim_8Nme_{12}$ adopting a lamellar morphology and PS–$Nme_{24}Nim_8$ adopting a hexagonally packed cylinder morphology (Figure A4). Further purification is desired to identify the self-assembly morphology of neat block copolymers, and for later salt-doping or quaternization to obtain ion-containing block copolymers.

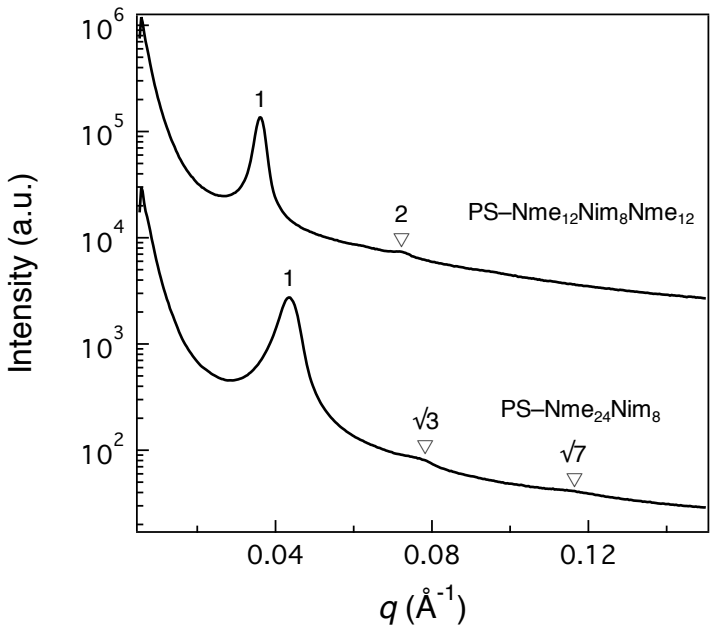

Figure A4. SAXS of preliminarily purified click reaction products
PS–Nme$_{12}$Nim$_8$Nme$_{12}$ exhibits a lamellar morphology while PS–Nme$_{24}$Nim$_8$ shows a hexagonally packed cylinder morphology. These preliminarily purified products likely contain unreacted homopolymers.

A4. Conclusions and Outlook

In establishing a model block copolymer system that allows precise placement of ions or metal–ligand coordination sites, we successfully synthesized sequence-defined polypeptoids with 25% of the repeat units bearing unprotected heterocyclic nitrogen-containing side chains. Attempts were made to obtain block copolymers from azide–alkyne click reactions, while optimization to increase reaction efficiency is needed or other synthesis strategies to conjugate polypeptoids with polystyrene may be further explored. Sequence-defined polypeptoids are demonstrated as a potential candidate to study fundamental structure–conductivity relationships in ion-containing block copolymers that will provide insight on designing solid polymer electrolytes.

References

1. Bates, F. S.; Fredrickson, G. H., Block copolymers - Designer soft materials. *Phys. Today* **1999,** *52* (2), 32-38.

2. Bates, F. S.; Fredrickson, G. H., Block Copolymer Thermodynamics - Theory and Experiment. *Annu. Rev. Phys. Chem.* **1990,** *41*, 525-557.

3. Leibler, L., Theory of Microphase Separation in Block Copolymers. *Macromolecules* **1980,** *13* (6), 1602-1617.

4. Matsen, M. W., Effect of Architecture on the Phase Behavior of AB-Type Block Copolymer Melts. *Macromolecules* **2012,** *45* (4), 2161-2165.

5. Cochran, E. W.; Garcia-Cervera, C. J.; Fredrickson, G. H., Stability of the gyroid phase in diblock copolymers at strong segregation. *Macromolecules* **2006,** *39* (12), 4264-4264.

6. Bates, F. S.; Schulz, M. F.; Khandpur, A. K.; Förster, S.; Rosedale, J. H.; Almdal, K.; Mortensen, K., Fluctuations, conformational asymmetry and block copolymer phase behaviour. *Faraday Discuss.* **1994,** *98* (0), 7-18.

7. Helfand, E.; Wasserman, Z. R., Block Copolymer Theory. 4. Narrow Interphase Approximation. *Macromolecules* **1976,** *9* (6), 879-888.

8. Helfand, E.; Wasserman, Z. R., Block Copolymer Theory. 5. Spherical Domains. *Macromolecules* **1978,** *11* (5), 960-966.

9. Helfand, E.; Wasserman, Z., Block Copolymer Theory. 6. Cylindrical Domains. *Macromolecules* **1980,** *13* (4), 994-998.

10. Hiemenz, P. C.; Lodge, T. P., *Polymer Chemistry*. CRC Press: **2007**.

11. Bates, F. S.; Fredrickson, G. H., Conformational Asymmetry and Polymer-Polymer Thermodynamics. *Macromolecules* **1994,** *27* (4), 1065-1067.

12. Bates, F. S.; Schulz, M. F.; Rosedale, J. H.; Almdal, K., Correlation of binary polyolefin phase behavior with statistical segment length asymmetry. *Macromolecules* **1992,** *25* (20), 5547-5550.

13. Fredrickson, G. H.; Liu, A. J.; Bates, F. S., Entropic Corrections to the Flory-Huggins Theory of Polymer Blends: Architectural and Conformational Effects. *Macromolecules* **1994,** *27* (9), 2503-2511.

14. Almdal, K.; Hillmyer, M. A.; Bates, F. S., Influence of conformational asymmetry on polymer-polymer interactions: An entropic or enthalpic effect? *Macromolecules* **2002,** *35* (20), 7685-7691.

15. Lee, S.; Bluemle, M. J.; Bates, F. S., Discovery of a Frank-Kasper σ Phase in Sphere-Forming Block Copolymer Melts. *Science* **2010,** *330* (6002), 349.

16. Lee, S.; Leighton, C.; Bates, F. S., Sphericity and symmetry breaking in the formation of Frank–Kasper phases from one component materials. *Proc. Natl. Acad. Sci. U.S.A.* **2014,** *111* (50), 17723.

17. Schulze, M. W.; Lewis, R. M.; Lettow, J. H.; Hickey, R. J.; Gillard, T. M.; Hillmyer, M. A.; Bates, F. S., Conformational Asymmetry and Quasicrystal Approximants in Linear Diblock Copolymers. *Phys. Rev. Lett.* **2017,** *118* (20), 207801.

18. Singh, C.; Goulian, M.; Liu, A. J.; Fredrickson, G. H., Phase Behavior of Semiflexible Diblock Copolymers. *Macromolecules* **1994,** *27* (11), 2974-2986.

19. Matsen, M. W.; Barrett, C., Liquid-crystalline behavior of rod-coil diblock copolymers. *J. Chem. Phys.* **1998,** *109* (10), 4108-4118.

20. Pryamitsyn, V.; Ganesan, V., Self-assembly of rod–coil block copolymers. *J. Chem. Phys.* **2004,** *120* (12), 5824-5838.

21. Mao, S.; MacPherson, Q.; Spakowitz, A. J., Polymer Semiflexibility Induces Nonuniversal Phase Transitions in Diblock Copolymers. *Phys. Rev. Lett.* **2018,** *120* (6), 067802.

22. Kumar, N. A.; Ganesan, V., Communication: Self-assembly of semiflexible-flexible block copolymers. *J. Chem. Phys.* **2012,** *136* (10), 101101.

23. Leigh, T.; Fernandez-Trillo, P., Helical polymers for biological and medical applications. *Nat. Rev. Chem.* **2020,** *4* (6), 291-310.

24. Rosales, A. M.; Murnen, H. K.; Kline, S. R.; Zuckermann, R. N.; Segalman, R. A., Determination of the persistence length of helical and non-helical polypeptoids in solution. *Soft Matter* **2012,** *8* (13), 3673-3680.

25. Suzuki, Y.; Watanabe, T.; Kosugi, H.; Ueda, K.; Kikuchi, M.; Narumi, A.; Kawaguchi, S., Chain Conformation of Poly(D-lactide) in Tetrahydrofuran by Static Light Scattering, Small-Angle X-ray Scattering, and Intrinsic Viscosity. *Macromolecules* **2020,** *53* (5), 1604-1612.

26. Davidson, E. C.; Rosales, A. M.; Patterson, A. L.; Russ, B.; Yu, B.; Zuckermann, R. N.; Segalman, R. A., Impact of Helical Chain Shape in Sequence-Defined Polymers on Polypeptoid Block Copolymer Self-Assembly. *Macromolecules* **2018,** *51* (5), 2089-2098.

27. Klok, H. A.; Lecommandoux, S., Supramolecular Materials via Block Copolymer Self-Assembly. *Adv. Mater.* **2001,** *13* (16), 1217-1229.

28. Mao, G.; Ober, C. K., Block copolymers containing liquid crystalline segments. *Acta Polym.* **1997,** *48* (10), 405-422.

29. Chen, J. T.; Thomas, E. L.; Ober, C. K.; Hwang, S. S., Zigzag Morphology of a Poly(styrene-b-hexyl isocyanate) Rod-Coil Block Copolymer. *Macromolecules* **1995,** *28* (5), 1688-1697.

30. Chen, J. T.; Thomas, E. L.; Ober, C. K.; Mao, G. p., Self-Assembled Smectic Phases in Rod-Coil Block Copolymers. *Science* **1996,** *273* (5273), 343.

31. Ho, R.-M.; Chiang, Y.-W.; Tsai, C.-C.; Lin, C.-C.; Ko, B.-T.; Huang, B.-H., Three-Dimensionally Packed Nanohelical Phase in Chiral Block Copolymers. *J. Am. Chem. Soc.* **2004,** *126* (9), 2704-2705.

32. Ho, R.-M.; Chiang, Y.-W.; Chen, C.-K.; Wang, H.-W.; Hasegawa, H.; Akasaka, S.; Thomas, E. L.; Burger, C.; Hsiao, B. S., Block Copolymers with a Twist. *J. Am. Chem. Soc.* **2009,** *131* (51), 18533-18542.

33. Ho, R.-M.; Li, M.-C.; Lin, S.-C.; Wang, H.-F.; Lee, Y.-D.; Hasegawa, H.; Thomas, E. L., Transfer of Chirality from Molecule to Phase in Self-Assembled Chiral Block Copolymers. *J. Am. Chem. Soc.* **2012,** *134* (26), 10974-10986.

34. Ho, R.-M.; Chiang, Y.-W.; Lin, S.-C.; Chen, C.-K., Helical architectures from self-assembly of chiral polymers and block copolymers. *Prog. Polym. Sci.* **2011,** *36* (3), 376-453.

35. Rubinstein, M.; Colby, R. H., *Polymer Physics*. Oxford University Press: New York, **2003**.

36. He, Z.; Yang, X.; Zhao, D., Numerical estimation of unperturbed dimensions of regioirregular poly(3-ethylthiophene)s. *Macromol. Theory Simul.* **1995,** *4* (2), 277-288.

37. Yamamoto, T.; Komarudin, D.; Arai, M.; Lee, B.-L.; Suganuma, H.; Asakawa, N.; Inoue, Y.; Kubota, K.; Sasaki, S.; Fukuda, T.; Matsuda, H., Extensive Studies on π-Stacking of Poly(3-alkylthiophene-2,5-diyl)s and Poly(4-alkylthiazole-2,5-diyl)s by Optical

Spectroscopy, NMR Analysis, Light Scattering Analysis, and X-ray Crystallography. *J. Am. Chem. Soc.* **1998,** *120* (9), 2047-2058.

38. Adachi, T.; Brazard, J.; Ono, R. J.; Hanson, B.; Traub, M. C.; Wu, Z.-Q.; Li, Z.; Bolinger, J. C.; Ganesan, V.; Bielawski, C. W.; Vanden Bout, D. A.; Barbara, P. F., Regioregularity and Single Polythiophene Chain Conformation. *J. Phys. Chem. Lett.* **2011,** *2* (12), 1400-1404.

39. McCulloch, B.; Ho, V.; Hoarfrost, M.; Stanley, C.; Do, C.; Heller, W. T.; Segalman, R. A., Polymer Chain Shape of Poly(3-alkylthiophenes) in Solution Using Small-Angle Neutron Scattering. *Macromolecules* **2013,** *46* (5), 1899-1907.

40. Gettinger, C. L.; Heeger, A. J.; Drake, J. M.; Pine, D. J., A photoluminescence study of poly(phenylene vinylene) derivatives: The effect of intrinsic persistence length. *J. Chem. Phys.* **1994,** *101* (2), 1673-1678.

41. Nakano, T.; Okamoto, Y., Synthetic Helical Polymers: Conformation and Function. *Chem. Rev.* **2001,** *101* (12), 4013-4038.

42. Chou, P. Y.; Fasman, G. D., Conformational parameters for amino acids in helical, β-sheet, and random coil regions calculated from proteins. *Biochemistry* **1974,** *13* (2), 211-222.

43. Bonduelle, C., Secondary structures of synthetic polypeptide polymers. *Polym. Chem.* **2018,** *9* (13), 1517-1529.

44. Wang, Z.-G., 50th Anniversary Perspective: Polymer Conformation—A Pedagogical Review. *Macromolecules* **2017,** *50* (23), 9073-9114.

45. Stuart, M. A. C.; Huck, W. T. S.; Genzer, J.; Müller, M.; Ober, C.; Stamm, M.; Sukhorukov, G. B.; Szleifer, I.; Tsukruk, V. V.; Urban, M.; Winnik, F.; Zauscher, S.;

Luzinov, I.; Minko, S., Emerging applications of stimuli-responsive polymer materials. *Nat. Mater.* **2010,** *9* (2), 101-113.

46. Lau, K. F.; Dill, K. A., A lattice statistical mechanics model of the conformational and sequence spaces of proteins. *Macromolecules* **1989,** *22* (10), 3986-3997.

47. Khokhlov, A. R.; Khalatur, P. G., Conformation-Dependent Sequence Design (Engineering) of AB Copolymers. *Phys. Rev. Lett.* **1999,** *82* (17), 3456-3459.

48. Murnen, H. K.; Khokhlov, A. R.; Khalatur, P. G.; Segalman, R. A.; Zuckermann, R. N., Impact of Hydrophobic Sequence Patterning on the Coil-to-Globule Transition of Protein-like Polymers. *Macromolecules* **2012,** *45* (12), 5229-5236.

49. Bloksma, M. M.; Rogers, S.; Schubert, U. S.; Hoogenboom, R., Secondary structure formation of main-chain chiral poly(2-oxazoline)s in solution. *Soft Matter* **2010,** *6* (5), 994-1003.

50. Kramer, J. R.; Deming, T. J., Glycopolypeptides via Living Polymerization of Glycosylated-l-lysine N-Carboxyanhydrides. *J. Am. Chem. Soc.* **2010,** *132* (42), 15068-15071.

51. Lu, H.; Wang, J.; Bai, Y.; Lang, J. W.; Liu, S.; Lin, Y.; Cheng, J., Ionic polypeptides with unusual helical stability. *Nat. Commun.* **2011,** *2* (1), 206.

52. Zuckermann, R. N.; Kerr, J. M.; Kent, S. B. H.; Moos, W. H., Efficient method for the preparation of peptoids [oligo(N-substituted glycines)] by submonomer solid-phase synthesis. *J. Am. Chem. Soc.* **1992,** *114* (26), 10646-10647.

53. Figliozzi, G. M.; Goldsmith, R.; Ng, S. C.; Banville, S. C.; Zuckermann, R. N., [25] Synthesis of N-substituted glycine peptoid libraries. *Methods Enzymol.* **1996**, *267*, 437-447.

54. Xuan, S.; Zuckermann, R. N., Engineering the atomic structure of sequence-defined peptoid polymers and their assemblies. *Polymer* **2020,** *202*, 122691.

55. Wu, C. W.; Sanborn, T. J.; Zuckermann, R. N.; Barron, A. E., Peptoid oligomers with alpha-chiral, aromatic side chains: Effects of chain length on secondary structure. *J. Am. Chem. Soc.* **2001,** *123* (13), 2958-2963.

56. Armand, P.; Kirshenbaum, K.; Falicov, A.; Dunbrack, R. L.; Dill, K. A.; Zuckermann, R. N.; Cohen, F. E., Chiral N-substituted glycines can form stable helical conformations. *Fold. Des.* **1997,** *2* (6), 369-375.

57. Kirshenbaum, K.; Barron, A. E.; Goldsmith, R. A.; Armand, P.; Bradley, E. K.; Truong, K. T. V.; Dill, K. A.; Cohen, F. E.; Zuckermann, R. N., Sequence-specific polypeptoids: A diverse family of heteropolymers with stable secondary structure. *Proc. Natl. Acad. Sci. U.S.A.* **1998,** *95* (8), 4303-4308.

58. Wu, C. W.; Kirshenbaum, K.; Sanborn, T. J.; Patch, J. A.; Huang, K.; Dill, K. A.; Zuckermann, R. N.; Barron, A. E., Structural and spectroscopic studies of peptoid oligomers with alpha-chiral aliphatic side chains. *J. Am. Chem. Soc.* **2003,** *125* (44), 13525-13530.

59. Stringer, J. R.; Crapster, J. A.; Guzei, I. A.; Blackwell, H. E., Extraordinarily Robust Polyproline Type I Peptoid Helices Generated via the Incorporation of alpha-Chiral Aromatic N-1-Naphthylethyl Side Chains. *J. Am. Chem. Soc.* **2011,** *133* (39), 15559-15567.

60. Wu, C. W.; Sanborn, T. J.; Huang, K.; Zuckermann, R. N.; Barron, A. E., Peptoid oligomers with alpha-chiral, aromatic side chains: Sequence requirements for the formation of stable peptoid helices. *J. Am. Chem. Soc.* **2001,** *123* (28), 6778-6784.

61. Shin, H.-M.; Kang, C.-M.; Yoon, M.-H.; Seo, J., Peptoid helicity modulation: precise control of peptoid secondary structures via position-specific placement of chiral monomers. *Chem. Comm.* **2014,** *50* (34), 4465-4468.

62. Crapster, J. A.; Guzei, I. A.; Blackwell, H. E., A Peptoid Ribbon Secondary Structure. *Angew. Chem. Int. Ed.* **2013,** *52* (19), 5079-5084.

63. Gorske, B. C.; Mumford, E. M.; Gerrity, C. G.; Ko, I., A Peptoid Square Helix via Synergistic Control of Backbone Dihedral Angles. *J. Am. Chem. Soc.* **2017,** *139* (24), 8070-8073.

64. Kaminker, R.; Kaminker, I.; Gutekunst, W. R.; Luo, Y.; Lee, S.; Niu, J.; Han, S.; Hawker, C. J., Tuning conformation and properties of peptidomimetic backbones through dual N/Cα-substitution. *Chem. Comm.* **2018,** *54* (41), 5237-5240.

65. Semenov, A. N., Contribution to the theory of microphase layering in block-copolymer melts. *Sov. Phys. JETP* **1985,** *61* (4), 733–742.

66. Semenov, A. N., Theory of block copolymer interfaces in the strong segregation limit. *Macromolecules* **1993,** *26* (24), 6617-6621.

67. Hashimoto, T.; Shibayama, M.; Kawai, H., Domain-Boundary Structure of Styrene-Isoprene Block Copolymer Films Cast from Solution. 4. Molecular-Weight Dependence of Lamellar Microdomains. *Macromolecules* **1980,** *13* (5), 1237-1247.

68. Hasegawa, H.; Tanaka, H.; Yamasaki, K.; Hashimoto, T., Bicontinuous microdomain morphology of block copolymers. 1. Tetrapod-network structure of polystyrene-polyisoprene diblock polymers. *Macromolecules* **1987,** *20* (7), 1651-1662.

69. Fredrickson, G. H.; Helfand, E., Fluctuation effects in the theory of microphase separation in block copolymers. *J. Chem. Phys.* **1987,** *87* (1), 697-705.

70. Lynd, N. A.; Meuler, A. J.; Hillmyer, M. A., Polydispersity and block copolymer self-assembly. *Prog. Polym. Sci.* **2008,** *33* (9), 875-893.

71. Gentekos, D. T.; Dupuis, L. N.; Fors, B. P., Beyond Dispersity: Deterministic Control of Polymer Molecular Weight Distribution. *J. Am. Chem. Soc.* **2016,** *138* (6), 1848-1851.

72. Kottisch, V.; Gentekos, D. T.; Fors, B. P., "Shaping" the Future of Molecular Weight Distributions in Anionic Polymerization. *ACS Macro Lett.* **2016,** *5* (7), 796-800.

73. Domanskyi, S.; Gentekos, D. T.; Privman, V.; Fors, B. P., Predictive design of polymer molecular weight distributions in anionic polymerization. *Polym. Chem.* **2020,** *11* (2), 326-336.

74. Gentekos, D. T.; Fors, B. P., Molecular Weight Distribution Shape as a Versatile Approach to Tailoring Block Copolymer Phase Behavior. *ACS Macro Lett.* **2018,** *7* (6), 677-682.

75. Rosenbloom, S. I.; Fors, B. P., Shifting Boundaries: Controlling Molecular Weight Distribution Shape for Mechanically Enhanced Thermoplastic Elastomers. *Macromolecules* **2020,** *53* (17), 7479-7486.

76. Gentekos, D. T.; Sifri, R. J.; Fors, B. P., Controlling polymer properties through the shape of the molecular-weight distribution. *Nat. Rev. Mater.* **2019,** *4* (12), 761-774.

77. Matsen, M. W.; Schick, M., Microphase Separation in Starblock Copolymer Melts. *Macromolecules* **1994,** *27* (23), 6761-6767.

78. Lequieu, J.; Koeper, T.; Delaney, K. T.; Fredrickson, G. H., Extreme Deflection of Phase Boundaries and Chain Bridging in A(BA′)n Miktoarm Star Polymers. *Macromolecules* **2020,** *53* (2), 513-522.

79. Lynd, N. A.; Oyerokun, F. T.; O'Donoghue, D. L.; Handlin, D. L.; Fredrickson, G. H., Design of Soft and Strong Thermoplastic Elastomers Based on Nonlinear Block Copolymer Architectures Using Self-Consistent-Field Theory. *Macromolecules* **2010,** *43* (7), 3479-3486.

80. Shi, W.; Lynd, N. A.; Montarnal, D.; Luo, Y.; Fredrickson, G. H.; Kramer, E. J.; Ntaras, C.; Avgeropoulos, A.; Hexemer, A., Toward Strong Thermoplastic Elastomers with Asymmetric Miktoarm Block Copolymer Architectures. *Macromolecules* **2014,** *47* (6), 2037-2043.

81. Shi, W.; Hamilton, A. L.; Delaney, K. T.; Fredrickson, G. H.; Kramer, E. J.; Ntaras, C.; Avgeropoulos, A.; Lynd, N. A.; Demassieux, Q.; Creton, C., Aperiodic "Bricks and Mortar" Mesophase: a New Equilibrium State of Soft Matter and Application as a Stiff Thermoplastic Elastomer. *Macromolecules* **2015,** *48* (15), 5378-5384.

82. Bates, C. M.; Bates, F. S., 50th Anniversary Perspective: Block Polymers—Pure Potential. *Macromolecules* **2017,** *50* (1), 3-22.

83. Rosales, A. M.; McCulloch, B. L.; Zuckermann, R. N.; Segalman, R. A., Tunable Phase Behavior of Polystyrene–Polypeptoid Block Copolymers. *Macromolecules* **2012,** *45* (15), 6027-6035.

84. Patterson, A. L.; Danielsen, S. P. O.; Yu, B.; Davidson, E. C.; Fredrickson, G. H.; Segalman, R. A., Sequence Effects on Block Copolymer Self-Assembly through Tuning Chain Conformation and Segregation Strength Utilizing Sequence-Defined Polypeptoids. *Macromolecules* **2019,** *52* (3), 1277-1286.

85. Patterson, A. L.; Yu, B.; Danielsen, S. P. O.; Davidson, E. C.; Fredrickson, G. H.; Segalman, R. A., Monomer Sequence Effects on Interfacial Width and Mixing in Self-Assembled Diblock Copolymers. *Macromolecules* **2020,** *53* (9), 3262-3272.

86. Sun, J.; Teran, A. A.; Liao, X.; Balsara, N. P.; Zuckermann, R. N., Nanoscale Phase Separation in Sequence-Defined Peptoid Diblock Copolymers. *J. Am. Chem. Soc.* **2013,** *135* (38), 14119-14124.

87. Shirvanyants, D.; Panyukov, S.; Liao, Q.; Rubinstein, M., Long-range correlations in a polymer chain due to its connectivity. *Macromolecules* **2008,** *41* (4), 1475-1485.

88. Venkataswamy, K.; Jamieson, A. M.; Petschek, R. G., Static and Dynamic Properties of Polystyrene in Good Solvents - Ethylbenzene and Tetrahydrofuran. *Macromolecules* **1986,** *19* (1), 124-133.

89. Benoit, H.; Doty, P., Light Scattering from Non-Gaussian Chains. *J. Phys. Chem.* **1954,** *57* (9), 958-963.

90. Piedra-Arroni, E.; Makni, F.; Severac, L.; Stigliani, J. L.; Pratviel, G.; Bonduelle, C., Smart Poly(imidazoyl-L-lysine): Synthesis and Reversible Helix-to-Coil Transition at Neutral pH. *Polymers* **2017,** *9* (7).

91. Murakami, H.; Norisuye, T.; Fujita, H., Dimensional and Hydrodynamic Properties of Poly(Hexyl Isocyanate) in Hexane. *Macromolecules* **1980,** *13* (2), 345-352.

92. Gu, H.; Nakamura, Y.; Sato, T.; Teramoto, A.; Green, M. M.; Andreola, C., Global conformations of chiral polyisocyanates in dilute solution. *Polymer* **1999,** *40* (4), 849-856.

93. Nakatsuji, M.; Hyakutake, M.; Osa, M.; Yoshizaki, T., Mean-square radius of gyration and second virial coefficient of poly(diisopropyl fumarate) in dilute solution. *Polym. J.* **2008,** *40* (6), 566-571.

94. Armand, P.; Kirshenbaum, K.; Goldsmith, R. A.; Farr-Jones, S.; Barron, A. E.; Truong, K. T. V.; Dill, K. A.; Mierke, D. F.; Cohen, F. E.; Zuckermann, R. N.; Bradley, E. K., NMR determination of the major solution conformation of a peptoid pentamer with chiral side chains. *Proc. Natl. Acad. Sci. U.S.A.* **1998,** *95* (8), 4309-4314.

95. Mukherjee, S.; Zhou, G.; Michel, C.; Voelz, V. A., Insights into Peptoid Helix Folding Cooperativity from an Improved Backbone Potential. *J. Phys. Chem. B* **2015,** *119* (50), 15407-15417.

96. Yu, B.; Danielsen, S. P. O.; Patterson, A. L.; Davidson, E. C.; Segalman, R. A., Effects of Helical Chain Shape on Lamellae-Forming Block Copolymer Self-Assembly. *Macromolecules* **2019,** *52* (6), 2560-2568.

97. Theisen, A.; Johann, C.; Deacon, M. P.; Harding, S. E., *Refractive Increment Data-Book for Polymer and Biomolecular Scientists*. Nottingham University Press: Nottingham, United Kingdom, **2000**.

98. Huglin, M. B., Specific Refractive Index Increments of Polymer Solutions .I. Literature Values. *J. Appl. Polym. Sci.* **1965,** *9* (12), 3963-4001.

99. Arnold, O.; Bilheux, J. C.; Borreguero, J. M.; Buts, A.; Campbell, S. I.; Chapon, L.; Doucet, M.; Draper, N.; Leal, R. F.; Gigg, M. A.; Lynch, V. E.; Markvardsen, A.; Mikkelson, D. J.; Mikkelson, R. L.; Miller, R.; Palmen, K.; Parker, P.; Passos, G.; Perring, T. G.; Peterson, P. F.; Ren, S.; Reuter, M. A.; Savici, A. T.; Taylor, J. W.; Taylor, R. J.; Tolchenoy, R.; Zhou, W.; Zikoysky, J., Mantid-Data analysis and visualization package for neutron scattering and mu SR experiments. *Nucl. Instrum. Meth. A* **2014,** *764*, 156-166.

100. Wignall, G. D.; Bates, F. S., Absolute Calibration of Small-Angle Neutron-Scattering Data. *J. Appl. Crystallogr.* **1987,** *20*, 28-40.

101. Pedersen, J. S.; Schurtenberger, P., Scattering Functions of Semiflexible Polymers with and without Excluded Volume Effects. *Macromolecules* **1996,** *29* (23), 7602-7612.

102. Chen, W.-R.; Butler, P. D.; Magid, L. J., Incorporating Intermicellar Interactions in the Fitting of SANS Data from Cationic Wormlike Micelles. *Langmuir* **2006,** *22* (15), 6539-6548.

103. Hudson, B. C.; Battigelli, A.; Connolly, M. D.; Edison, J.; Spencer, R. K.; Whitelam, S.; Zuckermann, R. N.; Paravastu, A. K., Evidence for cis Amide Bonds in Peptoid Nanosheets. *J. Phys. Chem. Lett.* **2018,** *9* (10), 2574-2578.

104. Shah, N. H.; Butterfoss, G. L.; Nguyen, K.; Yoo, B.; Bonneau, R.; Rabenstein, D. L.; Kirshenbaum, K., Oligo(N-aryl glycines): A New Twist on Structured Peptoids. *J. Am. Chem. Soc.* **2008,** *130* (49), 16622-16632.

105. Knight, A. S.; Zhou, E. Y.; Francis, M. B.; Zuckermann, R. N., Sequence Programmable Peptoid Polymers for Diverse Materials Applications. *Adv. Mater.* **2015,** *27* (38), 5665-5691.

106. Wang, H.-F.; Yang, K.-C.; Hsu, W.-C.; Lee, J.-Y.; Hsu, J.-T.; Grason, G. M.; Thomas, E. L.; Tsai, J.-C.; Ho, R.-M., Generalizing the effects of chirality on block copolymer assembly. *Proc. Natl. Acad. Sci. U.S.A.* **2019,** *116* (10), 4080.

107. Yamakawa, H., A New Framework of Polymer Solution Science. The Helical Wormlike Chain. *Polym. J.* **1999,** *31* (2), 109-119.

108. Berry, G. C., Thermodynamic and Conformational Properties of Polystyrene .I. Light-Scattering Studies on Dilute Solutions of Linear Polystyrenes. *J. Chem. Phys.* **1966,** *44* (12), 4550-4564.

109. Flory, P. J.; Fisk, S., Effect of Volume Exclusion on Dimensions of Polymer Chains. *J. Chem. Phys.* **1966,** *44* (6), 2243-2248.

110. Olsen, B. D.; Segalman, R. A., Self-assembly of rod–coil block copolymers. *Mater. Sci. Eng. R Rep.* **2008,** *62* (2), 37-66.

111. Olsen, B. D.; Shah, M.; Ganesan, V.; Segalman, R. A., Universalization of the Phase Diagram for a Model Rod−Coil Diblock Copolymer. *Macromolecules* **2008,** *41* (18), 6809-6817.

112. Pauling, L.; Corey, R. B.; Branson, H. R., The structure of proteins: Two hydrogen-bonded helical configurations of the polypeptide chain. *Proc. Natl. Acad. Sci. U.S.A.* **1951,** *37* (4), 205.

113. Perutz, M. F., New X-Ray Evidence on the Configuration of Polypeptide Chains: Polypeptide Chains in Poly-γ-benzyl-L-glutamate, Keratin and Hæmoglobin. *Nature* **1951,** *167* (4261), 1053-1054.

114. Shoulders, M. D.; Raines, R. T., Collagen Structure and Stability. *Annu. Rev. Biochem.* **2009,** *78* (1), 929-958.

115. Yashima, E.; Maeda, K.; Iida, H.; Furusho, Y.; Nagai, K., Helical Polymers: Synthesis, Structures, and Functions. *Chem. Rev.* **2009,** *109* (11), 6102-6211.

116. Schwartz, E.; Koepf, M.; Kitto, H. J.; Nolte, R. J. M.; Rowan, A. E., Helical poly(isocyanides): past, present and future. *Polym. Chem.* **2011,** *2* (1), 33-47.

117. Cornelissen, J. J. L. M.; Rowan, A. E.; Nolte, R. J. M.; Sommerdijk, N. A. J. M., Chiral Architectures from Macromolecular Building Blocks. *Chem. Rev.* **2001,** *101* (12), 4039-4070.

118. Yamamoto, T., Molecular Dynamics of Crystallization in a Helical Polymer Isotactic Polypropylene from the Oriented Amorphous State. *Macromolecules* **2014,** *47* (9), 3192-3202.

119. Mathieu, C.; Stocker, W.; Thierry, A.; Wittmann, J. C.; Lotz, B., Epitaxy of isotactic poly(1-butene): new substrates, impact and attempt at recognition of helix orientation in form I′ by AFM. *Polymer* **2001,** *42* (16), 7033-7047.

120. Bloksma, M. M.; Hoeppener, S.; D'Haese, C.; Kempe, K.; Mansfeld, U.; Paulus, R. M.; Gohy, J.-F.; Schubert, U. S.; Hoogenboom, R., Self-assembly of chiral block and gradient copolymers. *Soft Matter* **2012,** *8* (1), 165-172.

121. Hanson, J. A.; Li, Z.; Deming, T. J., Nonionic Block Copolypeptide Micelles Containing a Hydrophobic rac-Leucine Core. *Macromolecules* **2010,** *43* (15), 6268-6269.

122. Wang, Z.; Sheng, R.; Luo, T.; Sun, J.; Cao, A., Synthesis and self-assembly of diblock glycopolypeptide analogues PMAgala-b-PBLG as multifunctional biomaterials for protein recognition, drug delivery and hepatoma cell targeting. *Polym. Chem.* **2017,** *8* (2), 472-484.

123. Zhang, J.; Chen, X.-F.; Wei, H.-B.; Wan, X.-H., Tunable assembly of amphiphilic rod–coil block copolymers in solution. *Chem. Soc. Rev.* **2013,** *42* (23), 9127-9154.

124. Loo, Y.-L.; Register, R. A.; Ryan, A. J., Modes of Crystallization in Block Copolymer Microdomains: Breakout, Templated, and Confined. *Macromolecules* **2002,** *35* (6), 2365-2374.

125. Rosales, A. M.; Murnen, H. K.; Zuckermann, R. N.; Segalman, R. A., Control of Crystallization and Melting Behavior in Sequence Specific Polypeptoids. *Macromolecules* **2010,** *43* (13), 5627-5636.

126. Ilavsky, J., Nika: software for two-dimensional data reduction. *J. Appl. Crystallogr.* **2012,** *45* (2), 324-328.

127. Hamley, I. W., Form Factor of Helical Ribbons. *Macromolecules* **2008,** *41* (22), 8948-8950.

128. Bates, F. S.; Rosedale, J. H.; Fredrickson, G. H., Fluctuation effects in a symmetric diblock copolymer near the order–disorder transition. *J. Chem. Phys.* **1990,** *92* (10), 6255-6270.

129. Matsen, M. W.; Bates, F. S., Unifying Weak- and Strong-Segregation Block Copolymer Theories. *Macromolecules* **1996,** *29* (4), 1091-1098.

130. Sakamoto, N.; Hashimoto, T.; Han, C. D.; Kim, D.; Vaidya, N. Y., Order−Order and Order−Disorder Transitions in a Polystyrene-block-Polyisoprene-block-Polystyrene Copolymer. *Macromolecules* **1997,** *30* (6), 1621-1632.

131. Yu, B.; Danielsen, S. P. O.; Yang, K.-C.; Ho, R.-M.; Walker, L. M.; Segalman, R. A., Insensitivity of Sterically Defined Helical Chain Conformations to Solvent Quality in Dilute Solution. *ACS Macro Lett.* **2020,** *9* (6), 849-854.

132. Mayes, A. M.; de la Cruz, M. O., Concentration fluctuation effects on disorder–order transitions in block copolymer melts. *J. Chem. Phys.* **1991,** *95* (6), 4670-4677.

133. Qin, J.; Morse, D. C., Fluctuations in Symmetric Diblock Copolymers: Testing Theories Old and New. *Phys. Rev. Lett.* **2012,** *108* (23), 238301.

134. Delaney, K. T.; Fredrickson, G. H., Recent Developments in Fully Fluctuating Field-Theoretic Simulations of Polymer Melts and Solutions. *J. Phys. Chem. B* **2016,** *120* (31), 7615-7634.

135. Dair, B. J.; Honeker, C. C.; Alward, D. B.; Avgeropoulos, A.; Hadjichristidis, N.; Fetters, L. J.; Capel, M.; Thomas, E. L., Mechanical Properties and Deformation Behavior of the Double Gyroid Phase in Unoriented Thermoplastic Elastomers. *Macromolecules* **1999,** *32* (24), 8145-8152.

136. Pernot, H.; Baumert, M.; Court, F.; Leibler, L., Design and properties of co-continuous nanostructured polymers by reactive blending. *Nat. Mater.* **2002,** *1* (1), 54-58.

137. Meuler, A. J.; Fleury, G.; Hillmyer, M. A.; Bates, F. S., Structure and Mechanical Properties of an O70 (Fddd) Network-Forming Pentablock Terpolymer. *Macromolecules* **2008,** *41* (15), 5809-5817.

138. Cho, B. K.; Jain, A.; Gruner, S. M.; Wiesner, U., Mesophase Structure-Mechanical and Ionic Transport Correlations in Extended Amphiphilic Dendrons. *Science* **2004,** *305* (5690), 1598.

139. Crossland, E. J. W.; Kamperman, M.; Nedelcu, M.; Ducati, C.; Wiesner, U.; Smilgies, D. M.; Toombes, G. E. S.; Hillmyer, M. A.; Ludwigs, S.; Steiner, U.; Snaith, H. J., A Bicontinuous Double Gyroid Hybrid Solar Cell. *Nano Lett.* **2009,** *9* (8), 2807-2812.

140. Yan, L.; Rank, C.; Mecking, S.; Winey, K. I., Gyroid and Other Ordered Morphologies in Single-Ion Conducting Polymers and Their Impact on Ion Conductivity. *J. Am. Chem. Soc.* **2020,** *142* (2), 857-866.

141. Martín-Moreno, L.; García-Vidal, F. J.; Somoza, A. M., Self-Assembled Triply Periodic Minimal Surfaces as Molds for Photonic Band Gap Materials. *Phys. Rev. Lett.* **1999,** *83* (1), 73-75.

142. Urbas, A. M.; Maldovan, M.; DeRege, P.; Thomas, E. L., Bicontinuous Cubic Block Copolymer Photonic Crystals. *Adv. Mater.* **2002,** *14* (24), 1850-1853.

143. Dolan, J. A.; Wilts, B. D.; Vignolini, S.; Baumberg, J. J.; Steiner, U.; Wilkinson, T. D., Optical Properties of Gyroid Structured Materials: From Photonic Crystals to Metamaterials. *Adv. Opt. Mater.* **2015,** *3* (1), 12-32.

144. Hsueh, H.-Y.; Chen, H.-Y.; She, M.-S.; Chen, C.-K.; Ho, R.-M.; Gwo, S.; Hasegawa, H.; Thomas, E. L., Inorganic Gyroid with Exceptionally Low Refractive Index from Block Copolymer Templating. *Nano Lett.* **2010,** *10* (12), 4994-5000.

145. Hur, K.; Francescato, Y.; Giannini, V.; Maier, S. A.; Hennig, R. G.; Wiesner, U., Three-Dimensionally Isotropic Negative Refractive Index Materials from Block Copolymer Self-Assembled Chiral Gyroid Networks. *Angew. Chem. Int. Ed.* **2011,** *50* (50), 11985-11989.

146. Kim, M. I.; Wakada, T.; Akasaka, S.; Nishitsuji, S.; Saijo, K.; Hasegawa, H.; Ito, K.; Takenaka, M., Stability of the Fddd Phase in Diblock Copolymer Melts. *Macromolecules* **2008,** *41* (20), 7667-7670.

147. Meuler, A. J.; Hillmyer, M. A.; Bates, F. S., Ordered Network Mesostructures in Block Polymer Materials. *Macromolecules* **2009,** *42* (19), 7221-7250.

148. Matsen, M. W.; Bates, F. S., Origins of complex self-assembly in block copolymers. *Macromolecules* **1996,** *29* (23), 7641-7644.

149. Martínez-Veracoechea, F. J.; Escobedo, F. A., Simulation of the gyroid phase in off-lattice models of pure diblock copolymer melts. *J. Chem. Phys.* **2006,** *125* (10), 104907.

150. Matsen, M. W.; Bates, F. S., Block copolymer microstructures in the intermediate-segregation regime. *J. Chem. Phys.* **1997,** *106* (6), 2436-2448.

151. Matsen, M. W., Phase Behavior of Block Copolymer/Homopolymer Blends. *Macromolecules* **1995,** *28* (17), 5765-5773.

152. Martínez-Veracoechea, F. J.; Escobedo, F. A., Lattice Monte Carlo Simulations of the Gyroid Phase in Monodisperse and Bidisperse Block Copolymer Systems. *Macromolecules* **2005,** *38* (20), 8522-8531.

153. Winey, K. I.; Thomas, E. L.; Fetters, L. J., The Ordered Bicontinuous Double-Diamond Morphology in Diblock Copolymer Homopolymer Blends. *Macromolecules* **1992,** *25* (1), 422-428.

154. Tureau, M. S.; Rong, L.; Hsiao, B. S.; Epps, T. H., Phase Behavior of Neat Triblock Copolymers and Copolymer/Homopolymer Blends Near Network Phase Windows. *Macromolecules* **2010,** *43* (21), 9039-9048.

155. Lynd, N. A.; Hillmyer, M. A., Influence of Polydispersity on the Self-Assembly of Diblock Copolymers. *Macromolecules* **2005,** *38* (21), 8803-8810.

156. Meuler, A. J.; Ellison, C. J.; Hillmyer, M. A.; Bates, F. S., Polydispersity-Induced Stabilization of the Core−Shell Gyroid. *Macromolecules* **2008,** *41* (17), 6272-6275.

157. Xie, Q.; Qiang, Y.; Li, W., Regulate the Stability of Gyroids of ABC-Type Multiblock Copolymers by Controlling the Packing Frustration. *ACS Macro Lett.* **2020,** *9* (2), 278-283.

158. Alward, D. B.; Kinning, D. J.; Thomas, E. L.; Fetters, L. J., Effect of arm number and arm molecular weight on the solid-state morphology of poly(styrene-isoprene) star block copolymers. *Macromolecules* **1986,** *19* (1), 215-224.

159. Kinning, D. J.; Thomas, E. L.; Alward, D. B.; Fetters, L. J.; Handlin, D. L., Sharpness of the functionality-induced structural transition in poly(styrene-isoprene) star block copolymers. *Macromolecules* **1986,** *19* (4), 1288-1290.

160. Bates, M. W.; Lequieu, J.; Barbon, S. M.; Lewis, R. M.; Delaney, K. T.; Anastasaki, A.; Hawker, C. J.; Fredrickson, G. H.; Bates, C. M., Stability of the A15 phase in diblock copolymer melts. *Proc. Natl. Acad. Sci. U.S.A.* **2019,** *116* (27), 13194.

161. Sun, J.; Jiang, X.; Siegmund, A.; Connolly, M. D.; Downing, K. H.; Balsara, N. P.; Zuckermann, R. N., Morphology and Proton Transport in Humidified Phosphonated Peptoid Block Copolymers. *Macromolecules* **2016,** *49* (8), 3083-3090.

162. Grason, G. M.; DiDonna, B. A.; Kamien, R. D., Geometric Theory of Diblock Copolymer Phases. *Phys. Rev. Lett.* **2003,** *91* (5), 058304.

163. Grason, G. M.; Kamien, R. D., Interfaces in Diblocks: A Study of Miktoarm Star Copolymers. *Macromolecules* **2004,** *37* (19), 7371-7380.

164. Yadav, M.; Bates, F. S.; Morse, D. C., Effects of Segment Length Asymmetry in Ternary Diblock Co-polymer–Homopolymer Mixtures. *Macromolecules* **2019,** *52* (11), 4091-4102.

165. Seo, Y.; Brown, J. R.; Hall, L. M., Effect of Tapering on Morphology and Interfacial Behavior of Diblock Copolymers from Molecular Dynamics Simulations. *Macromolecules* **2015,** *48* (14), 4974-4982.

166. Luo, M.; Browns, J. R.; Remy, R. A.; Scott, D. M.; Mackay, M. E.; Halv, L. M.; Epps, T. H., Determination of Interfacial Mixing in Tapered Block Polymer Thin Films: Experimental and Theoretical Investigations. *Macromolecules* **2016,** *49* (14), 5213-5222.

167. Jinnai, H.; Nishikawa, Y.; Spontak, R. J.; Smith, S. D.; Agard, D. A.; Hashimoto, T., Direct measurement of interfacial curvature distributions in a bicontinuous block copolymer morphology. *Phys. Rev. Lett.* **2000,** *84* (3), 518-521.

168. Maurer, W. W.; Bates, F. S.; Lodge, T. P.; Almdal, K.; Mortensen, K.; Fredrickson, G. H., Can a single function for χ account for block copolymer and homopolymer blend phase behavior? *J. Chem. Phys.* **1998,** *108* (7), 2989-3000.

169. Kuan, W.-F.; Roy, R.; Rong, L.; Hsiao, B. S.; Epps, T. H., Design and Synthesis of Network-Forming Triblock Copolymers Using Tapered Block Interfaces. *ACS Macro Lett.* **2012,** *1* (4), 519-523.

170. Brown, J. R.; Sides, S. W.; Hall, L. M., Phase Behavior of Tapered Diblock Copolymers from Self-Consistent Field Theory. *ACS Macro Lett.* **2013,** *2* (12), 1105-1109.

171. Feng, X.; Burke, C. J.; Zhuo, M.; Guo, H.; Yang, K.; Reddy, A.; Prasad, I.; Ho, R.-M.; Avgeropoulos, A.; Grason, G. M.; Thomas, E. L., Seeing mesoatomic distortions in soft-matter crystals of a double-gyroid block copolymer. *Nature* **2019,** *575* (7781), 175-179.

172. Rosales, A. M.; Segalman, R. A.; Zuckermann, R. N., Polypeptoids: a model system to study the effect of monomer sequence on polymer properties and self-assembly. *Soft Matter* **2013,** *9* (35), 8400-8414.

173. Fetsch, C.; Gaitzsch, J.; Messager, L.; Battaglia, G.; Luxenhofer, R., Self-Assembly of Amphiphilic Block Copolypeptoids – Micelles, Worms and Polymersomes. *Sci. Rep.* **2016,** *6* (1), 33491.

174. Gangloff, N.; Ulbricht, J.; Lorson, T.; Schlaad, H.; Luxenhofer, R., Peptoids and Polypeptoids at the Frontier of Supra- and Macromolecular Engineering. *Chem. Rev.* **2016,** *116* (4), 1753-1802.

175. Xuan, S.; Zuckermann, R. N., Diblock copolypeptoids: a review of phase separation, crystallization, self-assembly and biological applications. *J. Mater. Chem. B* **2020,** *8* (25), 5380-5394.

176. Knight, A. S.; Zhou, E. Y.; Francis, M. B., Development of peptoid-based ligands for the removal of cadmium from biological media. *Chem. Sci.* **2015,** *6* (7), 4042-4048.

177. Sun, J.; Stone, G. M.; Balsara, N. P.; Zuckermann, R. N., Structure–Conductivity Relationship for Peptoid-Based PEO–Mimetic Polymer Electrolytes. *Macromolecules* **2012,** *45* (12), 5151-5156.

178. Blackmond, D. G., The origin of biological homochirality. *Cold Spring Harb. Perspect. Biol.* **2010,** *2* (5), a002147-a002147.

179. Wen, T.; Wang, H.-F.; Li, M.-C.; Ho, R.-M., Homochiral Evolution in Self-Assembled Chiral Polymers and Block Copolymers. *Acc. Chem. Res.* **2017,** *50* (4), 1011-1021.

180. Meek, K. M.; Elabd, Y. A., Polymerized ionic liquid block copolymers for electrochemical energy. *J. Mater. Chem. A* **2015,** *3* (48), 24187-24194.

181. Ganesan, V., Ion transport in polymeric ionic liquids: recent developments and open questions. *Mol. Syst. Des. Eng.* **2019,** *4* (2), 280-293.

182. Eshetu, G. G.; Mecerreyes, D.; Forsyth, M.; Zhang, H.; Armand, M., Polymeric ionic liquids for lithium-based rechargeable batteries. *Mol. Syst. Des. Eng.* **2019,** *4* (2), 294-309.

183. Schauser, N. S.; Seshadri, R.; Segalman, R. A., Multivalent ion conduction in solid polymer systems. *Mol. Syst. Des. Eng.* **2019,** *4* (2), 263-279.

184. Singh, M.; Odusanya, O.; Wilmes, G. M.; Eitouni, H. B.; Gomez, E. D.; Patel, A. J.; Chen, V. L.; Park, M. J.; Fragouli, P.; Iatrou, H.; Hadjichristidis, N.; Cookson, D.; Balsara, N. P., Effect of Molecular Weight on the Mechanical and Electrical Properties of Block Copolymer Electrolytes. *Macromolecules* **2007,** *40* (13), 4578-4585.

185. Panday, A.; Mullin, S.; Gomez, E. D.; Wanakule, N.; Chen, V. L.; Hexemer, A.; Pople, J.; Balsara, N. P., Effect of Molecular Weight and Salt Concentration on Conductivity of Block Copolymer Electrolytes. *Macromolecules* **2009,** *42* (13), 4632-4637.

186. Ganesan, V.; Pyramitsyn, V.; Bertoni, C.; Shah, M., Mechanisms Underlying Ion Transport in Lamellar Block Copolymer Membranes. *ACS Macro Lett.* **2012,** *1* (4), 513-518.

187. Epps, T. H.; Bailey, T. S.; Waletzko, R.; Bates, F. S., Phase Behavior and Block Sequence Effects in Lithium Perchlorate-Doped Poly(isoprene-b-styrene-b-ethylene oxide) and Poly(styrene-b-isoprene-b-ethylene oxide) Triblock Copolymers. *Macromolecules* **2003,** *36* (8), 2873-2881.

188. Young, W.-S.; Kuan, W.-F.; Epps, I. I. I. T. H., Block copolymer electrolytes for rechargeable lithium batteries. *J. Polym. Sci. B Polym. Phys.* **2014,** *52* (1), 1-16.

189. Thelen, J. L.; Inceoglu, S.; Venkatesan, N. R.; Mackay, N. G.; Balsara, N. P., Relationship between Ion Dissociation, Melt Morphology, and Electrochemical Performance of Lithium and Magnesium Single-Ion Conducting Block Copolymers. *Macromolecules* **2016,** *49* (23), 9139-9147.

190. Inceoglu, S.; Rojas, A. A.; Devaux, D.; Chen, X. C.; Stone, G. M.; Balsara, N. P., Morphology–Conductivity Relationship of Single-Ion-Conducting Block Copolymer Electrolytes for Lithium Batteries. *ACS Macro Lett.* **2014,** *3* (6), 510-514.

191. Ye, Y.; Choi, J.-H.; Winey, K. I.; Elabd, Y. A., Polymerized Ionic Liquid Block and Random Copolymers: Effect of Weak Microphase Separation on Ion Transport. *Macromolecules* **2012,** *45* (17), 7027-7035.

192. Sanoja, G. E.; Schauser, N. S.; Bartels, J. M.; Evans, C. M.; Helgeson, M. E.; Seshadri, R.; Segalman, R. A., Ion Transport in Dynamic Polymer Networks Based on

Metal–Ligand Coordination: Effect of Cross-Linker Concentration. *Macromolecules* **2018,** *51* (5), 2017-2026.

193. Sundberg, R. J.; Martin, R. B., Interactions of histidine and other imidazole derivatives with transition metal ions in chemical and biological systems. *Chem. Rev.* **1974,** *74* (4), 471-517.

194. la Cruz, D. S.-d.; Green, M. D.; Ye, Y.; Elabd, Y. A.; Long, T. E.; Winey, K. I., Correlating backbone-to-backbone distance to ionic conductivity in amorphous polymerized ionic liquids. *J. Polym. Sci. B Polym. Phys.* **2012,** *50* (5), 338-346.

195. Choi, U. H.; Ye, Y.; Salas de la Cruz, D.; Liu, W.; Winey, K. I.; Elabd, Y. A.; Runt, J.; Colby, R. H., Dielectric and Viscoelastic Responses of Imidazolium-Based Ionomers with Different Counterions and Side Chain Lengths. *Macromolecules* **2014,** *47* (2), 777-790.

196. Evans, C. M.; Bridges, C. R.; Sanoja, G. E.; Bartels, J.; Segalman, R. A., Role of Tethered Ion Placement on Polymerized Ionic Liquid Structure and Conductivity: Pendant versus Backbone Charge Placement. *ACS Macro Lett.* **2016,** *5* (8), 925-930.

197. Burkoth, T. S.; Fafarman, A. T.; Charych, D. H.; Connolly, M. D.; Zuckermann, R. N., Incorporation of unprotected heterocyclic side chains into peptoid oligomers via solid-phase submonomer synthesis. *J. Am. Chem. Soc.* **2003,** *125* (29), 8841-8845.

198. Gauthier, M. A.; Klok, H.-A., Peptide/protein–polymer conjugates: synthetic strategies and design concepts. *Chem. Comm.* **2008,** (23), 2591-2611.

199. Iha, R. K.; Wooley, K. L.; Nyström, A. M.; Burke, D. J.; Kade, M. J.; Hawker, C. J., Applications of Orthogonal "Click" Chemistries in the Synthesis of Functional Soft Materials. *Chem. Rev.* **2009,** *109* (11), 5620-5686.

200. Obermeyer, A. C.; Olsen, B. D., Synthesis and Application of Protein-Containing Block Copolymers. *ACS Macro Lett.* **2015,** *4* (1), 101-110.